

**ILRS Meeting on Retroreflector Arrays
Austria Center Vienna
Room SM2
April 6, 2006
13:30 – 17:00**

- 1. Specifications for high satellites: What cross sections do we need for Galileo, GPS and GEOS; compare with actual experience on GPS, GLONASS and LAGEOS (J. McGarry, D. Arnold, W. Gurtner)**
- 2. Progress at NASA on getting retroreflectors on GPS-III (J. McGarry)**
- 3. Description of the Galileo retro array on the two Engineering Missions and what are the options of the operational fleet? (G. Appleby)**
- 4. Configuration options to meet the specification (D. Arnold)**
- 5. Studies at GSFC on the hollow cubes (J. McGarry)**
- 6. Measurement Test Bed at INFN-LNF (S. Dell'Agnello)**
- 7. Westpac - Why isn't the performance better with the recessed cubes (J. Luck, J. Ries)**
- 8. Other concepts ; Luneberg Sphere (?), Lunar Lander (Jan McGarry)**
- 9. Any other business?**

Retroreflector Arrays for high altitude satellites

1. GPS 35,36

Each GPS 35,36 retroreflector array (shown below) has 32 hexagonal cubes 19 mm high and 27 mm across flats on the hexagonal front face. According to the GPS website the array is 239 mm long, 194 mm wide, and 37 mm thick, and has a mass of 1.27 kg.



The reflecting area of one hexagonal cube is

$$A = 2\sqrt{3}r^2$$

where r is the radius of the inscribed circle ($r = \text{half of } 27 \text{ mm} = 13.5 \text{ mm}$). This gives a face area of 6.3 sq cm. For 32 cubes this is a total reflecting area of 202 sq cm. The area of the array is $23.9 \times 19.4 = 463 \text{ sq cm}$. The retroreflectors are 44 % of the total area.

The volume of a hexagonal cube corner is

$$V = \frac{5}{\sqrt{6}}r^3 = 2.04r^3 \quad (1)$$

With $r = 1.35 \text{ cm}$ this is 5 cc. Since the density of quartz is about 2.2 g/cc the mass is 11 grams per cube. For 32 cubes this is 353 g = .353 kg. The cubes are 28 % of the total array mass of 1.27 kg. The actual cube corners vary in mass. According to Vladimir Vasiliev, "The mass of a single GPS cube corner prism is 11.3 +/- 0.45 grams. With the correct value of the used type of quartz glass density (2.21), the volume is 5.1 cm³."

Since the specifications of the GPS cubes are unknown there is no way to do an accurate calculation of the cross section. One way of estimating the cross section is to use the cross section for an optimized dihedral angle offset. This gives about 1.25 million sq meters without accounting for reflection losses.

The Russian cubes use aluminum coated back faces which have a lower reflectivity than silver. Information from Vladimir Vasiliev gives a measured reflectivity of about 50 %. This would be a cross section of $1.25/2 = .625$ million sq m per cube. For 32 cubes this is 20 million sq meters.

To get 100 million sq meters with this design of cube corner would require 160 cubes. The total reflecting area would be 1008 sq cm. The total mass would be 1760 g = 1.76 kg.

2. Galileo

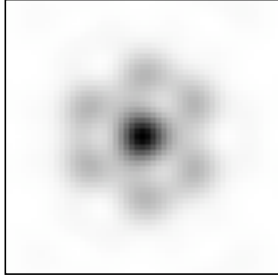
The velocity aberration is about 24 microradians. This is a little lower than the velocity aberration for GPS which is about 26 microradians. The wavelength used is 532 nm. The cross section needed to obtain good signal is between 50 and 200 million sq meters. Calculations have been done to estimate the number of cubes needed to obtain a cross section of 100 million sq meters. The results can be scaled for other values of cross section. Since the spacecraft rotates to keep the solar panels aligned it is necessary to have a circular far field diffraction pattern to account for velocity aberration.

The cross section at 24 microradians velocity aberration is optimized by varying the size, dihedral angle offset, and using coated or uncoated cubes. The cross section can be optimized as maximum cross section per unit reflecting area or maximum cross section per unit volume (mass). It turns out that both methods give similar results so only one case is given for each possible design.

A. Circular uncoated cube corner

Because of polarization effects, a dihedral angle offset gives a complicated pattern in an uncoated cube. With no dihedral angle offset, the central peak is lower by about a factor of 4 than for a coated cube of the same size. For this reason it does not work well to design an uncoated cube to work on the central peak or use dihedral angle offsets unless other factors require it. The best option is to work on the side lobes that are present naturally from the polarization effects. These side lobes look similar to what one would obtain with a dihedral angle offset in a coated cube.

For a circular uncoated cube corner the optimum size (no dihedral angle offset) for 24 microradians velocity aberration and 532 nm wavelength is in the range 1.3 to 1.4 inches in diameter. For a 1.3 inch cube the cross section per cube is about 2 million sq meters per cube including reflection losses at the front face. There are no other reflection losses to consider since the reflection at the back faces is total. To get 100 million sq meters cross section would require 50 cubes. This result can be scaled for other desired value of cross section. The diffraction pattern is shown below. The scale is -50 to $+50$ microradians in each dimension.



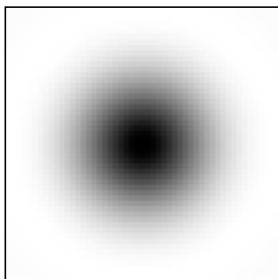
The reflecting area of one cube corner is $A = \pi r^2$ where r is the radius of the front face. The radius of a 1.3 inch diameter cube is .65 in = 1.65 cm. The reflecting area is 8.56 sq cm per cube. For 50 cubes the total reflecting area is 428 sq cm.

I do not have a formula for the volume of a circular cube corner. It should be a little less than that of a hexagonal cube with the same inscribed diameter of the front face. Using the formula for a hexagonal cube in equation (1) gives a volume of 9 cc per cube. With a density of 2.2 g/cc this is 20 g per cube. For 50 cubes the mass is 1000 g = 1 kg.

B. Circular coated cube corner

In coated solid cube corners, there can be thermal gradients due to absorption of sunlight at the back faces. The change in optical path length is proportional to the square of the diameter of the cube corner. For this reason is better to keep the size as small as possible. Since there are no polarization effects to reduce the central peak, a good approach is to use a cube with the cross section optimized on the central peak.

For a circular coated cube corner with no dihedral angle offset the optimum size for 532 nm wavelength on the central peak is in the range .4 to .5 inches in diameter. For a .5 inch cube the cross section per cube is about .276 million sq meters including reflection losses at the front face. If the back faces are silver coated with a triple reflection coefficient of .9 the effective cross section is .25 million sq meters per cube. To obtain a cross section of 100 million sq m requires 400 cube corners. This value can be scaled for other cross sections. The diffraction pattern is shown below. The scale is -50 to +50 microradians.



The radius of the cube is .25 inches = .635 cm. The area per cube is 1.27 sq cm. For 400 cubes the total reflecting area is 508 sq cm.

The volume of one cube (over estimated slightly by using the formula for a hexagonal cube) is .523 cc. The mass with a density of 2.2 is 1.15 grams. The total mass for 400 cubes is 460 grams.

C. Hollow cube corner

A 2 inch diameter hollow cube corner consists of three orthogonal plates 1.4 x 1.4 x .12 inches. This is 3.5 x 3.5 x .3 cm. The plates are $\sqrt{2}$ larger than the radius (one inch). The ratio of the plate width to the thickness is $3.5/.3 = 11.666$. As a function of the radius of the aperture the volume of the hollow cube corner is

$$V = .7273r^3 \quad (2)$$

Comparing this with equation (1) for the volume of a hexagonal cube we see that the volume of the plates in a hollow cube is smaller by a factor of $.7273/2.04 = .356$. The density of quartz is 2.2, the density of aluminum is 2.7 and the density of beryllium is 1.85. The weight ratio between solid and hollow depends on the material used for the hollow cube.

In a solid cube corner there are reflection losses at the front face on entering and leaving the cube corner that give a transmission factor of about .93. In a hollow cube the cross section would be greater by $1/.93 = 1.075$ since there is no reflection loss at the front face.

In a hollow cube corner there is no optical path through fused silica to distort the wavefront if there are thermal gradients. There is only the issue of mechanical distortion of the reflecting faces due to thermal gradients. This effect should be much less than the effect of thermal gradients in fused silica.

In either a solid coated cube or a hollow cube with metal reflecting faces it is possible to use a dihedral angle offset to create a smooth ring in the diffraction pattern at the radius of the first diffraction ring. This is done by setting the dihedral angle offset to give the same beam spread as the radius of the first diffraction ring. The only reason not to do this in a solid cube is the problem of thermal gradients in large cubes.

The divergence of the exiting wavefront due to offsetting all three dihedral angles by the same amount is given by the formula

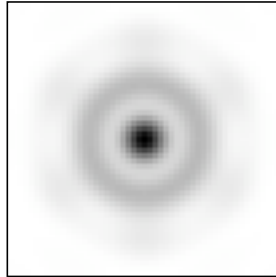
$$\gamma = \frac{4}{3} \sqrt{6} n \vartheta \quad (3)$$

where γ is the divergence of the wavefront, n is the index of refraction, and ϑ is the dihedral angle offset. For a divergence of 24 microradians with $n = 1.00$ (hollow cube), the dihedral angle offset is 7.35 microradians = 1.5 arcsec.

The position of the first diffraction ring is given by the formula

$$\gamma = 1.635 \frac{\lambda}{D} \tag{4}$$

where γ is the radius of the ring, λ is the wavelength, and D is the diameter of the cube corner. For a wavelength of 532 nm the diameter required to put the first diffraction ring at 24 microradians is 1.4 inches. The diffraction pattern is shown below. The scale is -50 to +50 microradians.



For a circular 1.4 inch hollow cube corner with each dihedral angle offset by 1.5 arcsec, the cross section at 24 microradians is about 3.1 million sq meters per cube. There is no reflection loss at the front face since the cube is hollow. If the reflecting faces are silver, there is a triple reflection coefficient of about .9 which gives an effective cross section of 2.8 million sq meters. To get a cross section of 100 million requires 36 cubes.

The radius of one cube is .7 inches = 1.78 cm. The area of one cube is 9.9 sq cm. The area of 36 cubes is 356 sq cm. The volume of one cube is 4.1 cc. The mass if aluminum is used is 11.07g per cube. The mass for 36 cubes is 400 g.

D. Small hollow cube corner.

The dimensions used in section B for a circular coated cube could also be used for a small hollow cube. The area would be the same. The volume with $r = .25$ inches = .635 cm using equation (2) is .186 cc. For aluminum with density 2.7, the mass is .5 g/cube. The mass of 400 cubes is 201 g.

E. Summary

The table below gives a summary of options for achieving a cross section of 100 million sq meters at the altitude of Galileo. The values can be scaled for another cross section.

Design	# of cubes	Diam. in	Area sq cm	Mass g
uncoated	50	1.3	428	1000
coated	400	0.5	508	460
hollow	400	0.5	508	201
hollow	36	1.4	356	400

GPS	160	1.06	1008	1760
-----	-----	------	------	------

3. Geosynchronous.

The velocity aberration at geosynchronous altitude is about 18 microradians. The part due to the orbital motion is about 20 microradians. The part due to the earth rotation has a magnitude of about 3 microradians. The component of the earth rotation that is parallel to the orbital velocity depends on the location of the observing station. The velocity aberration is constant for each station. For a station on the equator directly under the satellite the velocity aberration would be 17 microradians. Since the satellite is in an equatorial orbit, the satellite velocity and the earth rotational velocity are always coplanar. There is no across track component of velocity aberration.

The direction of the velocity aberration is always perpendicular to the earth's rotation axis and varies only slightly in magnitude depending on the location of the station. If the satellite is tri-axially stabilized it is possible to use a single dihedral angle offset to split the return into two high gain spots to increase the cross section.

The cross section needed is between about 500 million and 2 billion sq meters. A cross section of 1 billion sq meters has been used in this analysis. The results can be scaled for other cross section values.

A. Circular uncoated cube corner

Because the diffraction pattern already has side lobes due to polarization effects it is not feasible to use a single dihedral angle offset for this design. Adding a dihedral angle offset would decrease the cross section. All that can be done is to optimize the size for the particular velocity aberration. Since the velocity aberration is lower than for the Galileo the cube corner should be larger to create a tighter return beam.

The optimum size for this velocity aberration is about 1.7 inches. The cross section at 18 microradians for wavelength 532 nm is about 6.07 million sq meters per cube. To obtain a cross section of 1 billion sq meters requires 165 cubes. The area of a single cube is 14.64 sq cm. The total area for 165 cubes is 2415 sq cm. The volume of a single cube is 20.54 cc. The mass is 45.2 grams per cube. The total mass for 165 cubes is 7457 grams = 7.457 kg.

B. Circular coated cube corner.

With no dihedral angle offset, the optimum size for this velocity aberration is about .7 inches. The cross section at 18 microradians is about .964 million sq meters per cube. If the reflection losses give a factor of .9 this reduces to .867 million sq m. To obtain a cross section of 1 billion sq meters requires 1153 cubes. The area of one cube is 2.48 sq cm. The area of 1153 cubes is 2863 sq cm. The volume of one cube is 1.434 cc. The mass of one cube is 3.15 g. The mass of 1153 cubes is 3638 g = 3.638 kg.

C. Hollow cube corner with 3 dihedral angle offsets.

Using equation (3) with a velocity aberration of 18 microradians gives a dihedral angle offset of 1.136 arcsec. From equation (4) the optimum size to put the receiver on the first diffraction ring is 1.902 inches. Runs for various sizes show that the optimum cross section per unit area is obtained with a size of about 1.8 inches. The cross section at 18 microradians is about 9.117 million sq meters. With a reflection loss of about .9 this gives about 8.2 million sq meters per cube. To obtain a cross section of 1 billion sq meters requires 122 cubes. The area of one cube is 16.4 sq cm. The total area is 2003 sq cm. The volume of one cube is 8.69 cc. The mass using aluminum is 23.46 grams per cube. The total mass is 2862 g = 2.862 kg.

D. Small hollow cube.

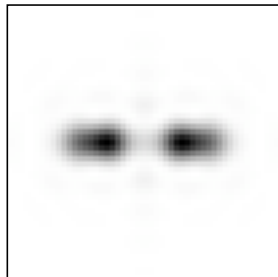
If the .7 inch cube described in section B were hollow the volume of one cube would be .511 cc. For aluminum the mass would be 1.38 grams. The total mass for 1153 cubes would be 1590 grams = 1.59 kg.

E. Hollow cube with single dihedral angle offset.

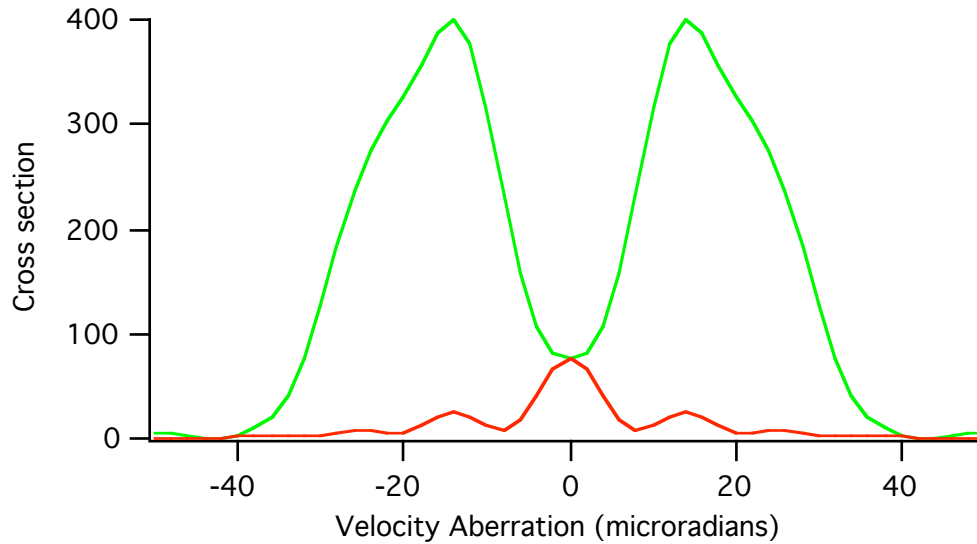
Thermal distortion in sunlight may limit the size of a hollow cube to around 2 inches. Using a large cube with a single dihedral angle offset gives two high gain spots in the far field. The separation of the spots as a function of the single dihedral angle offset is half the value given by equation (3). We have

$$\gamma = \frac{2}{3}\sqrt{6n\delta} \quad (5)$$

The dihedral angle offset needed to give a divergence of 18 microradians is 2.27 arcsec. Runs with various dihedral angle offsets show that the optimum value is around 2.4 arcsec. The diffraction pattern is shown below.



The cross section along the horizontal and vertical axes is shown below



The green curve is horizontal and the red curve is vertical. The units are $4\pi \times 10000$ sq m. The data are shown in the table below. The units are $4\pi \times 10000$ sq m.

Microradians	Horizontal	Vertical
0.0	76.0649190000	76.0649190000
2.0	82.3193370000	65.6734690000
4.0	106.4345880000	41.3876230000
6.0	157.3004130000	18.4337570000
8.0	233.2242680000	8.7527660000
10.0	315.4219170000	12.9339850000
12.0	376.8902410000	21.8597250000
14.0	399.8891570000	25.5428280000
16.0	387.0119490000	20.9442310000
18.0	356.5317490000	12.5876820000
20.0	326.6843830000	6.8791880000
22.0	302.6618980000	6.2435980000
24.0	276.4752350000	8.1470650000
26.0	237.8112080000	8.7226950000
28.0	185.0585830000	6.6561140000
30.0	127.2670530000	3.7119870000
32.0	77.0256960000	2.2149730000
34.0	41.8296300000	2.6105670000
36.0	21.1335870000	3.4568740000
38.0	9.8636300000	3.3012100000
40.0	3.6124560000	2.1427330000
42.0	0.7769240000	1.0893610000
44.0	1.0962180000	0.9472980000
46.0	3.5016240000	1.4282950000
48.0	5.8705670000	1.6772170000
50.0	6.5083970000	1.2970590000

The cross section at 18 microradians in the horizontal direction is $356 \times 4\pi \times 10000 = 44.7$ million sq meters. In the table the maximum cross section occurs at 14 microradians.

However, increasing the dihedral angle offset does not increase the cross section at 18 microradians. It decreases all the values.

To obtain a cross section of 1 billion sq meters requires 22 cube corners. The area of one cube corner is 20.27 sq cm. The total area is 446 sq cm. The volume of one cube is 11.92 cc. The mass using aluminum is 32.2 g/cube. The total mass is 708 grams.

F. Summary

The table below gives a summary of options for achieving a cross section of 1 billion sq meters at geosynchronous altitude.

Design	# of cubes	Diam. In.	Area sq cm	Mass g
Uncoated	165	1.7	2415	7457
Coated	1153	.7	2863	3638
Hollow	1153	.7	2863	1590
Hollow	122	1.8	2003	2863
Single dihedral	22	2.0	446	708

The area and mass listed are for the cube corners only. The total area and mass will depend on the type of mounting. For GPS 35,36, the area of the cubes is 44% of the total and the mass of the cubes is 28% of the total.

Late breaking news

Reinhart Neubert has suggested using a Zerodur plate with a dielectric reflector instead of a Beryllium plate with a silver coating. The advantage is that the dielectric materials have a low solar absorptivity and high thermal emissivity to keep the reflector cool, and a low thermal expansion coefficient to minimize thermal distortion of the plates.

The dielectric is a polarizing reflector that will change the diffraction pattern. The effect is similar to the polarization changes caused by total internal reflection in uncoated cubes. This may spread the beam somewhat but might allow larger cubes to be manufactured. It would simplify the thermal design. There is currently no model for computing the cross section. It could probably be estimated using the model for an uncoated cube.

Comments from Reinhart Neubert:

1. Yes, I mean Zerodur. It can be produced with near zero expansion at a given temperature. Unfortunately the useful temperature range is small, about 0....50 °C. I am going to get more precise information from Schott Inc., what is technically possible.
2. Dielectric coatings are used for laser mirrors because of its low loss. This are multiple layers of about $\lambda/2$ thickness with alternating index of

refraction. Usually they have high reflection in a limited wavelength band, but broad band systems are possible also. I am not sure that they can be optimized for all possible lasers, but surely they can be optimized for a fundamental and its second harmonic (for instance 850/425 nm).

3. The flatness of the dielectric mirrors is no problem.

4. Dielectric mirrors are of course polarizing. This has to be considered. In addition they depend on the angle of incidence. But for high satellites the angle does not vary so much.

5. The designers of multi layer dielectric coatings have software to compute the properties. This software is used to tailor the system to the customers needs. The reflection properties have to be tested of course.

6. Yes, I expect the thermal emissivity of Zerodur to be similar to glass.

7. The accuracy requirements for future GPS and GALILEO satellites you should discuss in Vienna with the Geodesists. The main data source for the orbit is the surely the radio system itself (the ground based receiver network). However the laser measurements are welcome to validate the orbit. I am quite sure that for future applications laser measurements on the cm level will be useful for certain applications of the navigation systems.

8. I am not up to date informed what is technically possible in the field of thin layers. But I am sure that $\lambda/10$ for a 2 inch mirror is no problem. There are high quality Fabry Perot etalons available with this useful diameter. I'll ask the experts. Broad band mirrors are widely used for dye lasers. The number of layers for such mirrors is high (more than 20 layers).

9. Another option is a silver coating with additional dielectric layers to increase the reflectivity to 99 per cent or more. We are using such mirrors in our laser telescope. But the dielectric only would be of course fine.

Galileo

Design	# of cubes	Diam. in	Area sq cm	Mass g
uncoated	50	1.3	428	1000
coated	400	0.5	508	460
hollow	400	0.5	508	201
hollow	36	1.4	356	400
GPS	160	1.06	1008	1760

Geosynchronous

Design	# of cubes	Diam. In.	Area sq cm	Mass g
Uncoated	165	1.7	2415	7457
Coated	1153	.7	2863	3638
Hollow	1153	.7	2863	1590
Hollow	122	1.8	2003	2863
Single dihedral	22	2.0	446	708

Wavelength correction for LAGEOS 850nm-425nm

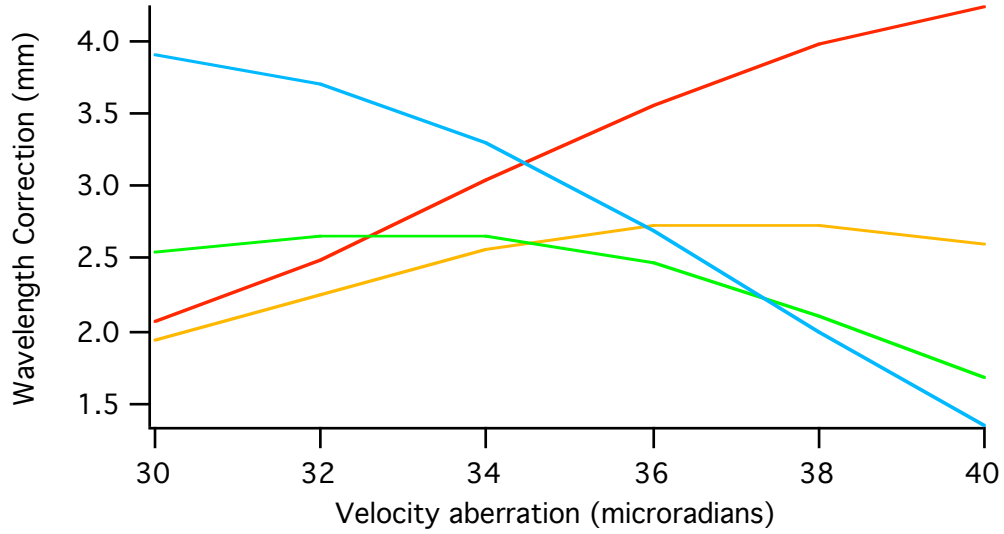


Figure 1. Wavelength correction vs velocity aberration for four dihedral angle offsets.

Curve Dihedral (arcseconds)

Red	1.00
Orange	1.25
Green	1.50
Blue	1.75

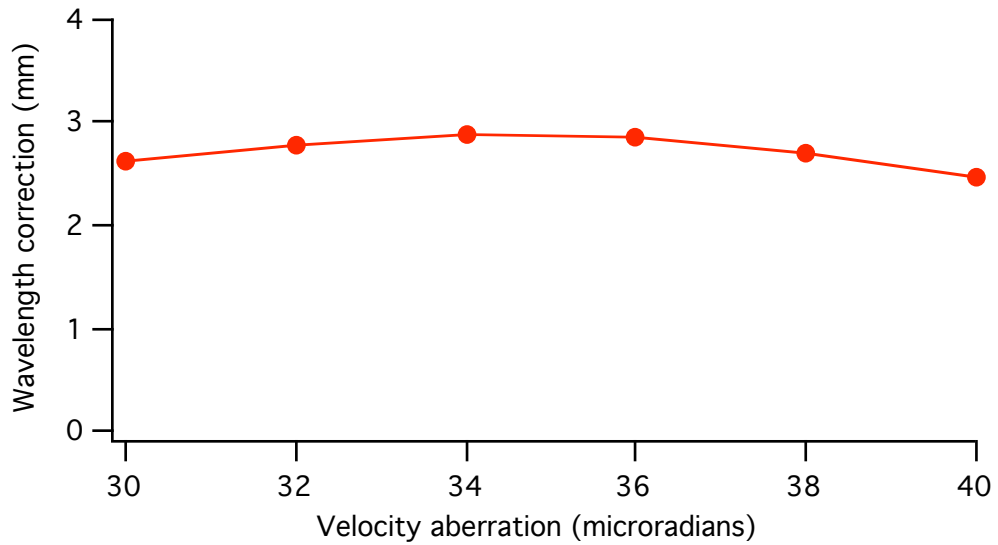


Figure 2. Wavelength correction vs velocity aberration averaged over four dihedral angle offsets.

Microradians	1.00	1.25	1.50	1.75
30.000000	2.064000	1.944000	2.537000	3.915000
32.000000	2.494000	2.249000	2.648000	3.703000
34.000000	3.035000	2.560000	2.664000	3.308000
36.000000	3.568000	2.735000	2.467000	2.691000
38.000000	3.978000	2.725000	2.098000	1.984000
40.000000	4.242000	2.592000	1.683000	1.346000

Table 1. Data used to plot Figure 1. in millimeters. The dihedral angle is listed in arcseconds above each column.

30	32	34	36	38	40
2.615000	2.773500	2.891750	2.865250	2.696250	2.465750

Table 2. Data used to plot the average wavelength correction (mm) in Figure 2. The velocity aberration in microradians is listed above each entry.

The average wavelength correction between 32 and 38 microradians is 2.806 mm +/- .2 mm.

The range bias is the result of three physical effects.

A. Diffraction

The diffraction pattern is different at each wavelength. As a result the contribution of each retroreflector is different at each wavelength. This results in a variation of a few millimeters in the range bias at different parts of the diffraction pattern. If the dihedral angle offset is optimized for the velocity aberration the average effect of diffraction is minimized. In the tables, the range bias is smallest at around 1.5 arcsec and increases for larger or smaller dihedral angle offsets.

B. Refraction

In a solid cube corner the light is bent into the cube corner by refraction at the front face of the cube. The refraction depends on the phase velocity V_p . The phase index of refraction is $N_p = c/V_p$. A larger N_p increases the acceptance angle of the cube corner and gives larger signal for cubes at large incidence angles. For a circular array the effect is that the centroid closer to the center of the array for larger N_p . This makes the range correction smaller.

C. Group velocity

The optical path length depends on the group velocity V_g of the light in the quartz. The group index of refraction is $N_g = c/V_g$.

wavelength	phase index	group index
0.355	1.476	1.533
0.4235	1.468	1.508
0.532	1.461	1.484
0.85	1.452	1.465
1.064	1.450	1.462

Table 3. N_p and N_g vs wavelengths (microns) provided by Stefan Riepl.

Dihedral Angle	Diffraction	Refraction	Group Vel.	Total
0.75	2.46	0.98	1.23	4.67
1.50	0.29	0.94	1.23	2.46

Table 4. The contribution to the range bias (mm) from each of the three physical effects.

The values in Table 4 are the average for velocity aberration 32, 34, 36, and 38 microradians. The contributions from Refraction and Group Velocity do not change much as the dihedral angle offset changes. The changes are due almost entirely to diffraction effects.

Simulations for LAGEOS with various dihedral angle offsets give the following range bias (850nm-425nm). The wavelength correction is most stable if the dihedral angle is optimized for the particular velocity aberration.

Dihedral Angle (arcsec)	Range Bias (mm)
0.00	13.18
0.25	10.91
0.50	7.23
0.75	4.67
1.00	3.24
1.25	2.56
1.50	2.46
1.75	2.92
2.00	4.52
2.25	6.66

2.50 10.18

Table 5. Wavelength correction (mm) vs dihedral angle offset (arcseconds)

The data in this report are based on simulations at a large number of orientations of the satellite. Data points were at 2 deg intervals in longitude at the equator with fewer points near the poles. The points were on and between each row of cube corners in latitude. At each orientation simulations were done for both wavelengths and 4 different dihedral angle offsets. About 19000 simulations were averaged to obtain the final results.

Summary. The average wavelength correction between 32 and 38 microradians is 2.806 mm +/- .2 mm.

SLR2000 Retro-Reflector Requirements

- Assumptions:
 - New 30% QE PMT.
 - 40 microrad divergence.
 - atmospheric transmission of 0.5 at zenith.
 - 60 microJoules / pulse out of telescope.
- Want 10 pes/sec for LEO, 6 for LAGEOS, and 3 for GPS/GEO.

Lidar Cross Section in M sq. meters	Marginal ≥ 30 deg night	Better ≥ 30 deg day	Best ≥ 20 deg day	Current Value
LEO (1000 km)			≥ 0.03	STELLA=0.65
LAGEOS (6000 km)			≥ 5	LAGEOS=7
HEO (20,000 km)	17	35	≥140	GPS=19
GEO (36,000 km)	150	300	≥1200	N/A

- MOBILAS systems average 100 returns / normal point (out of 1500 possible returns) for GPS-35/36. Twilight and night. Implies GPS retros are marginal.

SLR2000 return signal strength from GPS

$E := 0.000060$	laser energy (out of telescope) in Joules (eyesafe limit)
$\eta := 0.3$	receiver Q.E. (current QE=0.12, new detector QE=0.30)
$h\nu := 3.73 \cdot 10^{-19}$	conversion Joules to photons
$\theta_t := 20 \cdot 10^{-6}$	laser divergence (radians)
$a_e := 6378 \cdot 10^3$	radius of earth (meters)
$\tau_z := 0.5$	atmospheric transmission
$\sigma := 19 \cdot 10^6$	lidar cross-section (meters squared)
$A := 0.1256$	area of telescope (meters squared)
$\tau_{sys} := 0.5$	system transmission
$R_z := 20000 \cdot 10^3$	spacecraft altitude (meters)
$\varepsilon_{deg} := 30$	elevation of mount (degrees)

$$\varepsilon_r := \varepsilon_{deg} \cdot \frac{\pi}{180} \quad \theta_2 := \left(\frac{\pi}{2} - \varepsilon_r \right) \quad \theta_1 := \text{asin} \left[\frac{a_e}{(a_e + R_z)} \cdot \sin(\theta_2) \right]$$

$$\tau_a := \tau_z \left(\frac{1}{\sin(\varepsilon_r)} \right) \quad R_e := (a_e + R_z) \cdot \left(\frac{\sin(\theta_2 - \theta_1)}{\sin(\theta_2)} \right)$$

$$\tau_a = 0.25 \quad R_e = 2.2604 \times 10^7$$

$$n_s := \eta \cdot \left(\frac{E}{h\nu} \right) \cdot \tau_{sys} \cdot \tau_a^2 \cdot \left(\frac{\sigma}{2 \cdot \pi \cdot \theta_t^2 \cdot R_e^2} \right) \cdot \left(\frac{A}{\pi \cdot R_e^2} \right) \cdot 0.5$$

received photoelectrons

$$n_s = 8.7293 \times 10^{-4}$$

expected returns per second

$$n_r := n_s \cdot 2000$$

$$n_r = 1.7459$$

SLR2000 Noise Calculations

$$N := 2 \cdot 10^9 \quad \text{solar irradiance (watts/meter}^2\text{): 532nm}$$

$$\theta_r := 25 \cdot 10^{-6} \quad \text{S2K receiver FOV (radians) - half angle}$$

$$\Delta\lambda := 4 \cdot 10^{-10} \quad \text{S2K optical bandpass filter (meters)}$$

$$bw := 1 \cdot 10^{-9} \quad \text{bin width (sec) - range histogram for signal processing}$$

$$N_{bs} := \left(\frac{\eta}{4hv} \right) \cdot N \cdot \Delta\lambda \cdot A \cdot \tau_z \cdot \tau_{sys} \cdot \theta_r^2 \quad \text{worst case noise due to sun thru local atmosphere}$$

$$N_{bs} = 3.1568 \times 10^6 \quad \text{solar photons per second from sky background}$$

Noise counts per range histogram bin per fire:

$$N_{bs} \cdot bw = 0.0032$$

SIGNAL

$$n_s = 8.7293 \times 10^{-4}$$

$$\Delta t := \frac{9 \cdot N_{bs} \cdot bw}{n_s^2 \cdot 2000}$$

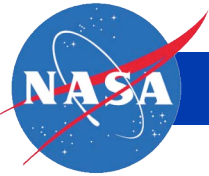
seconds to resolve signal from noise background: day

$$\Delta t = 18.6425$$

seconds to resolve signal: night

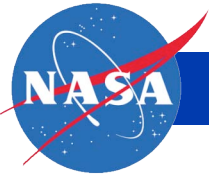
$$\Delta t := \frac{10}{n_r}$$

$$\Delta t = 5.7278$$



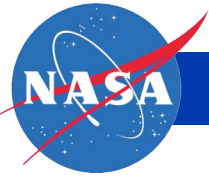
Excerpts from Mike Moreau's presentation

- **Through participation in GPS III Phase A program, NASA raised concern that there was no requirement to maintain the current laser ranging capability on GPS beyond the two reflector arrays (on 35,36).**
- **NASA prepared briefing citing technical justifications and rationale for flying laser retro-reflectors on subset of future GPS satellites**
 - **Presented at NASA/JPO "Space Day" June 2005 & IFOR August 2005**
- **There is broad (moral) support from across civil and DoD agencies**
 - **Generally considered the "smart thing to do"**
 - **...but, there are no existing positioning or timing requirements in GPS III that explicitly require a laser ranging capability**
- **Difficult to justify flying retro-reflectors based on requirements – benefits are mostly in-direct and for specialized applications**
- **Air Force has raised some specific technical concerns regarding impacts to the spacecraft**



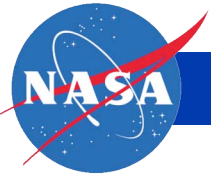
Recommended way forward

- **Work with the JPO to arrange a forum for the discussion of their technical concerns/risks**
 - **NASA will bring information on current and future laser ranging operations (wavelengths, intensities, duty cycles)**
 - **Air Force will bring information on specific technical concerns, as well as operational experiences with SV 35, 36**
- **Work with AFSPC/DRN to formally document the rationale, benefits, and costs of including laser retro-reflectors on future GPS satellites.**
- **Develop the recommended implementation approach**
 - **How many GPS satellites will fly the arrays**
 - **Selection of array (glass or beryllium), plan for procurement, testing, etc. Leverage existing testing being done by NASA.**
 - **Which agency will manage effort**



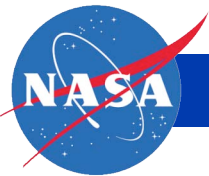
Top 10 Reasons GPS Should Carry Laser Retro-reflectors

10. To help validate improvements to orbit determination and overall performance
 - It is the only independent way to assess actual orbit accuracy; GPS-based approaches such as orbit overlap, formal errors, and user positioning can be useful, but they are circular to some extent
9. To improve our understanding of satellite dynamics and kinematics (such as antenna phase patterns); allowing us to test and improve new models, and advance the state of the art in satellites modeling; Particularly important for new satellites (IIF, III)
8. To help understand the GPS error budget, and in particular, separate radial orbit errors from clock errors
7. To help tie GPS to the terrestrial reference frame (which SLR significantly influences)
6. To help tie GPS reference frame to other GNSS (Galileo) carrying retro-reflectors
5. To validate compliance with the challenging performance Specs for Block III (e.g., decimeter-level URE), while the spacecrafts get harder to model
4. To avoid the appearance of Galileo as a technologically superior GNSS
3. To facilitate future utility of GPS for advanced science and civil applications consistent with its dual-use mandate, and to avoid actually lagging in performance behind Galileo
2. To get NASA and science community to stop harassing Air Force about this
1. Because we do not yet understand the large biases between SLR-based and GPS-based ranges



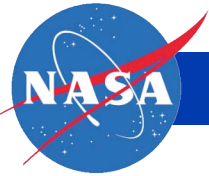
Future of Satellite Laser Ranging of GPS Spacecraft

Mike Moreau
2 March 2006



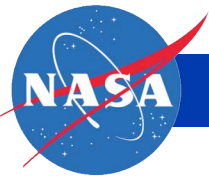
Background

- Through participation in GPS III Phase A program, NASA raised concern that there was no requirement to maintain the current laser ranging capability on GPS beyond the two reflector arrays flying on SV 35,36
- NASA prepared briefing citing technical justifications and rationale for flying laser retro-reflectors on subset of future GPS satellites
 - Presented at NASA/JPO “Space Day” June 2005
 - Presented at IFOR Meeting, Aug 2005



Background (continued)

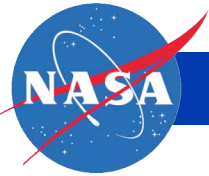
- There is broad (moral) support from across civil and DoD agencies
 - Generally considered the “smart thing to do”
- ...but, there are no existing positioning or timing requirements in GPS III that explicitly require a laser ranging capability
 - Both phase A contractors indicated they did NOT require independent, on-orbit validation of URE performance (ie laser ranging) in order to prove they can meet 20 cm URE requirement
 - Current antenna phase center location uncertainties are significant fraction of 20 cm
- Difficult to justify flying retro-reflectors based on requirements – benefits are mostly in-direct and for specialized applications



Recent Activities

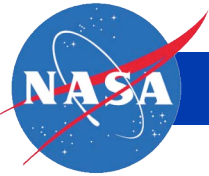
- GSFC (led by Jan McGarry) has been studying the performance of the new hollow beryllium cubes
 - Includes thermal testing and performance simulation
 - This work will help to validate these new arrays for use in space
 - Could do more with additional funding
- Carroll Alley (a key player in getting the laser reflector arrays on SV 35, 36) has possession of a third array and has expressed interest in donating it, if it furthers the cause
- Several recent inquiries as to the status of the laser ranging issue from stakeholders at Aerospace, Air Force, NGA, NASA...





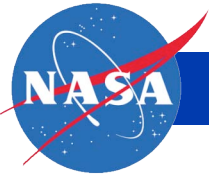
Potential Roadblocks

- Air Force has raised some specific technical concerns regarding impacts to the spacecraft
- Recommended way forward:
 - Setup a meeting via an appropriate forum to discuss specific concerns
 - NASA will bring information on current and future laser ranging operations (wavelengths, intensities, duty cycles)
 - Air Force will bring information on specific technical concerns, as well as operational experiences with SV 35, 36



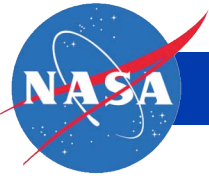
Potential Roadblocks (cont.)

- Source of Funding
 - Costs to procure and test retro-reflector arrays
 - Recent estimates for single array range from roughly \$100K to \$250K
 - Fidelity of these estimates is unclear
 - Cost impacts to spacecraft integration and testing
 - Impacts should be minor for GPS III if adopted now
 - Costs for IIR-M or IIF could be more significant
 - Costs associated with the actual operation of the SLR network to collect and process data
- Way forward:
 - Is there a way to leverage funding across agencies?



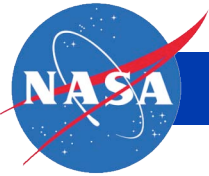
Potential Roadblocks (cont)

- Difficult to justify simply based on position, navigation, or timing requirements
 - Benefits wide range of users, no single stakeholder...
- Way forward:
 - Need to work with AFSPC/DRN to document rationale/benefits/stakeholders
 - Conform to formal requirements process (IFOR)
 - NASA has “taken up the cause”, but process to work this issue is not clear
 - Perhaps this would be a good issue for the NPCO to take on...



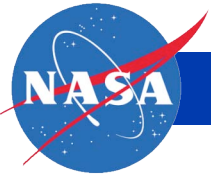
Partial List of Stakeholders

- Bill Feess, Aerospace/JPO
- Clyde Edgar, Aerospace/JPO
- Geoff Harris, Aerospace/JPO
- Col. Mark Crews, JPO
- Tom Powell, Aerospace/JPL
- Aaron Trask, NRL
- Frank Mueller, NGA
- Carroll Alley, U of Maryland
- Jim Slater, NGA
- Barbara Wiley, NGA
- Tom Creel, NGA/JPO
- Randall Taylor, NGA
- Everett Swift, NSWCCD/NGA
- Mike Pearlman, Harvard
- Gerald Mader, NOAA
- Larry Hothem, USGS
- Yoaz Bar-Sever, JPL
- Ruth Neilen, JPL
- John LaBrecque, NASA
- Jan McGarry, NASA
- David Carter, NASA
- *Partial listing of individuals who have either expressed support for this issue or have participated in meetings where this topic was discussed...*
- *Expect an actual list of the stakeholders would be much larger, touching on most civil and military agencies*
- *Use GSEF forum to develop more extensive stakeholders list*



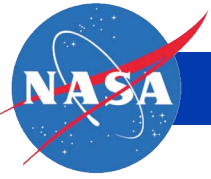
Proposed Way Forward – Some Recommendations

- Develop list of stakeholders and develop consensus position on issue across agencies
 - Engage GSEF, NPCO?
- Work with the JPO to arrange a forum for the discussion of their technical concerns/risks
- Work with AFSPC/DRN to formally document the rationale, benefits, and costs of including laser retro-reflectors on future GPS satellites.
- Develop the recommended implementation approach
 - How many GPS satellites will fly the arrays, which satellites (IIR-M, IIF, III)
 - Selection of array (glass or beryllium), plan for procurement, testing, etc. Leverage existing testing being done by NASA.
 - Which agency will manage effort

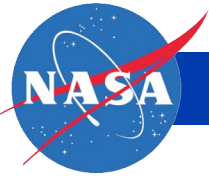


Parting Thought

- Why was this a no-brainer for Galileo and Glonass?

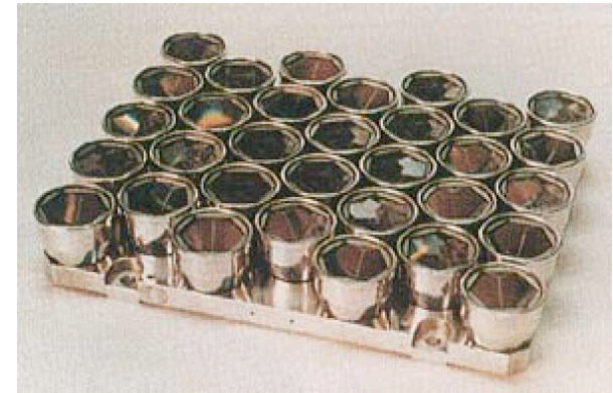


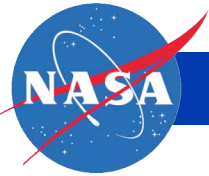
Background Information



Current Reflector Technology

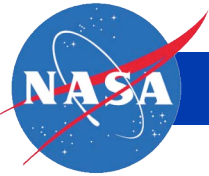
- **Retro-reflectors flown on existing GPS satellites (SV 35,36)**
 - Made of fused silica with aluminum coating on the reflecting surfaces
 - Array consists of 32 cubes each ~ 1" in diameter
 - 1.27 kg
 - Produces a lidar cross section of about 20 million square meters (inadequate for tracking by many laser ranging stations)
 - Supplier a Russian company, IPIE
- **Same company supplies arrays flown on GLONASS satellites**
- **74 cube array of the same kind flown on the Surrey Galileo prototype satellite**
- **SVs 35, 36 nearing end of life; GPS will lose SLR capability in the near future!**
- ***Carroll Alley of the University of Maryland has a third array that could be used for testing or flown***





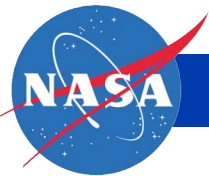
Beryllium Hollow Cube Technology

- Very light-weight, with substantial increases in lidar cross section
- Likely some NRE costs for performance testing/validation
- Array consisting of twenty 2" cubes, including holder:
 - 800 grams
 - ~0.5 to 1 billion square meters lidar cross section
 - Comparable in size to existing arrays
 - Performance gain of 25X versus current GPS satellites, on par with LAGEOS
- Potential vendor PLX Inc., www.plxinc.com



Top 10 Reasons GPS Should Carry Laser Retro-reflectors

10. To help validate improvements to orbit determination and overall performance
 - It is the only independent way to assess actual orbit accuracy; GPS-based approaches such as orbit overlap, formal errors, and user positioning can be useful, but they are circular to some extent
9. To improve our understanding of satellite dynamics and kinematics (such as antenna phase patterns); allowing us to test and improve new models, and advance the state of the art in satellites modeling; Particularly important for new satellites (IIF, III)
8. To help understand the GPS error budget, and in particular, separate radial orbit errors from clock errors
7. To help tie GPS to the terrestrial reference frame (which SLR significantly influences)
6. To help tie GPS reference frame to other GNSS (Galileo) carrying retro-reflectors
5. To validate compliance with the challenging performance Specs for Block III (e.g., decimeter-level URE), while the spacecrafts get harder to model
4. To avoid the appearance of Galileo as a technologically superior GNSS
3. To facilitate future utility of GPS for advanced science and civil applications consistent with its dual-use mandate, and to avoid actually lagging in performance behind Galileo
2. To get NASA and science community to stop harassing Air Force about this



Top Reason why GPS Should Carry Laser Retro-reflectors

1. Because we do not yet understand the large biases between SLR-based and GPS-based ranges

SLR Measured Range - GPS Computed Range

Overall statistics from GPS weeks 1147 through 1324

From JPL's weekly analysis of SLR residuals http://gipsy.jpl.nasa.gov/gps_slr/

Center	Number of Points	Mean (mm)	RMS (mm)	STD (mm)
IGR	5519	-55.5	60.3	23.7
IGS	5475	-53.9	59.1	24.2
COD	5390	-67.8	72.9	26.7
JPL	5283	-47.5	54.6	27.0
GFZ	5354	-59.7	65.7	27.4
EMR	5431	-47.1	55.3	29.0
MIT	3637	-35.4	50.3	35.8
NGS	5322	-47.7	59.8	36.1
SIO	5304	-36.0	53.8	40.0
ESA	1904	-53.3	66.8	40.3

Center	Number of Points	Mean (mm)	RMS (mm)	STD (mm)
IGR	5532	-55.9	60.8	23.9
JPL	5169	-50.8	56.2	24.1
IGS	5523	-52.4	58.2	25.2
COD	5334	-72.5	77.5	27.5
GFZ	5311	-64.7	70.9	28.9
EMR	5449	-49.2	57.2	29.1
NGS	5222	-40.3	54.0	35.9
MIT	3855	-11.4	39.5	37.9
ESA	1827	-55.7	67.8	38.6
SIO	5238	11.8	51.3	50.0

Hollow Cube Study at GSFC – Status April 2006

- Mechanical simulations show good performance of cubes through thermal gradients and thermal changes up to 80 deg.C. Real issue is integrity of cube.
- Recent thermal studies show range of temperatures for cubes to be ~ 48 to 63 deg.C if cubes can radiate off back (up to 145 deg.C if not).
- ProSystems has design (being patented) for bolted cube which we believe will be able to survive thermal changes. They have built us a 2.5” cube and will be testing it shortly in thermal chamber. Will provide wavefront error, beam deviation and far field patterns at room temperature, 60 deg.C and 150 deg.C.
- Unfortunately ProSystems can no longer sell retro-reflectors (litigation with PLX) so we will have to go through PLX if we want to purchase.
- Simulations will then be performed: (1) using recent thermal analysis in simulations, (2) comparing simulations to ProSystems tests.



Beryllium Hollow Cube Retroreflector

Thermal Distortion Analysis

C. Powell/542

T. Carnahan/542

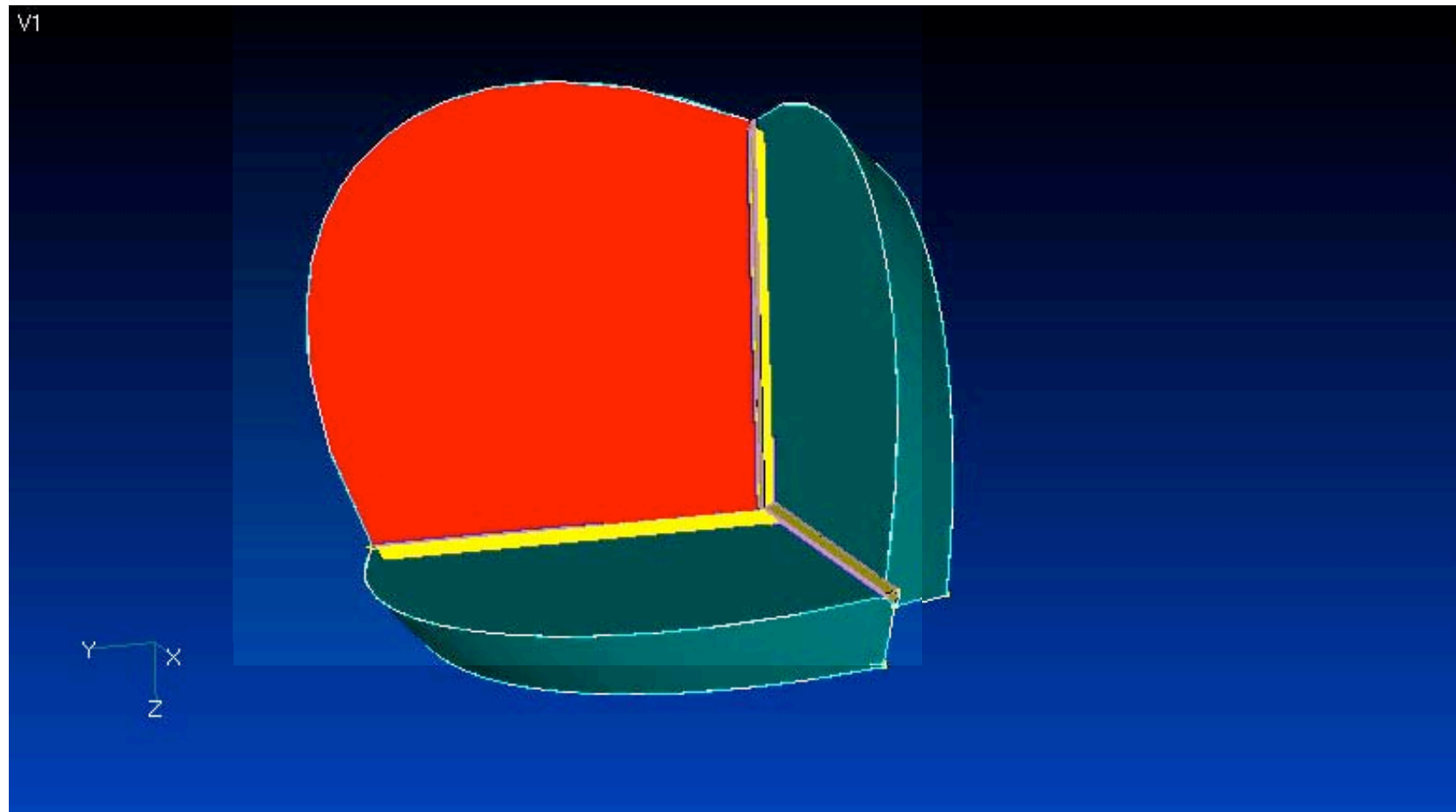
S. Irish/542

A. Morell/544



Retroreflector

Materials: Beryllium Plates Stycast 2850 Bonding (.05" thick)



Material Properties Used in Analysis



Beryllium:

- Young's Modulus - $40E+6$ psi
- Poisson's Ratio - .1
- Density - $.067$ lb/in³
- CTE - $11.2E-6$ /°C
- Yield Strength - 10,000 psi

Stycast 2850:

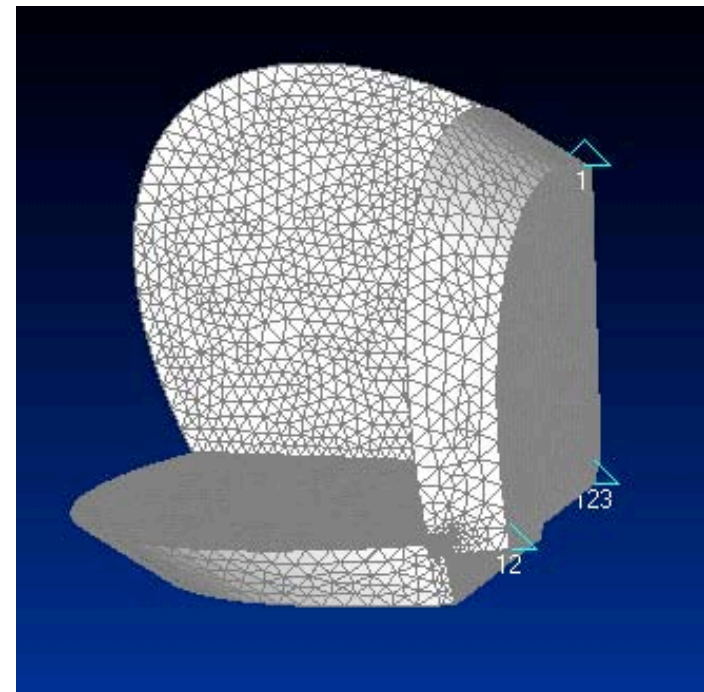
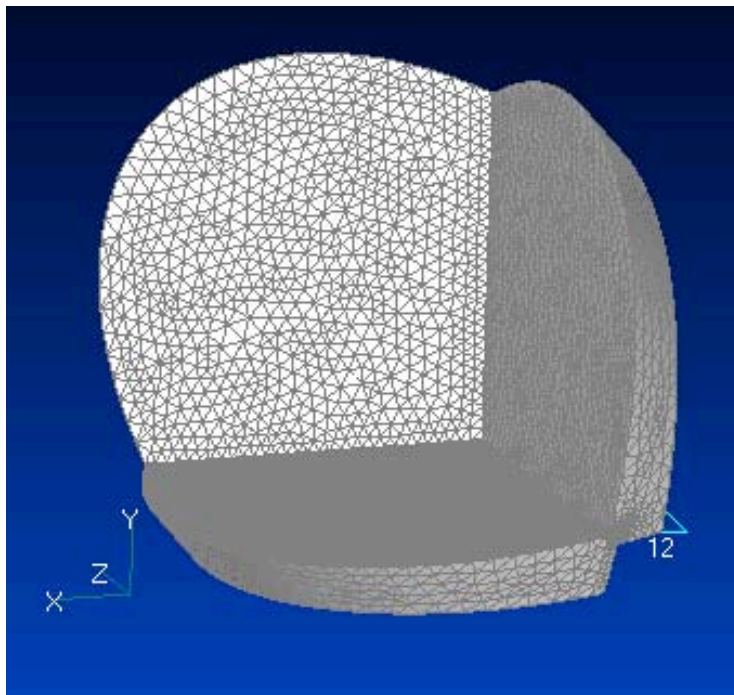
- Young's Modulus - $4.0E+6$ psi
- Poisson's Ratio - .3
- Density - $.087$ lb/in³
- CTE - $3.5E-5$ /°C
- Yield Strength - 5100 psi (lowest of possible values)*

*Various material sources have indicated a yield strength range from 5100 psi to 8400 psi.

Structural Model



Kinemetically mounted on Beryllium plate lying in Y Z plane



Blue triangles represent location of constraint. 1, 2, and 3 represent being fixed in the x, y, and z directions respectively.



1 °C Bulk Temperature Change for pure Be FEM and a FEM with Stycast bonding

- A FEM made up of entirely Be will expand without any surface distortion.
- Change temperature of both FEM from 20 °C to 21 °C. Compare both models' deflections.
- Purpose: Determine the distortion caused by the CTE mismatch in Beryllium and Stycast. Determine the maximum stress value and location in Stycast in order to see whether a 80 °C temperature increase is feasible.

Types of Temperature Loads Performed in Analysis Cont.



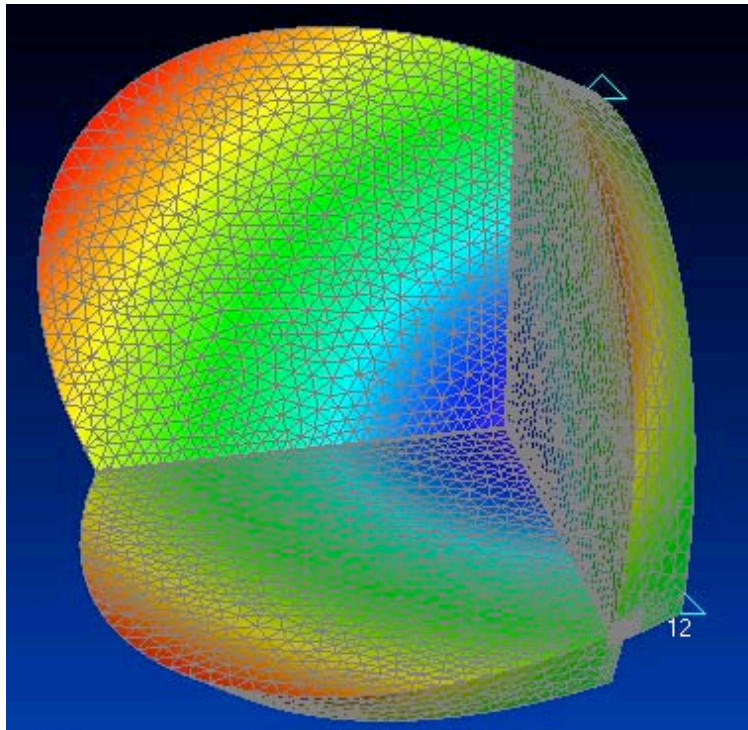
1 °C Temperature Gradient in X, Y, and Z Directions for a pure Be FEM and a FEM with Stycast bonding

- Apply a 1 °C linear temperature gradient load along x, y, and z directions for both models. Compare both models' deflections.
- Purpose: Determine the difference in deflections between a FEM made of only Be versus a FEM with Stycast bonding. Determine maximum stress quantity and location in Stycast in order to determine the maximum temperature gradient through the retroreflector.

1 °C Bulk Temperature Analysis Results



Contour Plot of Maximum Deflections



Contour map applies for FEM with and without Stycast bonding. Keys are defined for each case.

With Stycast

- .559 μm
- .526 μm
- .490 μm
- .454 μm
- .419 μm
- .384 μm
- .351 μm
- .315 μm
- .279 μm
- .245 μm
- .210 μm
- .175 μm
- .140 μm
- .106 μm
- .070 μm
- .035 μm
- 0

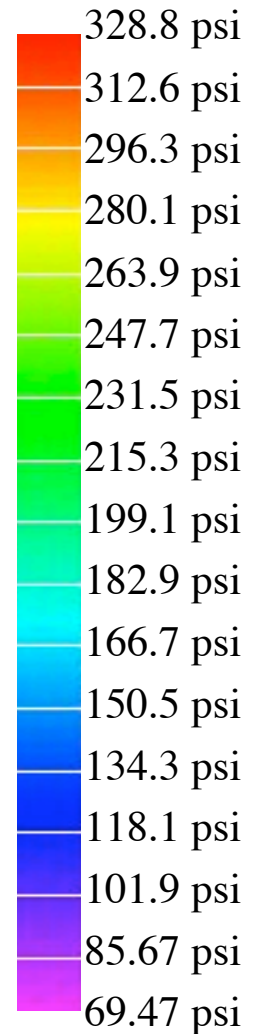
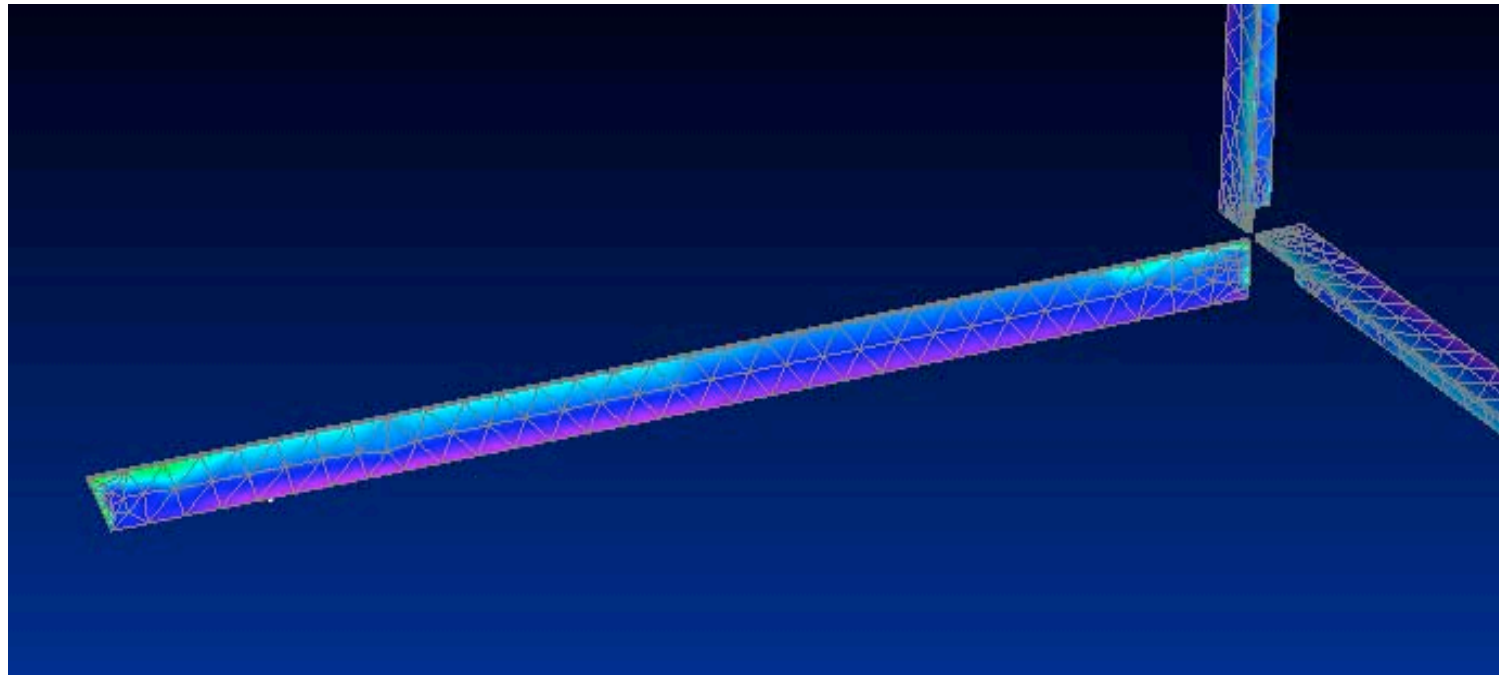
Pure Beryllium

- .556 μm
- .521 μm
- .488 μm
- .452 μm
- .417 μm
- .383 μm
- .348 μm
- .312 μm
- .277 μm
- .243 μm
- .208 μm
- .174 μm
- .139 μm
- .104 μm
- .069 μm
- .035 μm
- 0



1 °C Bulk Temperature Analysis Results Cont.

Contour Plot of Maximum Stresses
Stycast – limiting factor, only Stycast is shown



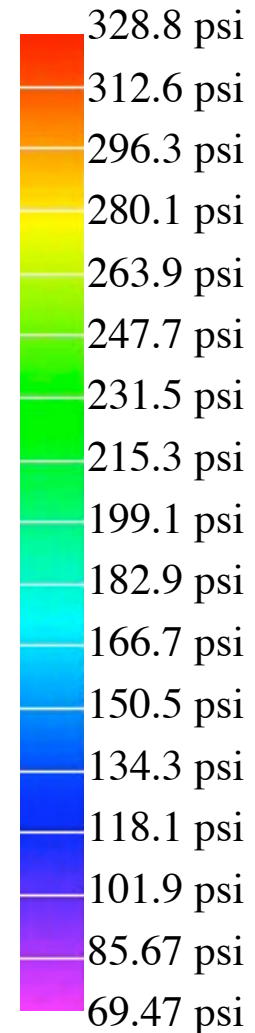
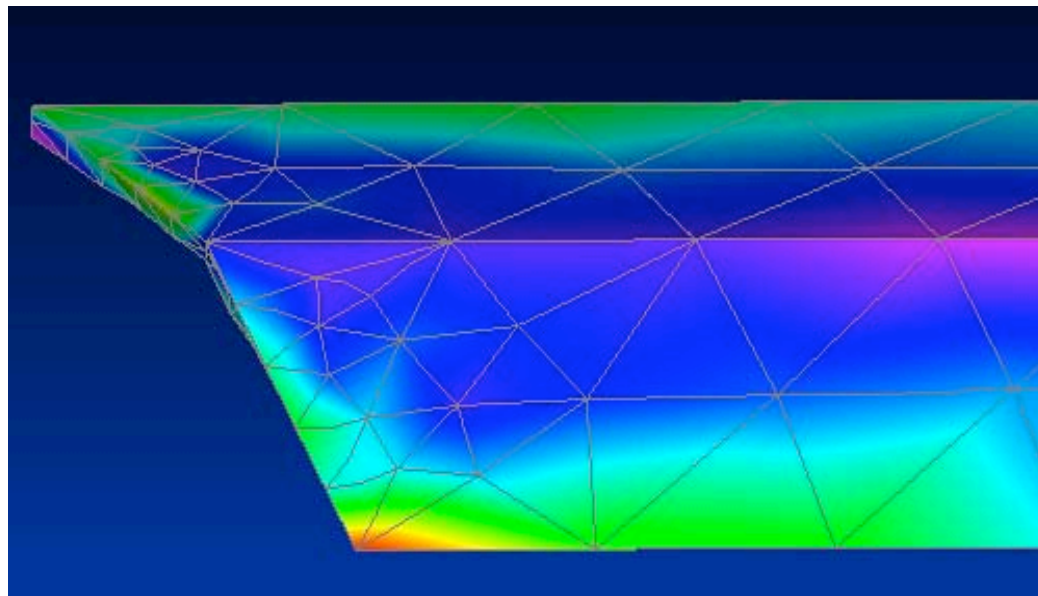


1 °C Bulk Temperature Analysis Results Cont.

Max Stress = 328.8 psi

Using a factor of safety of 2 yields a margin of safety of 6.756 for a 1°C bulk temperature change.

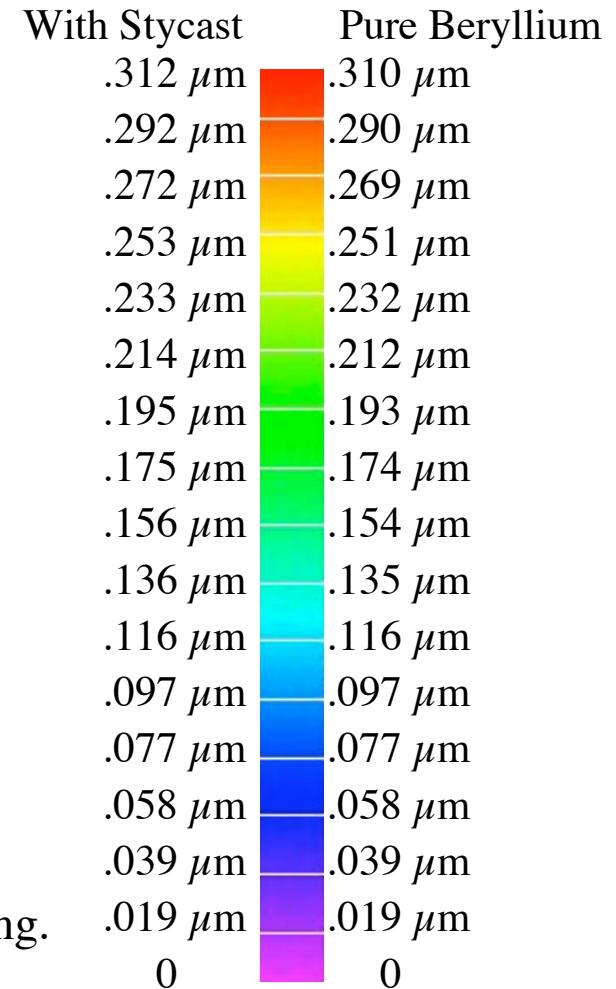
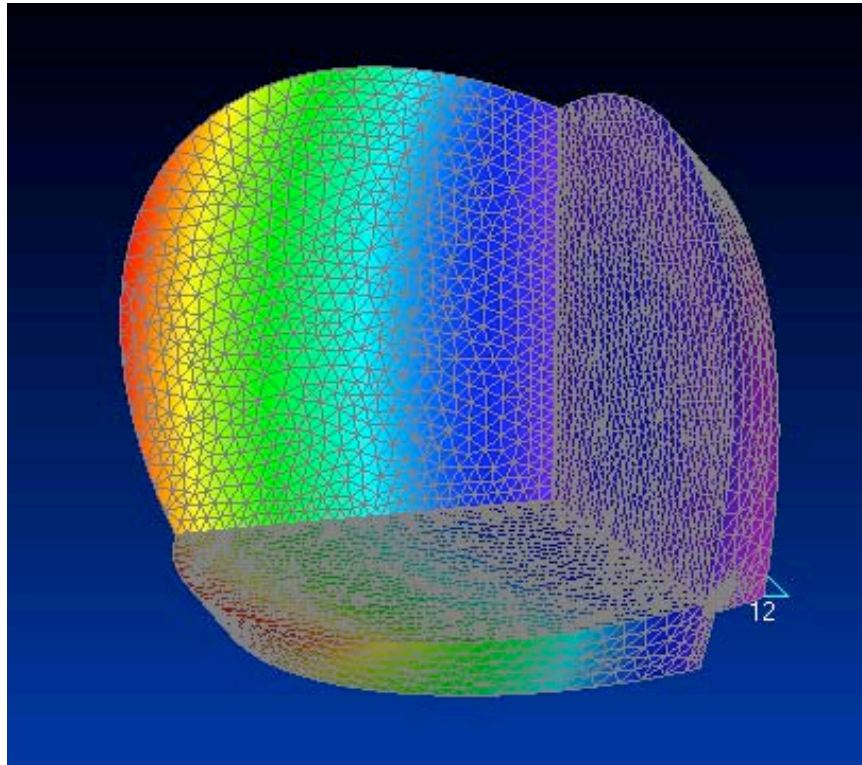
Contour Plot of Maximum Stress in Stycast Bonding





1 °C Linear Temperature Gradient Load in X Direction

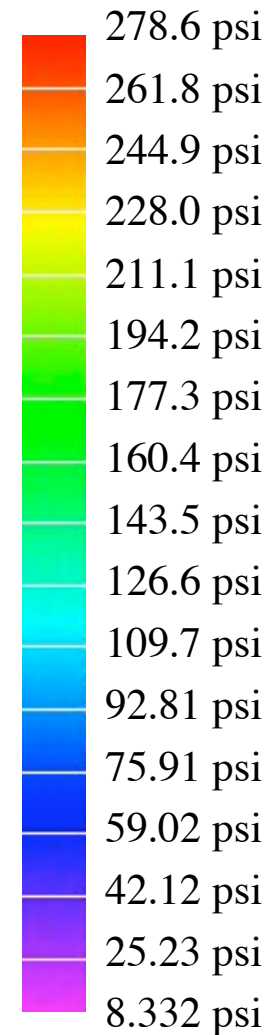
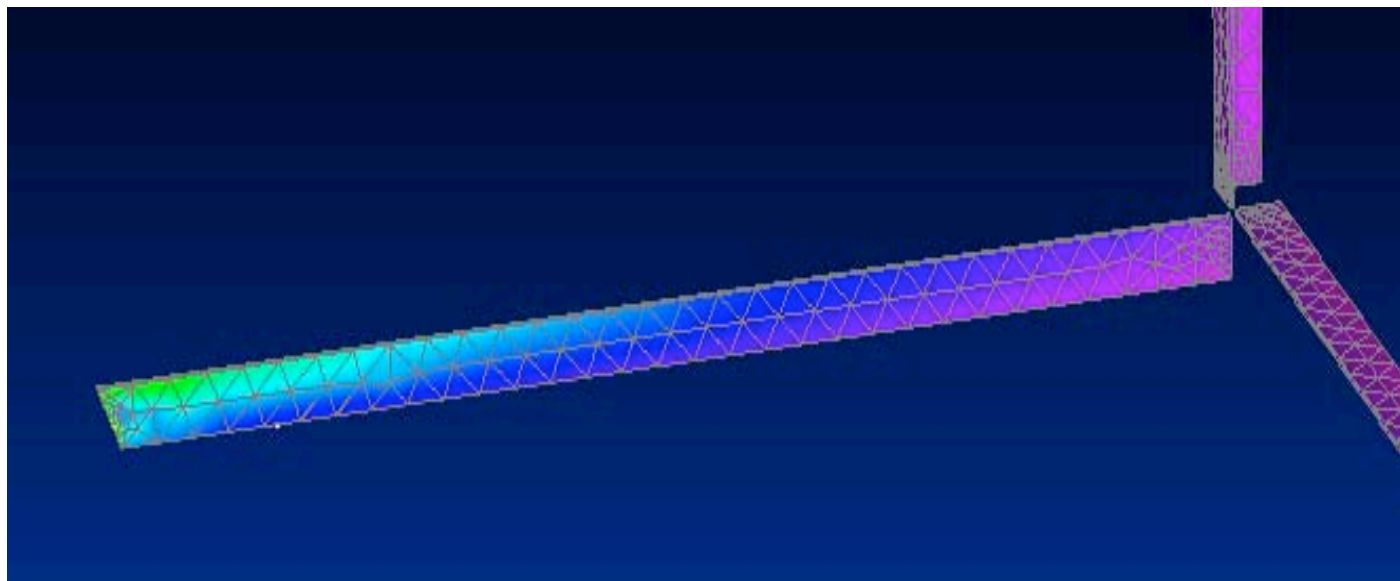
Contour Plot of Displacement due to 1°C Gradient in X Direction



Contour Plot applies for FEM with and without Stycast bonding.



Contour Plot of Maximum Stresses in Stycast Bonding

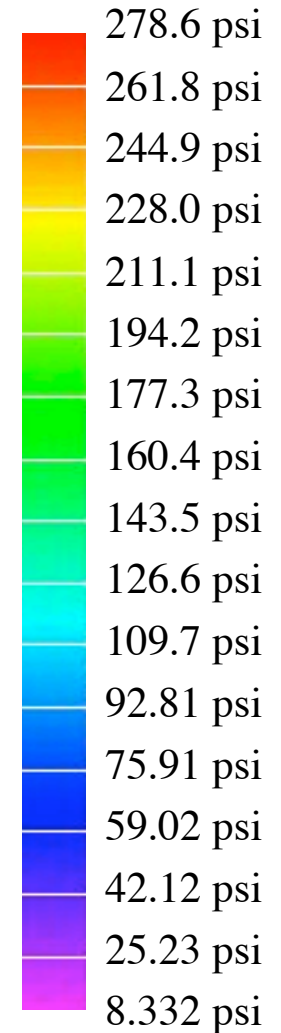
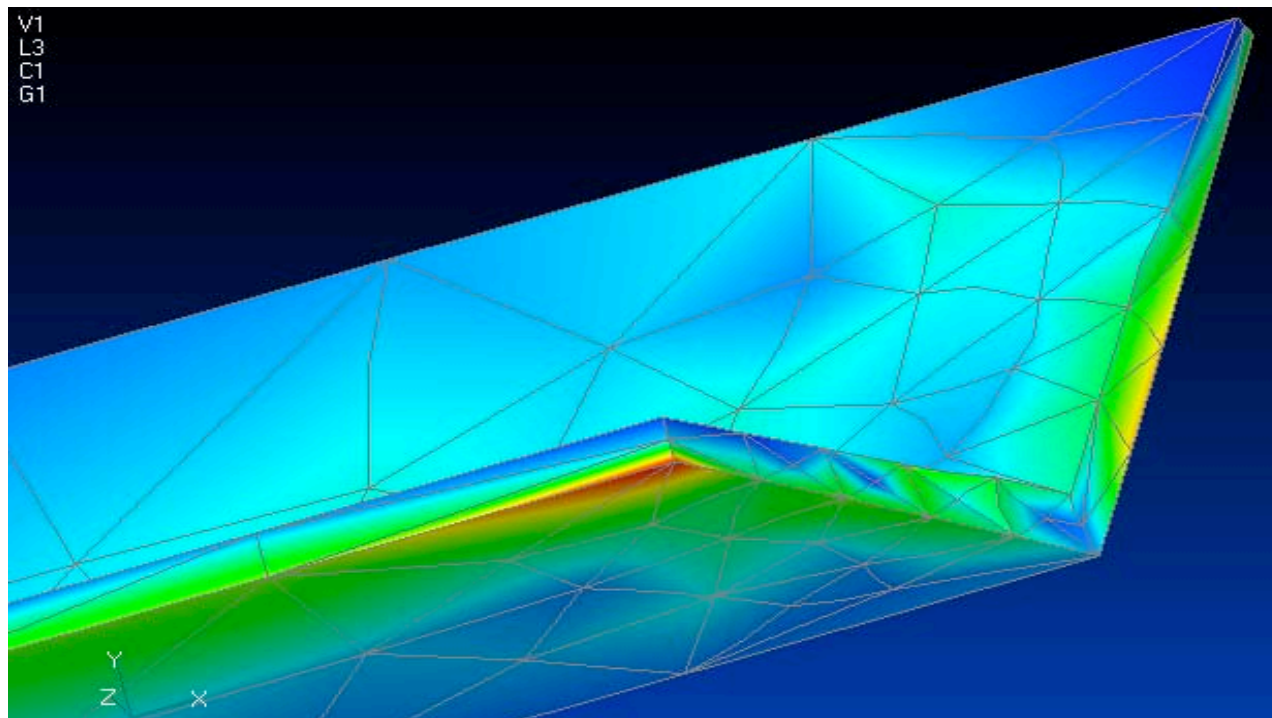


1 °C Linear Temperature Gradient Load in X Direction Cont.



Using a Factor of Safety of 2 yields a Margin of Safety of 8.153 for a 1 °C temperature gradient in the x direction.

Contour Plot of Maximum Stresses in Stycast Bonding





Maximum Deflections

Temp Gradient in Y direction with Stycast - $.396 \mu\text{m}$

Temp Gradient in Y direction without Stycast - $.394 \mu\text{m}$

Temp Gradient in Z direction with Stycast - $.376 \mu\text{m}$

Temp Gradient in Z direction without Stycast - $.374 \mu\text{m}$

Maximum Stress in Stycast Bonding

Temp Gradient in Y direction – 278.7 psi

Temp Gradient in Z direction – 277 psi

Summary of Results (FEM with Stycast only)



1 °C Bulk Temperature Change:

Maximum Distortion due to CTE mismatch in Beryllium and Stycast = $.0051 \mu\text{m}$

1 °C Temperature Gradient in X, Y, and Z directions

Distortion Between Maximums = $.00254, .00508, .00254 \mu\text{m}$ respectively

Conclusion:

Distortion is not a concern when the Beryllium retroreflector with Stycast bonding is subjected to a large temperature increase. Largest delta deflection was found to be $.005 \mu\text{m}$ which meets the requirements of less than $.01 \mu\text{m}$.

Summary of Results (FEM with Stycast only) Cont.



1 °C Bulk Temperature Change:

Using a Factor of Safety equal to 2, margin of safety = 6.756

Maximum Allowable Temperature Change = 7.756 °C

1 °C Temperature Gradient in X, Y, and Z directions

Using a Factor of Safety equal to 2, margin of safety = 8.153, 8.150, and 8.206 respectively

Maximum Allowable Temperature Change = 9.153, 9.150, and 9.206 °C respectively

Conclusion:

The structural analysis indicates that the stress in the Stycast is not able to withstand a 80°C delta temperature increase. However, it is believed that the analysis is conservative using a high factor of safety and a low yield strength. Also, an instrument design developed at GSFC utilized a glass part bonded with Stycast and it was able to withstand a temperature decrease from room temperature to 80K without degradation to the bond. Surface preparation is critical to the strength of bonded joints and the structural analysis is not able to model this effect.

Recommendations and Further Work



- The structural analysis is currently using the most conservative yield strength for Stycast 2850.
 - It is recommended that strength testing be performed to determine the appropriate yield strength of Stycast due to thermal loading. Various surface preparations should be considered.

- The structural analysis is currently assuming that the retroreflector design must be able to withstand a temperature of 100 C (ie, a 80 C delta temperature increase).
 - It is recommended that a thermal analysis be performed to determine the actual temperature environment.

Hollow retroreflectors

1. Advantages

- Lighter than solid cubes
- Transparent at all wavelengths
- No transmission through glass that may have thermal gradients
- No polarization effects
- High gain by using a single dihedral angle offset

2. Disadvantages

- Smaller acceptance angle
- Low range of velocity aberration if narrow return beam is used

3. Potential problems

- Joints may be unstable under thermal stress
- Thermal gradients can warp the surfaces or change the dihedral angles

4. Types of retroreflectors

- Solid block of material (no such thing)
- Beryllium with epoxy joints
- Aluminum with bolted joints
- Coated quartz reflecting plates

5. Potential applications

- GPS
- GALILEO
- Geosynchronous
- Lunar

The incidence angle on the array does not vary much so the small acceptance angle is not a problem. In low earth orbit more cubes would be needed to cover the large range of incidence angles.

6. Existing hollow cubes in space

- RME (6" cube tracked by 48" telescope)
- ADEOS (.5 meter coated quartz plates - tracked by the network)
- TES (inside instrument at -90C.)

7. Thermal modeling

A. Design tolerances.

Since there is no quartz, the performance of the cube depends only on maintaining the mechanical tolerances to $\lambda/10$. The main problem is solar heating of the cube.

B. Absolute temperature.

Metals run hot because they have a high α/ϵ ratio. This may damage the epoxy used to join the reflecting surfaces. Any thermal control needs to be passive through the use of materials with low absorptivity and high emissivity.

C. Thermal gradients

Suppose we have a square plate of area $l \times l$ and thickness w . The thermal parameters are

α = solar absorptivity

ε_1 = emissivity of the front surface

ε_2 = emissivity of the back surface

S = solar constant = 1412.5 Watts/sq meter

k = thermal conductivity of Beryllium = 225
Watts/m-°K

c = linear expansion coefficient of
Beryllium = $11.3 \times 10^{-6} K^{-1}$

σ = Stefan Boltzman constant =
 $5.6697 \times 10^{-8} W m^{-2} K^{-4}$

f = fraction of the solar radiation conducted
through plate.

Parametric equations have been derived for estimating the mechanical distortion due to thermal gradients in the cube as a function of the mechanical and thermal parameters.

Conduction through a plate.

All plates are being equally heated. The heat is being conducted through the plate and radiated from the back surfaces.

$$d = \frac{c l^2 f \alpha S}{2k}$$

If one side of the plate is warmer than the other the plate would warp into a spherical cap where d is the deflection.

Conduction along a plate.

The solar heating is only on one plate. Heat is being conducted to the other plates that are not being heated significantly.

$$d = \frac{c f \alpha S l^3}{k w}$$

The change in linear dimensions d could distort the dihedral angles.

The equations show that thermal warping is proportional to the square of the size of the cube corner for both types of thermal gradients.

Calculations using the formulas above indicate the thermal warping of a cube in the size range 1.5 to 2.0 inches is acceptable. The unresolved issue is the stability of the joints under thermal stress.

More detailed engineering studies are now being done at NASA to evaluate the mechanical distortion and possible damage to the joints due to thermal problems.

The best design would be a single block of material. Unfortunately, there is no existing technology for polishing the inside surfaces.

The next best choice would be a reflector with no dissimilar materials to cause differential expansion and contraction.

Composite cubes have been successfully used under thermally controlled conditions.

8. Conclusions

The use of hollow cubes for laser ranging appears to be feasible if the issue of the stability of the joints can be resolved.

Preliminary Analysis for Single Cube on Lunar Lander

- Potential use for RLEP II Lunar Lander. Would extend the use of lander to decades. Location: southern pole.
- Motivation is recent success by Tom Murphy (APOLLO system) – achieving > 1000 returns per minute from Apollo 15 (implying APOLLO could see returns from individual cube).
- Velocity aberration is < 2 arcsec implying would not need to spoil angles on 2" cube.
- Would need to have method for orienting cube toward earth or would require multiple cubes.
- Link analysis (returned photo-electrons per minute)

	Apollo 15	Single Apollo cube	2" hollow cube
APOLLO	2160	7	22
MLRS	4	0.01	0.04
Matera	60	0.2	0.6
Grasse (LLR)	20	0.07	0.2

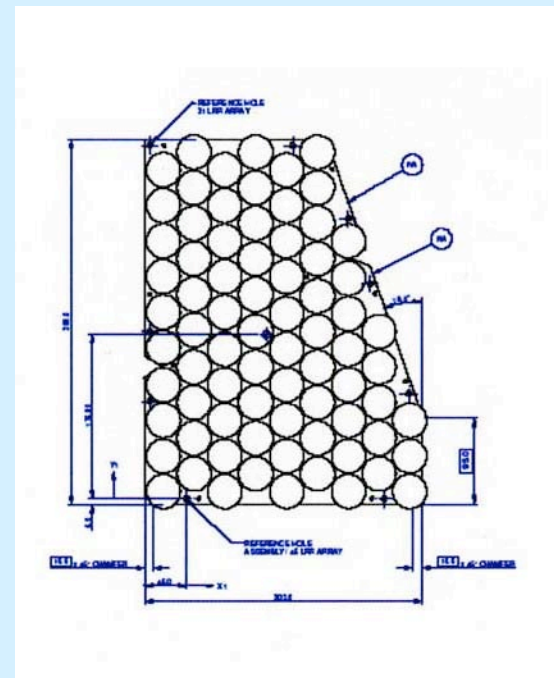
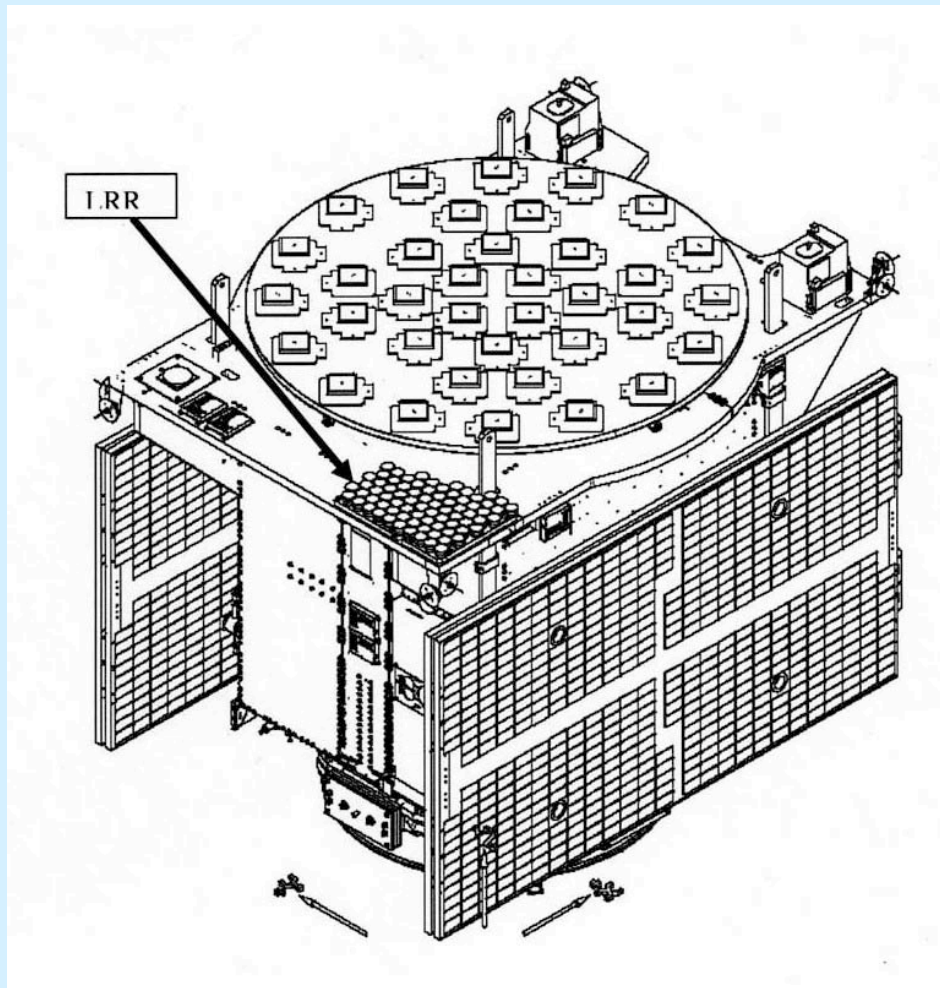
GIOVE-A and B laser arrays

from the ESA document 'Specification of GALILEO and GSTB-V2 Space Segment Properties Relevant for Satellite Laser Ranging, ESTEC, Nov 2005.'

(copy at:

http://ilrs.gsfc.nasa.gov/docs/galileo_description_v22.pdf)

GIOVE-A with 76-cube array – launched Dec 2005



GSTBV2/B with 67-cube array. To be launched Spring 2006?

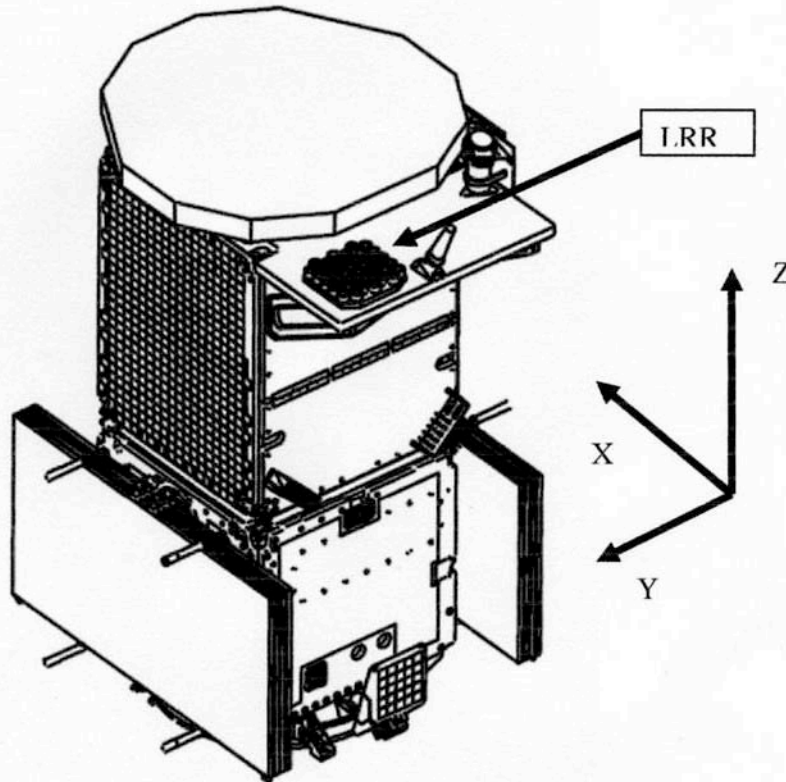
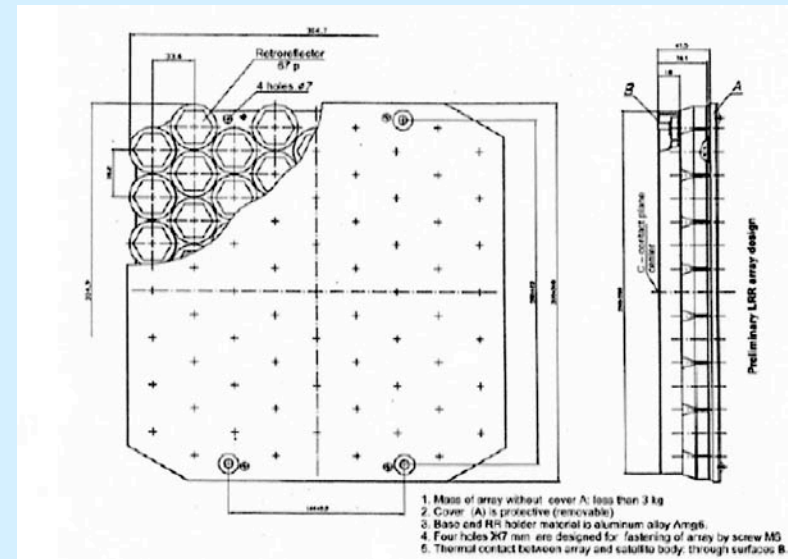
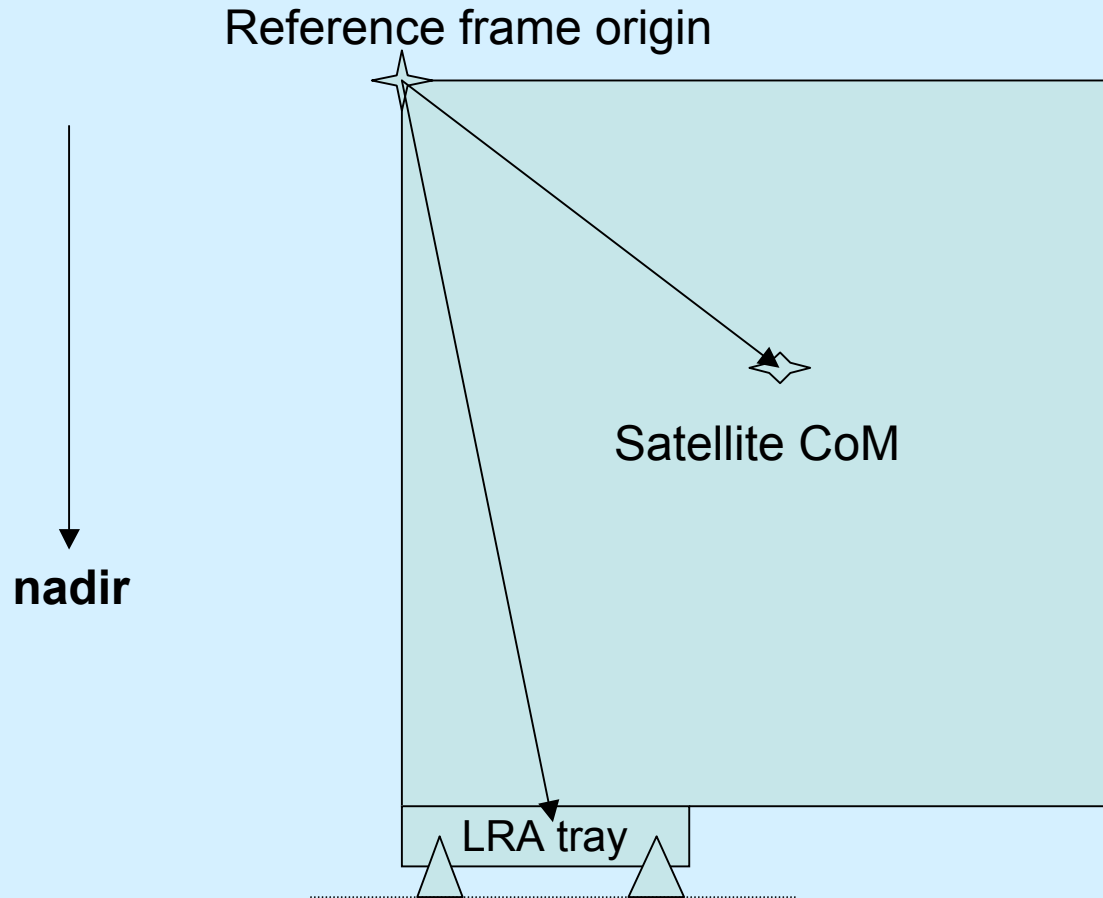


**Fig 2. Position of LRR in GSTBV2/B.
Spacecraft is shown with solar array in stowed configuration**



GIOVE-A schematic



We **have** the vector in satellite-fixed frame to the satellite CoM

We **also have** the vector in satellite-fixed frame to the **CoM** of the LRA tray

Need (say) location of plane of front faces of cubes wrt CoM of LRA tray:-

Can then compute cubes' phase centres wrt CoM of LRA tray;

Hence vector from satellite CoM to LRA phase centre.

SPECIFICATION OF GALILEO AND GSTB-V2 SPACE SEGMENT PROPERTIES RELEVANT FOR SATELLITE LASER RANGING

prepared by/*préparé par* Galileo Project Office

reference/*référence* ESA-EUING-TN/10206

issue/*édition* 2

revision/*révision* 2

date of issue/*date d'édition* 01/11/2005

status/*état*

Document type/*type de* Technical Note

document

Distribution/*distribution*

A P P R O V A L

Title <i>titre</i>	issue 2 <i>issue</i>	revision 2 <i>revision</i>
-----------------------	-------------------------	-------------------------------

author <i>auteur</i> R. Zandbergen, D. Navarro	date <i>date</i> 01/11/2005
---	--------------------------------

approved by <i>approuvé by</i> Marco Falcone	date <i>date</i>
---	---------------------

C H A N G E L O G

reason for change / <i>raison du changement</i>	issue/ <i>issue</i>	revision/ <i>revision</i>	date/ <i>date</i>
Enclose information about positions of LRR, CoG, and phase centre, together with yaw steering, mass, and cross-section area for satellites GSTBV2/A and GSTBV2/B. Change structure of document to focus it on the different satellites.	2	1	10/10/2005
Corrected Z component of phase centre for GSTBV2/B. Rephrased attitude law description for both GSTBV2A and B.	2	2	01/11/2005

C H A N G E R E C O R D

Issue: 2 Revision: 1

reason for change/ <i>raison du changement</i>	page(s)/ <i>page(s)</i>	paragraph(s)/ <i>paragraphe(s)</i>
	All Document	
Rephrased description of attitude law for GSTBV2A	Page 11	Section 3.3
Rephrased description of attitude law for GSTBV2B	Page 14	Section 4.3

<i>reason for change/raison du changement</i>	<i>page(s)/page(s)</i>	<i>paragraph(s)/parag raph(s)</i>
Corrected Z component of phase centre for GSTBV2/B and reformat table	Page 14	Table is section 4.4

T A B L E O F C O N T E N T S

1	INTRODUCTION	5
1.1	Objectives and Scope	5
1.2	Reference Documents	5
1.3	List of abbreviations.....	6
2	MISSION OBJECTIVES	7
2.1	General	7
2.2	GSTB-V2	7
2.3	Galileo.....	7
3	GSTB-V2/A (SSTL)	9
3.1	LRR Array Specifications	9
3.2	LRR and CoG positions	10
3.3	Attitude Law	11
3.4	Other navigation data	12
4	GSTB-V2/B (GAIN)	13
4.1	LRR Array Specifications	13
4.2	LRR and CoG positions	13
4.3	Attitude Law	14
4.4	Other navigation data	15
5	GALILEO	16

1 INTRODUCTION

1.1 Objectives and Scope

This document provides information about the relevant characteristics of the Galileo Spacecraft and orbits in order to allow an assessment by the International Laser Ranging Service of its capability to perform Satellite Laser Ranging support.

In addition, this document provides information (when available) about spacecraft properties crucial for precise orbit determination such as LRR position, centre of mass position, attitude law, navigation signal phase centre, etc. Some of these values are still subject to verification (for instance, during GSTBV2/A QAR) and will be updated in following versions of this document.

The document applies both to the two experimental spacecraft flown as part of the Galileo System Test Bed V2, henceforth referred to as GSTB-V2/A and GSTB-V2/B, and to the operational Galileo spacecraft. For the latter, distinction is made between the In-Orbit Validation (IOV) and Full Operational Capability (FOC) phases.

1.2 Reference Documents

RD-1	Galileo Satellite Laser Ranging Retro-Reflector Specifications, ESA MEMO	-DEUI-NG-MEMO/01280, Issue 1.0, 6-8-2004	Issue 1.0 6-8-2004
RD-2	Galileo Global Component System Requirements Document		Issue 4.2 27-7-2004
RD-3	Space Segment Design and Justification	GSTBV2-SS-DD-SST-SC-0004	Issue 5 28/01/05
RD-4	Antenna ICD (Alenia)	GSTBV2-SS-DR-SST-SC-0005	Rev 1 D 03/05/05
RD-5	GSTBV2A Laser Retroreflector	01733-ITM (no ESA ref code)	Rev 2 03/07/04
RD-6	GSTBV2 - LASER REFLECTOR GSTBV2 LRR Technical note - Response to RID 4383	GSTBV2-SS-TN-SST-PL-0022	N/A
RD-7	Navigation Antenna Mechanical Design and Analysis	RPT-GT2-0025-ALS	Issue 3 16/02/05
RD-8	GSTBV2A RF Test Report	RPT-GT2-0040-ALS	Issue 1 18/02/05
RD-9	Propulsion Bay ICD	GSTBV2-SS-DR-SST-SC-0001	Rev B 10/02/05
RD-10	AOCS Design Description and	GSTBV2-SS-TN-SST-SC-	Issue 2

	Justification File	0016	22/02/05
RD-11	Space-Segment DDDJF	GSTBV2-DD-GAIN-0030	Issue 2A 29/11/04
RD-12	Mechanical Design Description	GSTBV2-DD-GAIN-0282	Issue 3 15/11/04
RD-13	Navigation Antenna PFM Design Verification and Compliance Matrix	GSTBV2-SS-CAS-ENG-13 B	Issue 5 19/01/05
RD-14	Navigation Antenna ICD PFM-FM	GSTBV2-SS-CAS-ENG-16-B	Issue 1 Rev 1 06/09/04
RD-15	Satellite Budgets	GSTBV2-BG-GAIN-0037	Issue 5 03/12/04
RD-16	Yaw Steering Guidance	TN_60_0023	Issue 1 17/10/03

1.3 *List of abbreviations*

AOCS	Attitude and Orbit Control System
FOC	Full Operational Capability
GSTB	Galileo System Test Bed
GTRF	Galileo Terrestrial Reference Frame
IOV	In-Orbit Validation
ITRF	International Terrestrial Reference Frame
LRR	Laser Retro-Reflector
MEO	Medium Earth Orbit
RA	Right Ascension
S/C	Spacecraft
SLR	Satellite Laser Ranging
SSTL	Surrey Satellite Technology Ltd
TBC	To Be Confirmed

2 MISSION OBJECTIVES

2.1 *General*

This section specifies the mission objectives for the different S/C and operations phases, and includes the orbit parameters.

2.2 *GSTB-V2*

GSTB-V2/A, built by Surrey Satellite Technology Ltd (SSTL) of the UK, is foreseen to be launched by the end of 2005. GSTB-V2/B, built by Galileo Industries (GaIn), is foreseen to be launched in the 2nd quarter of 2006.

Both satellites missions have the same objectives:

- to secure the Galileo frequency allocations by providing a signal in space
- to allow early experimentation with critical hardware (Signal In Space and On-Board Clocks) and software systems
- to demonstrate navigation service
- to characterization of the MEO environment
- additional experimentation

Precise evaluation characterisation of the performance of the on-board atomic clocks, of antenna infrastructure, and of signal properties requires a precise orbit determination, in which SLR will play an important role. Both routine SLR tracking and occasional campaigns with higher-intensity tracking will be required.

The orbit defined for the operational test bed satellite is a near-circular ground track repeat orbit of 17 revolutions in (approximately) 10 sidereal days, with an inclination of 56°. The relevant orbit parameters are:

Semi-major axis:	29601 km
Eccentricity:	0.002
Inclination:	56°
Argument of perigee:	0° (TBC)
RA of ascending node:	182° for GSTBV2/A (TBC)

2.3 *Galileo*

The final constellation will consist of 27 operational spacecraft equipped with identical Laser Retro-Reflectors (LRR). The satellites will be evenly distributed over 3 orbit planes, in a 27/3/1 Walker constellation. That means that the R.A. of ascending nodes of the three planes are separated by 120° and the spacecraft in each plane are separated by 40° in-plane. The orbit is the same as for the GSTB-V2 spacecraft, i.e. a 10-day ground-track repeat orbit with 17 revolutions and an inclination of 56°. Each plane will include an additional (inactive) spare satellite, for which no SLR tracking will be requested as long as it is inactive.

The relevant orbit parameters are:

Semi-major axis:	29601 km
Eccentricity:	0.002
Inclination:	56°
Argument of perigee:	0° (TBC)
RA of ascending node:	0°, 120°, 240° (TBC)

The (up to) four Galileo satellites used in IOV will be launched in the 4th quarter of 2007 for a foreseen IOV phase duration of 6 months (extendable to 1 year). They will be identical to the FOC S/C, and they will have the same orbit parameters - no change in semi-major axis or inclination between IOV and FOC is foreseen.

The IOV S/C will be collocated to allow simultaneous reception of the navigation signals, but the final decision whether all four S/C will be in one plane or subdivided over two planes, and whether they will also be separated by 40°, is not yet made.

The objectives of SLR during IOV are similar to those for the GSTBV2 mission: to characterise on-board instrument properties using precise orbit determination, both on a routine basis and in occasional campaigns with more intensive tracking.

During FOC, SLR data will contribute to the verification of the precise orbits based on microwave data and to the tie between the Galileo Terrestrial Reference Frame (GTRF) and ITRF.

3 GSTB-V2/A (SSTL)

3.1 LRR Array Specifications

Originally, GSTB-V2/A was planned to be equipped with a pair of identical LRR arrays separated by some distance on the nadir-facing side of the spacecraft. The final design deviates from this original approach, whereby the two patches have been co-located and form one integrated array of 76 coated cubes with a diameter of 27 mm each. The overall shape is trapezoidal.

Specifications (RD-5):

1. OVERALL ENVELOPE (WITH COVER): 308 x 408 x 48 mm (excluding heads of mounting screws)
 OVERALL ENVELOPE (WITH COVER): 308 x 408 x 54.5 mm (including heads of mounting screws)

 OVERALL ENVELOPE (WITHOUT COVER): 306.8 x 405.5 x 41.5 mm
 45 LRR ARRAY (WITHOUT COVER): 306.8 x 271.8 x 41.5 mm
 31 LRR ARRAY (WITHOUT COVER): 239.5 x 254 x 41.5 mm
2. TOTAL WEIGHT (WITHOUT COVER): < 3.8 Kg
 45 LRR ARRAY (WITHOUT COVER): < 2.2 Kg
 31 LRR ARRAY (WITHOUT COVER): < 1.6 Kg
3. COORDINATES OF CENTRE OF GRAVITY OF 76 LRR ARRAY AS AN ASSEMBLY.
 Xg=89 mm, Yg=176.8 mm, Zg=24.37 mm (Referred to reference hole)
4. CENTRE OF GRAVITY OF 45 LRR ARRAY: Xg = 113.7 mm
 (Referred to reference hole) Yg = 100.0 mm
 Zg = 24.5 mm

 CENTRE OF GRAVITY OF 31 LRR ARRAY: Xg = 53.2 mm
 (Referred to reference hole) Yg = 289.0 mm
 Zg = 24.2 mm
5. MOMENT OF INERTIA OF 76 LRR ARRAY: Jx = 47964 Kg x mm²
 (Referred to 76 LRR array CofG) Jy = 21881 Kg x mm²
 Jz = 69038.6 Kg x mm²

 MOMENT OF INERTIA OF 45 LRR ARRAY: Jx = 8887.9 Kg x mm²
 (Referred to 45 LRR array CofG) Jy = 15133.4 Kg x mm²
 Jz = 23546.8 Kg x mm²

 MOMENT OF INERTIA OF 31 LRR ARRAY: Jx = 4319.5 Kg x mm²
 (Referred to 31 LRR array CofG) Jy = 7261.8Kg x mm²
 Jz = 11250.3 Kg x mm²
6. MATERIAL (BASE AND RR HOLDER): ALUMINIUM ALLOY AMr6

7. MOUNTING SCREWS: 9 pcs. M5 x 20.0 mm LONG CAP HEAD,
STAINLESS STEEL A2-70
8. MOUNTING WASHER: 9 pcs. DIA 5.3 mm, STAINLESS STEEL A2
9. CONTACT AREA (): 1,876.0 mm²
45 LRR ARRAY: 1061 mm²
31 LRR ARRAY: 815 mm²
10. OVERALL MOUNTING SURFACE FLATNESS: < 0.2 mm
Actual flatness is 0.04 mm
11. FLATNESS FOR EACH FOOT: same as for item 10
12. MOUNTING SURFACE ROUGHNESS: Ra1.6
13. SURVIVAL TEMPERATURE RANGE: from -150°C to +125°C

A detailed drawing is attached as Annex A.

3.2 *LRR and CoG positions*

Coordinate of the Centre of gravity of 76 LRR array with respect satellite reference frame (RD-4 and RD-6):

X = -832 mm
Y = -654 mm
Z = 1489 mm

Coordinate of the S/C centre of gravity (beginning of life, deployed solar array configuration; communication by email from Paul Charman on 14 September 2005)

X = -4 mm
Y = 1 mm
Z = 788 mm

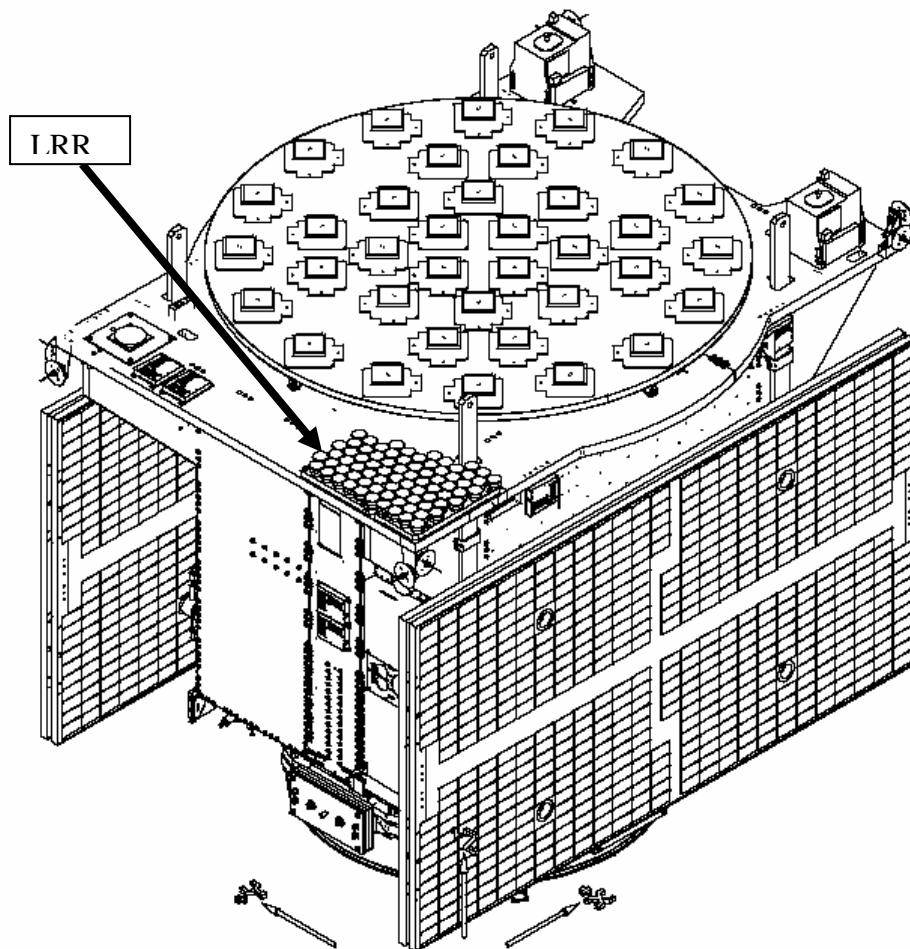


**Fig 1. Position of the LRR in the GSTB2/A spacecraft.
 Spacecraft is shown with solar array in stowed configuration**

3.3 *Attitude Law*

The GSTB-V2/A AOCS Normal Mode must maintain the spacecraft attitude such that the payload line of sight (nominally aligned with the spacecraft +Z Body axis) is always nadir-pointing and the solar array panels (aligned with the spacecraft body Y axis) can always achieve normal solar incidence by a rotation of the solar panels around the body Y axis. To be achieved this, the spacecraft follows an attitude profile that keeps the +Z body axis nadir-pointing and the spacecraft-Sun vector nominally in the spacecraft X-Z body plane by using only a spacecraft yaw rotation throughout the orbit. In practice there are two solutions which can be used to satisfy the requirements. The selected solution maintains the +X facet of the spacecraft in a deep-space pointing attitude.

It is foreseen that the theoretical attitude will not be achieved at times where the beta angle (angle between the sun and the orbital plane) is small, due to limitations in the reactions wheels and to poor yaw measurement (sun co-linearity). In addition, during eclipse, it is expected that the yaw error can reach values of up to 18 degrees.

3.4 *Other navigation data*

The phase centre for the navigation signal is provided here to complement the necessary information needed to perform precise orbit determination (RD-4, RD-7 and RD-8)

E5a + E5b	E6	E2/L1/E2
X = 0.0 mm	X = 0.0 mm	X = 0.0 mm
Y = 0.0 mm	Y = 0.0 mm	Y = 0.0 mm
Z = 1690.0 mm	Z = 1665.0 mm	Z = 1658.0 mm

The s/c mass at launch will be 614 kg. The approximate cross-section Area is 9 squared metres.

4 GSTB-V2/B (GAIN)

4.1 *LRR Array Specifications*

Specifications have been extracted from industrial documentation. (RD-11)

Size: 305mm x 305mm x 42 mm
Number of prisms: 67
Prism diameter: 27 mm (light area)
Material: optical grade fused silica, aluminium-coated
Temperature range: from -125°C to +125°C
Field of view: 12 degrees (half-cone)

A detailed drawing is attached as Annex B.

4.2 *LRR and CoG positions*

Coordinate of the Centre of gravity of the LRR array with respect satellite reference frame:

X = -807.5 mm
Y = 297.5 mm
Z = 2267.0 mm

Coordinate of the S/C centre of gravity (beginning of life, deployed solar array configuration)

X = 0.0 mm
Y = 0.0 mm
Z = 940.6 mm

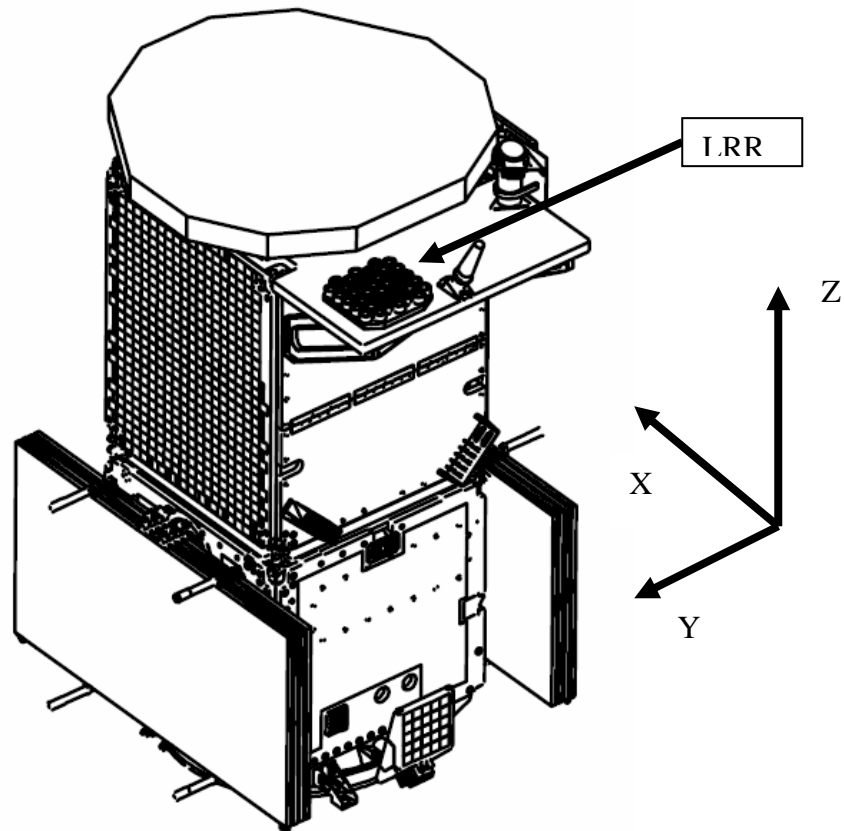


**Fig 2. Position of LRR in GSTBV2/B.
 Spacecraft is shown with solar array in stowed configuration**

4.3 Attitude Law

GSTBV2/B follows a yaw steering law such that the body +Z axis points continuously to Nadir, together with a rotation performed around the Z axis that maintains the S/C Y axis perpendicular to the Sun. The +X spacecraft panel is maintained away from the sun. (RD-10).

As with GSTBV2/A, it is foreseen that the theoretical attitude will not be achieved at times where the beta angle (angle between the sun and the orbital plane) is small, due to limitations in the reactions wheels and to poor yaw measurement (sun co-linearity). In addition, during eclipse, it is expected that the yaw error can reach values of the same order as GSTBV2/A.

4.4 *Other navigation data*

L-band phase centres (RD-13 and RD-14)

E5a + E5b	E6	E2/L1/E2
X = 0.0 mm	X = 0.0 mm	X = 0.0 mm
Y = 0.0 mm	Y = 0.0 mm	Y = 0.0 mm
Z = 2288.7 mm	Z = 2287.6 mm	Z = 2289.15 mm

5 GALILEO

The current specifications by industry of the LRR size are extracted from industrial documentation and confirmed by D. Smith of Astrium on 27 August 2004. Source document used (for the purpose of traceability of the information) is Annex 1 to Space Segment and Satellite Design Description and Justification File, Doc-no: GAL-DD-ASTD-SS-R-0002, Issue 3, Rev. 1 draft. 31.07.2004.

Size: 435mm x 540mm x 53mm

Number of prisms: 100

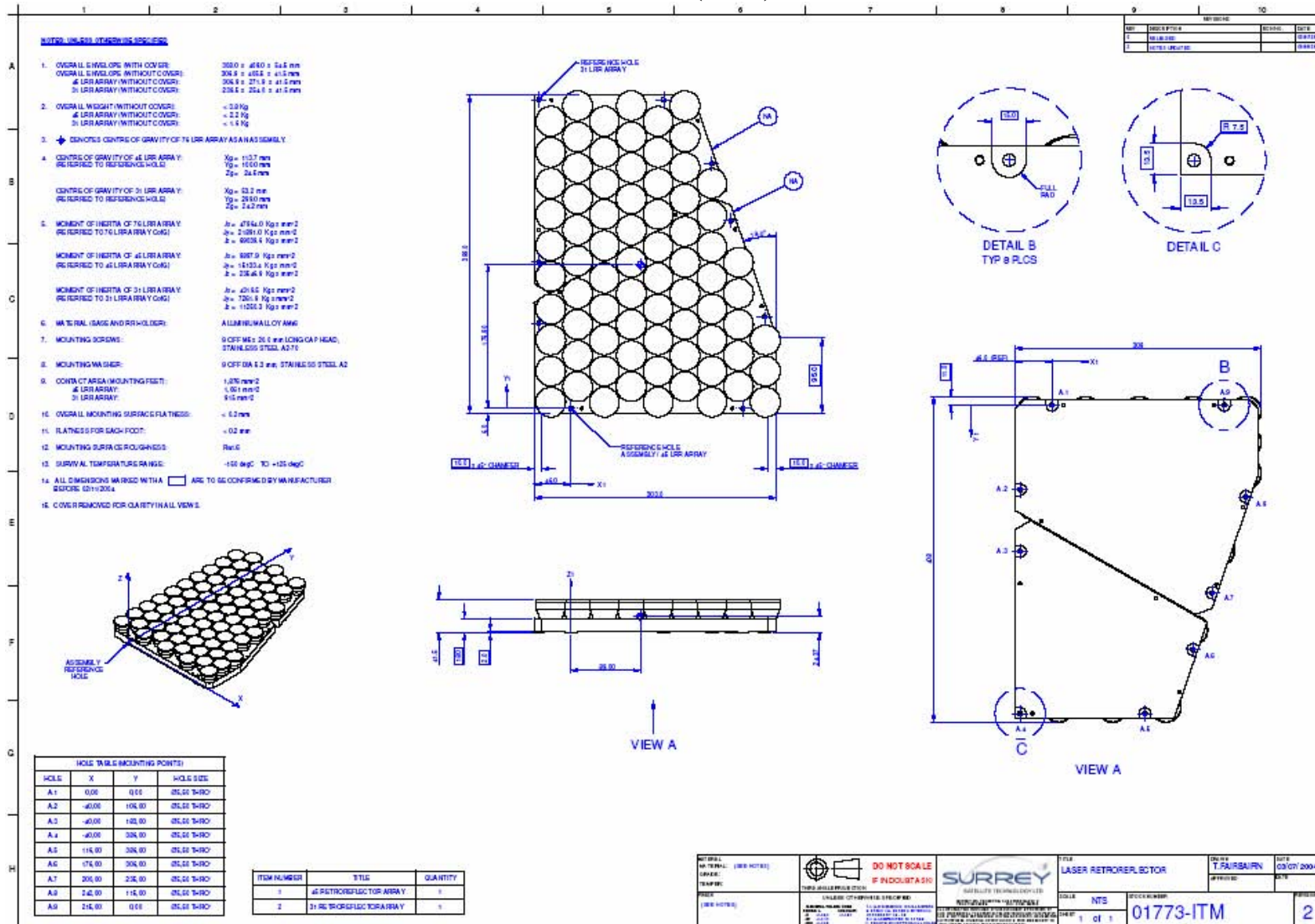
Mass: 5 kg

Prism diameter, dihedral offset, or the choice: coated or uncoated are not yet known.

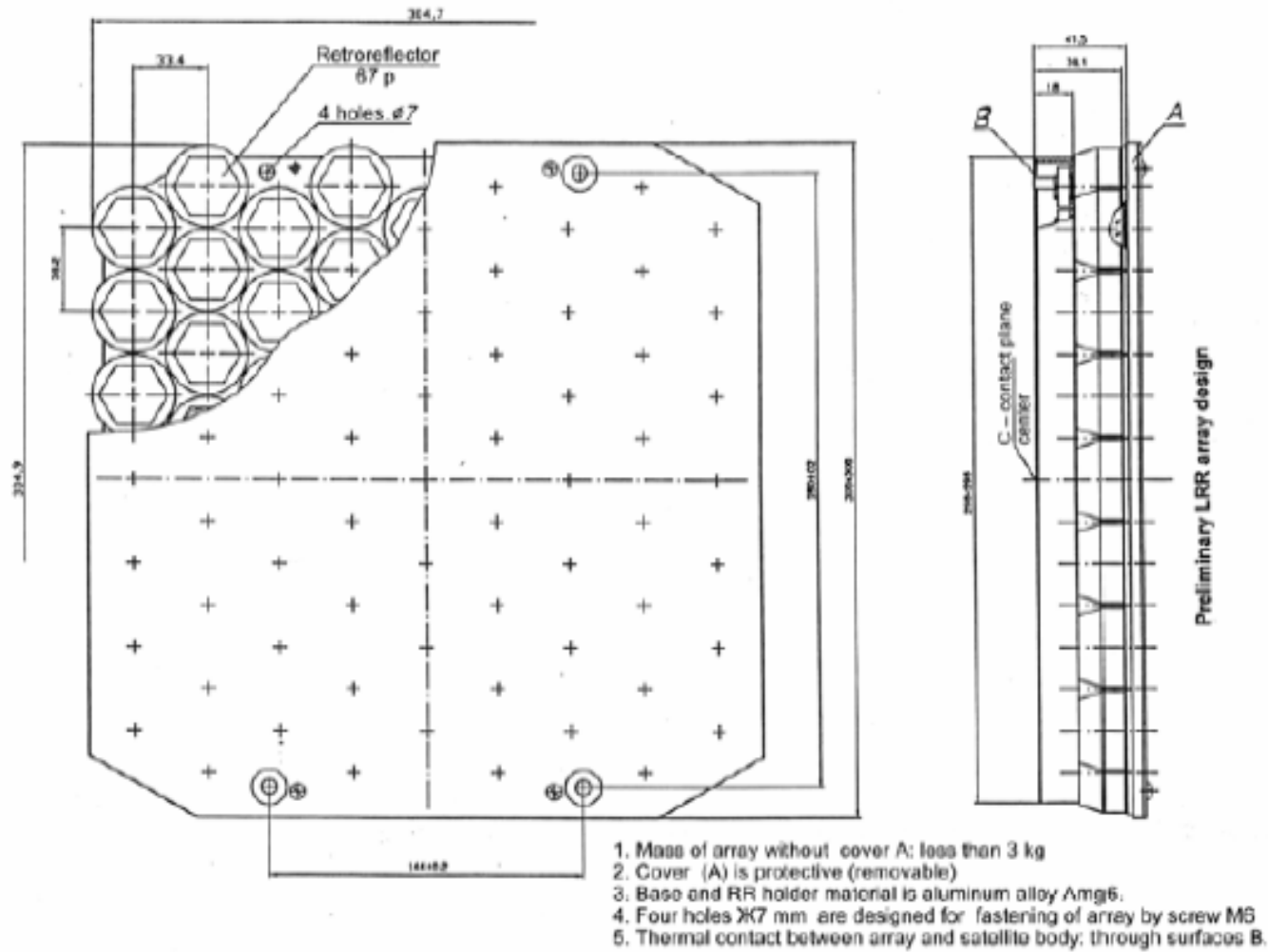
These values are now subject to change, since the Galileo System Requirements Document (RD-2) currently requires a minimum aggregate effective reflective LRR surface area of 660 square cm, viewed from any point on the Earth (i.e. assuming nominal S/C attitude).

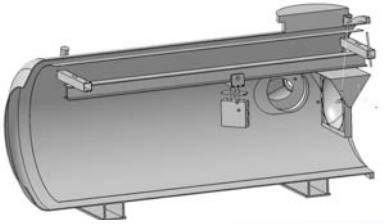
END OF DOCUMENT

ANNEX A (RD-5)



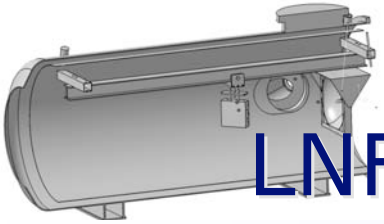
ANNEX B (RD-11)





Testing LAGEOS, LARES and GPS3 CCR prototypes at the LNF Space Climatic Facility

G. Delle Monache
Laboratori Nazionali di Frascati dell'INFN Frascati
for the LARES Collaboration
(I. Ciufolini PI)



INFN Space Climatic Facility (SCF)

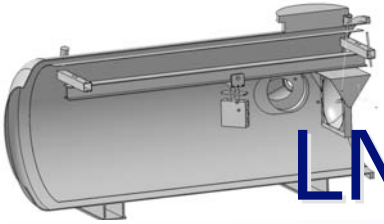
In Fall 2004 the full characterization of the LAGEOS/LARES satellites urged for thermal vacuum tests.

Soon we discovered difficulties in finding a facility equipped with the two main features for precision measurements:

 IR Camera










 "Hi FI" Sun Simulator

The interest of INFN in setting up in-house facility plus the chance of acquiring resources which can be shared among different activities and the availability of four nice dismissed cryostats led to the final decision of building a **SCF**

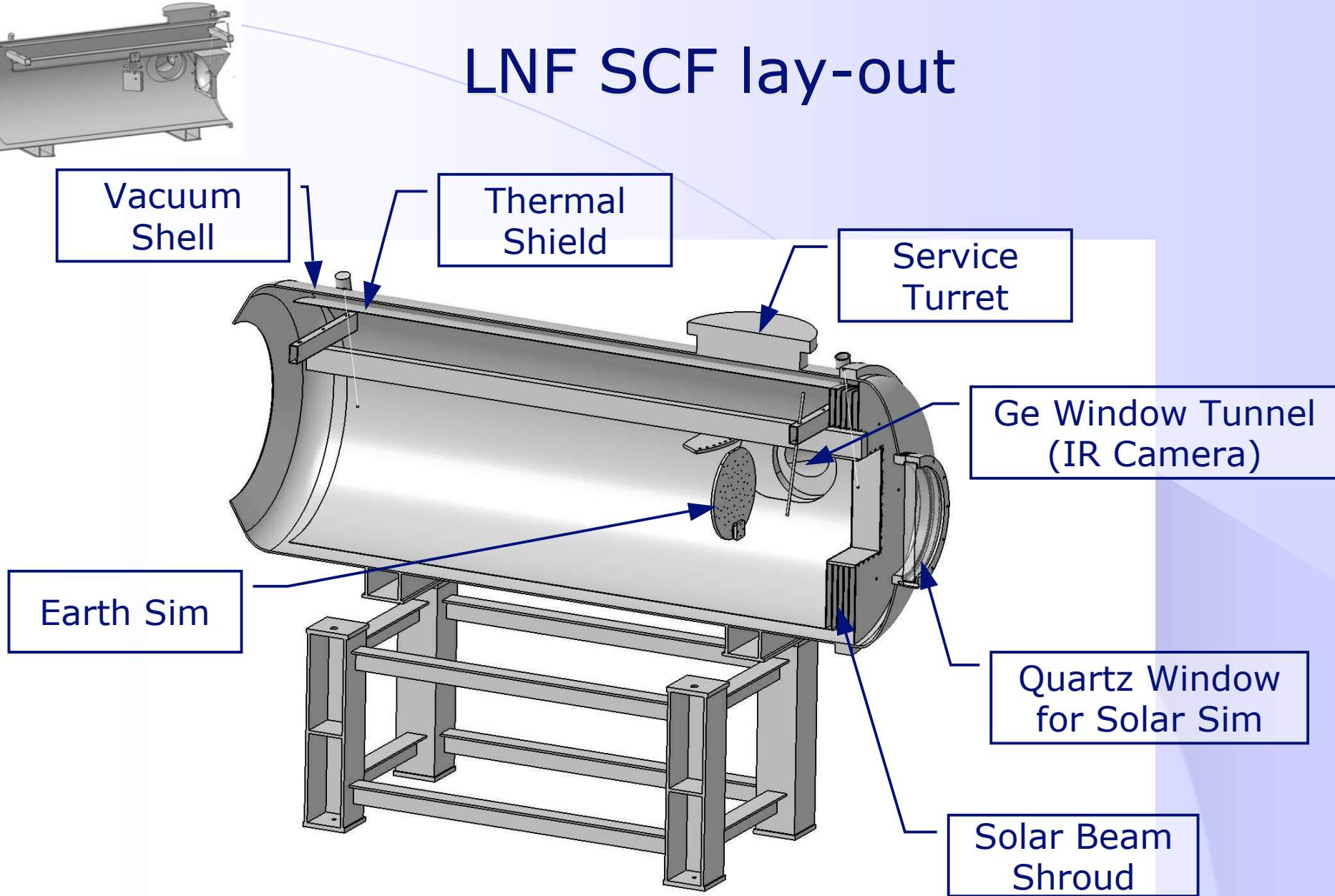


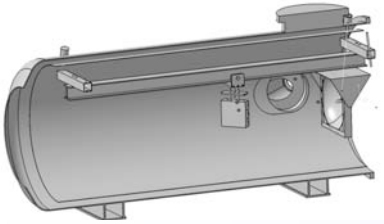
LNFSF: Main Components

The main components of the facility are:

-  Cryostat
-  Thermal Shield
-  Thermometry System
-  Ge Window
-  Sun Simulator
-  Quartz Window
-  IR Earth Simulator
-  Thermal Analysis Software
-  Lasers for Optical Tests

LNf SCF lay-out





The Cryostat

Dismissed SC RF cavities of the LISA accelerator prototype

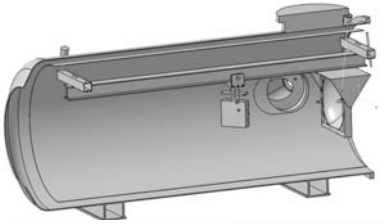
Internal dimensions (inside Cu thermal shields)

Cylinder:

\varnothing 800 mm H=1800 mm

The shield is provided with brazed coil for forced cooling with LN2





The Thermal Shield

AEROGLAZE

The **inside** part of the thermal shield has been painted with:

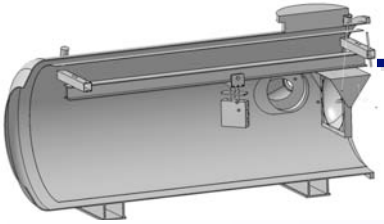
1. 9924 A/B bi-component primer (1 hand)
2. Z306 flat black absorptive Polyurethane, low outgassing (2 hands); Solar absorption (Gier-Dunkle integrating sphere) ≥ 0.95

No MLI or few Al layer foresee between the shield and the vacuum shell

The Solar beam shroud shapes the radiation to avoid radiance on the back of the thermal shield



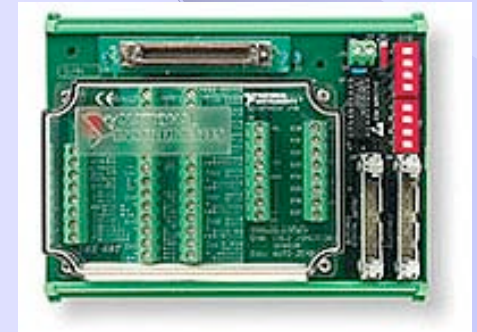
Baking in vacuum will be carried out in the next few days.

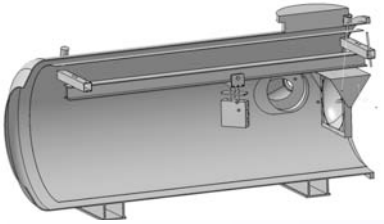


The Thermometry System

The thermometry System is composed of two main subsystems:

1. IR Camera FLIR Thermacam® E320 for non invasive temperature measurement
2. Probes system DAQ for:
 - cross check
 - IR Camera tuning
 - measurement of non visible parts made with:
 - NI PCI-4351 High-Precision temperature and Voltage Logger
 - NI TBX-68T Terminal Block for Thermocouples





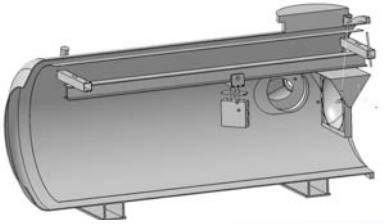
The IR Camera

- The ThermaCAM® EX320 has a true, built-in 320 x 240 pixel array
- Field of view/min focus distance 25° x 19° / 0.3 m
- Thermal Sensitivity 80 mK
- Detector Type Focal plane array (FPA) uncooled Vanadium Oxide microbolometer
- Spectral Range 7.5 ÷ 13 μm



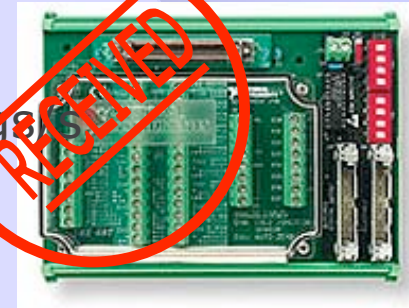
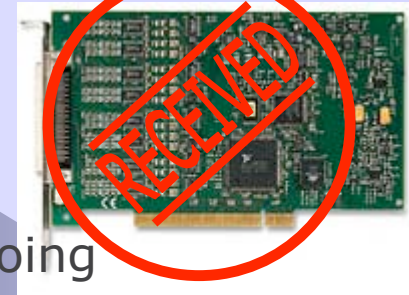
ThermaCAM® EX320

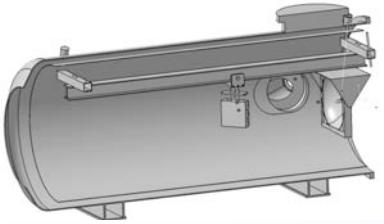
The camera will be used also in predictive maintenance, diagnostics and R&D activities in both LNF AD and RD



The Probes' System

1. NI PCI-4351 High-Precision temperature and Voltage Logger:
 - 14 unconditioned temperature or voltage inputs
 - Isothermal design, plastic cover to minimize thermal gradients across the terminal block
 - Built-in cold-junction compensation sensor and autozeroing circuitry
2. NI TBX-68T Terminal Block for Thermocouples:
 - Accuracy -- 0.42 °C for J-type thermocouples, 0.03 °C for thermistors, 0.12 °C for RTDs
 - 8 TTL Digital I/O lines
 - Autozero and cold-junction compensation
 - 16 voltage or 14 thermocouple inputs; up to 60 readings
 - 24-bit ADC resolution





The Ge Window

A Ge window is needed to "look inside" the SCF with the IR Camera to collect temperatures data



Company Specification:

Design of part:: plano-plano window

Material: optical grade germanium

Diameter: 100.0 (+0/-0.25) mm

Thickness: 10.0 (+/-0.25) mm

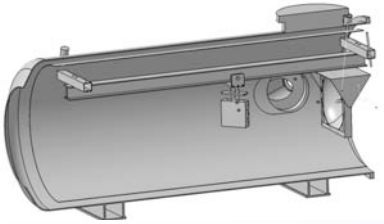
Surfaces quality: 80/50 scr/dig

Parallelism: < 5 arc. min.

Chamfer: 0.4(+0.3) mm x 45 deg.

Coating: both faces BBAR/BBAR coating for
7.5 ÷ 13 μm





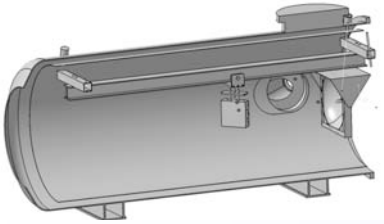
The Sun Simulator

Solar simulation with a lamp as heating method has several advantages; it does not assume a prior known environment, has a minimal interference and accurately simulates space environment. On the other side is expensive and the set can be difficult.

The choice of a Sun simulator comes from the cruciality of the temperature measurement in the LAGEOS/LARES satellites.

The specifications for the Sun Simulator are:

1. Close match to AM0 Spectrum (ASTM E 490-00a) over a surface $\text{\O}350$ mm
2. 2D uniformity better than $\pm 5\%$

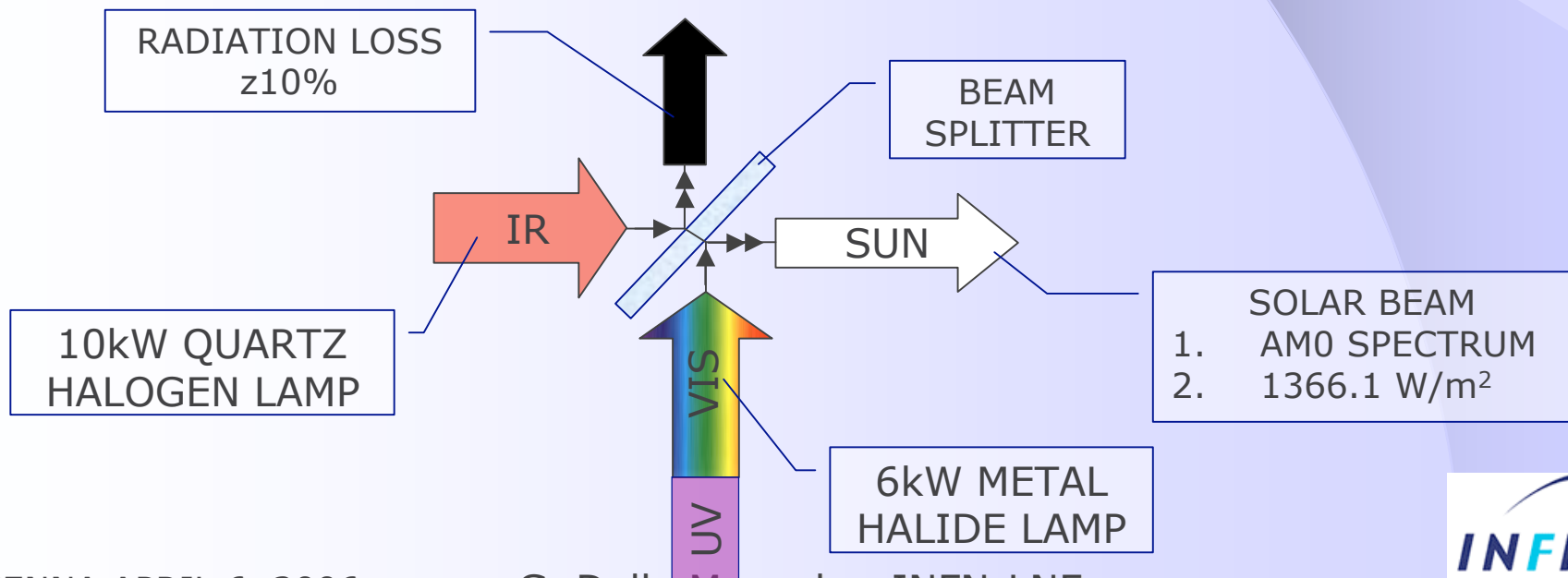


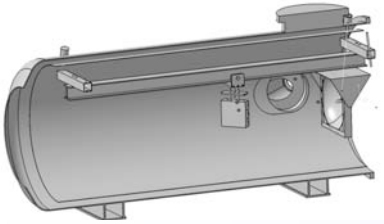
The Sun Simulator

To match the Solar spectrum 2 lamp types (plus filters) must be used:

1. QH: Quartz Halogen Lamp (IR)
2. HMI: Metal Halide Lamp (UV+Visible)

The geometry of the satellite (sphere) does not allow to use a lamp array focused on target. A beam-splitter configuration allows also to change the target distance without modifying the SS set up



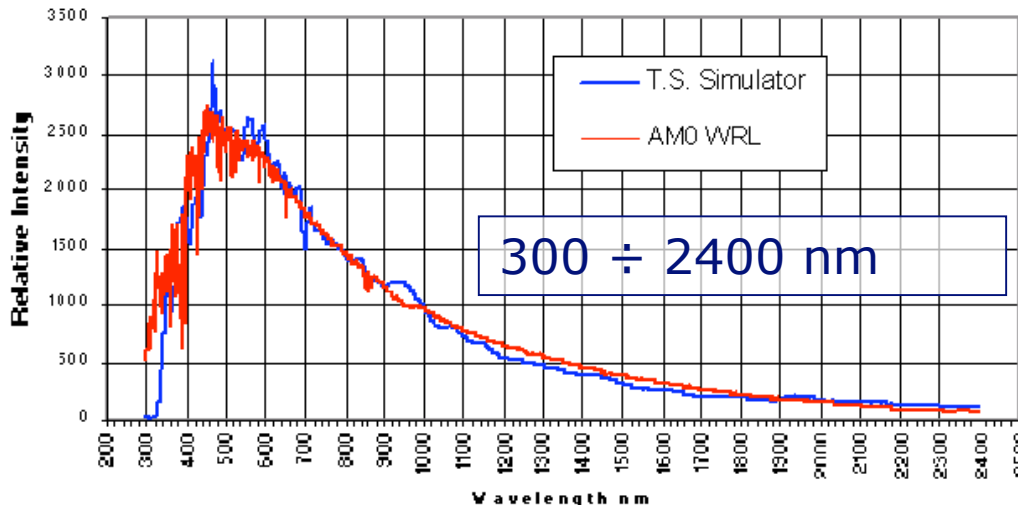


The Sun Simulator

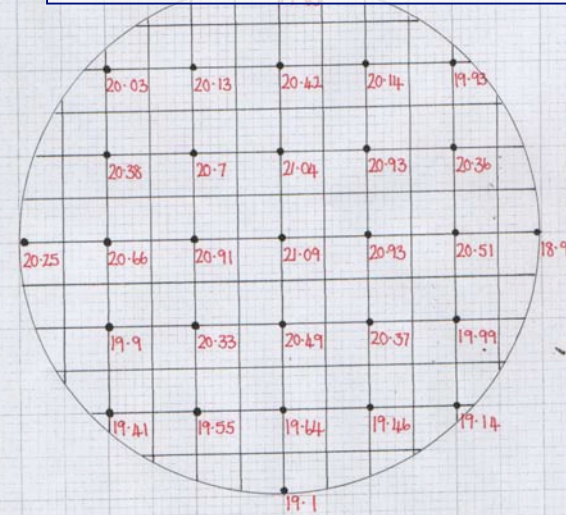
The two spectra are merged at the beam splitter, so as to produce the final one.

Each lamp is equipped with optical feedback (**Solarimeter**), which is fed to a PID controller. Each controller calibrates the output of its power unit, so as to compensate for lamp ageing.

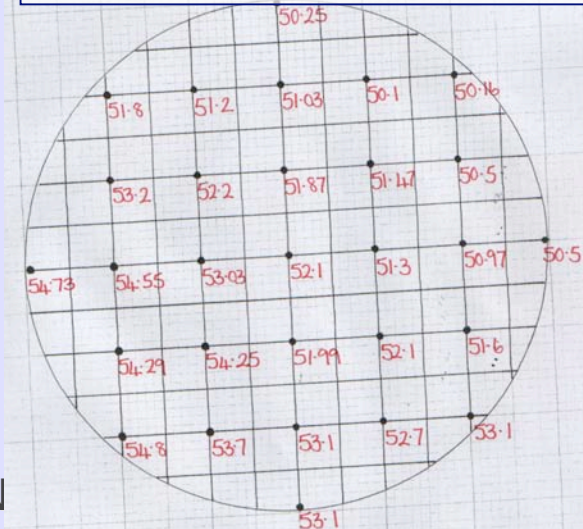
Close Match Simulator AM0

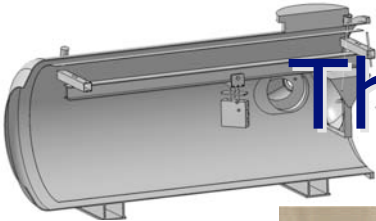


QH: uniformity $\pm 3\%$



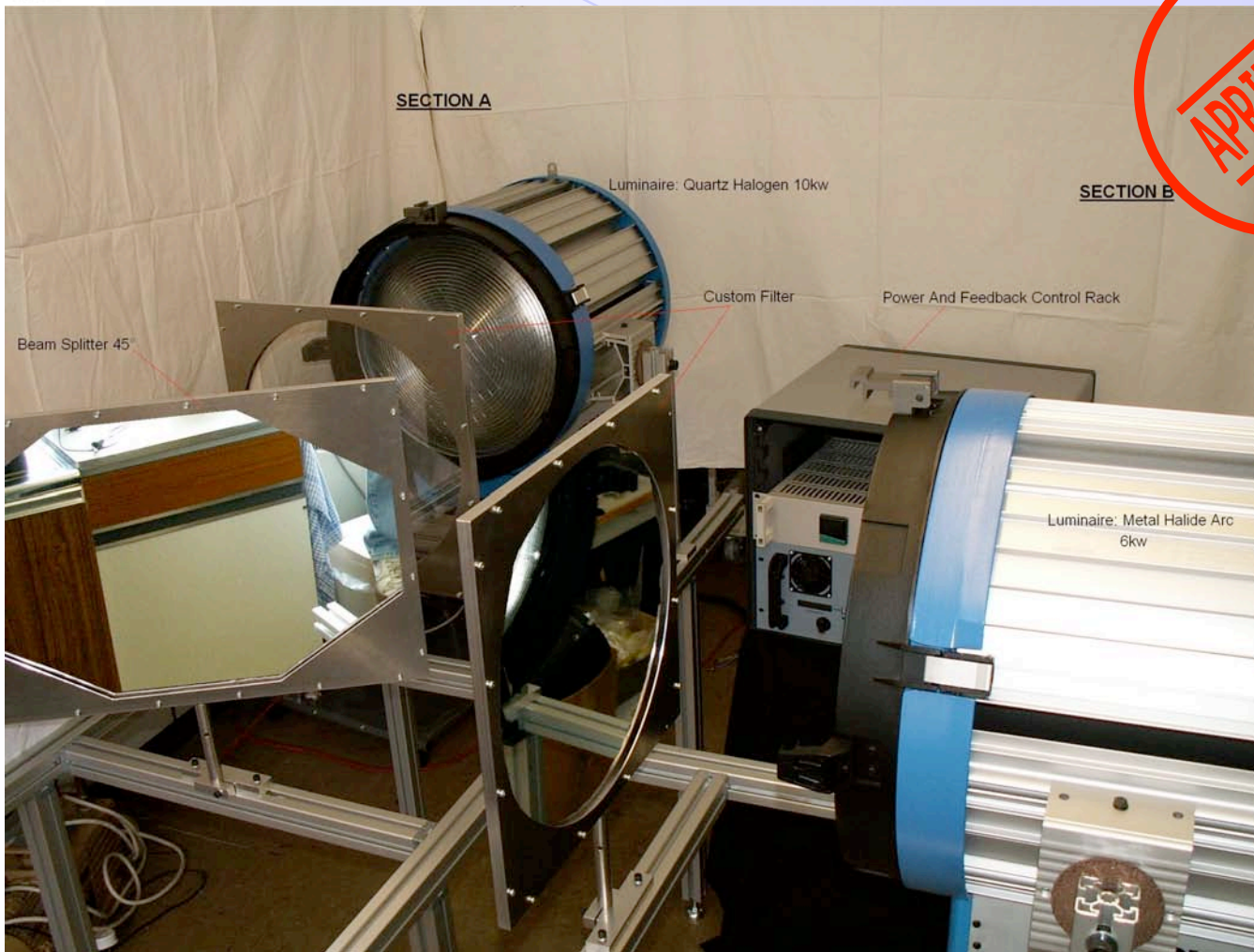
HMI: uniformity $\pm 3\%$



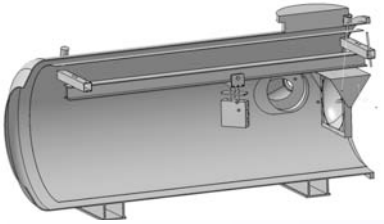


The Sun Simulator: here it is!

APRIL 2006



TS-Space Systems

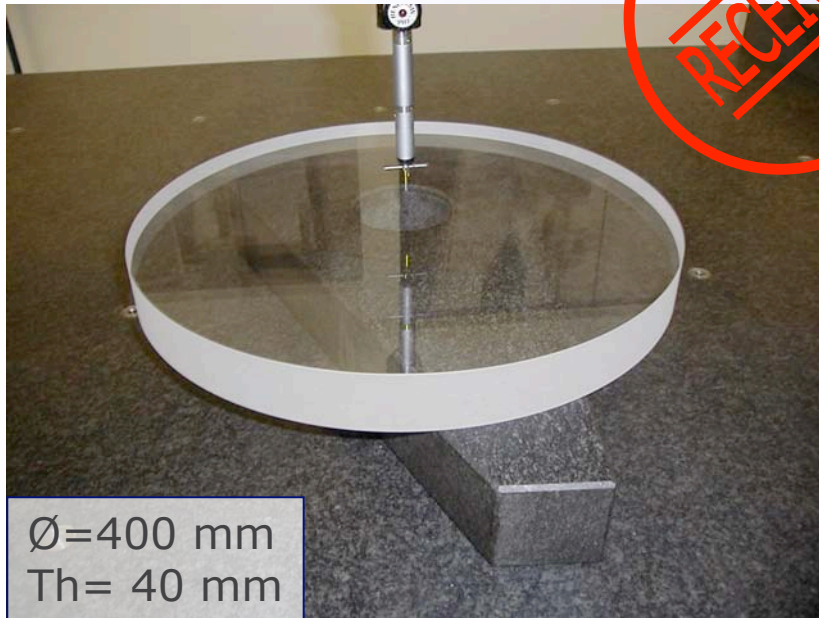


The Quartz Window

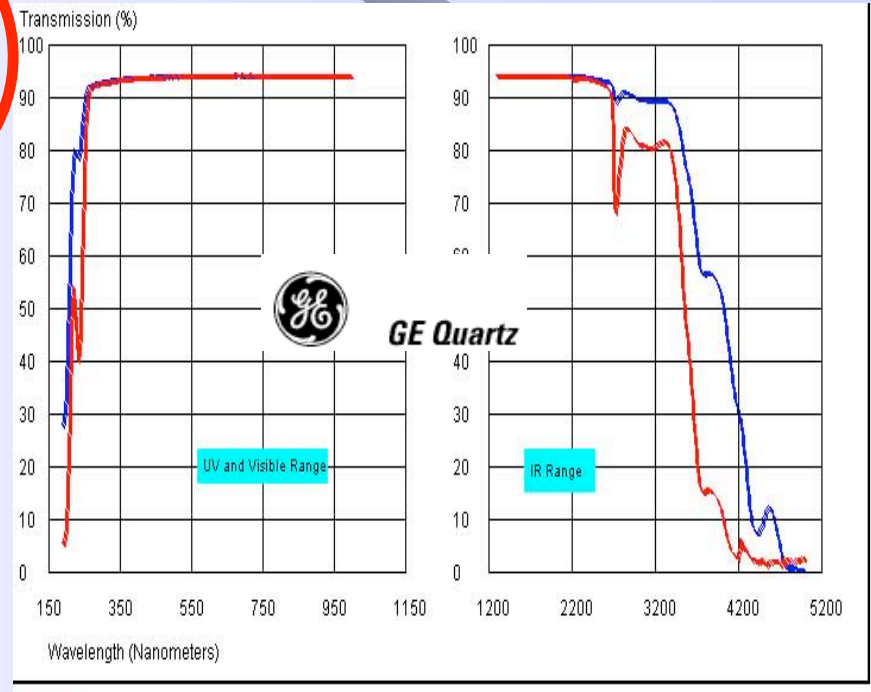
The Quartz window allows the SS beam to get inside the vacuum chamber (GE 144 type, Blu line)

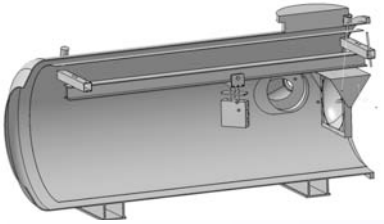
$\tau_{\text{vis}} > 95\%$

$\tau_{\text{IR}} > 85\%$



$\text{Ø} = 400 \text{ mm}$
 $\text{Th} = 40 \text{ mm}$



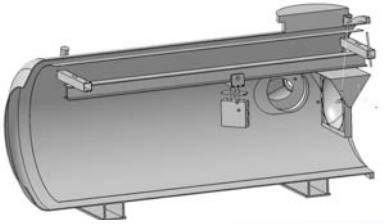


The IR Earth simulator

The IR Earth Simulator is an Al disk painted with Z306 set at 250 K by Thermo Electric Cooler (TEC) controlled by a PWM feedback system

TEC layout not yet defined as well as chance to "thermally link" the disk to the shield or the vacuum case





The IR Earth Simulator

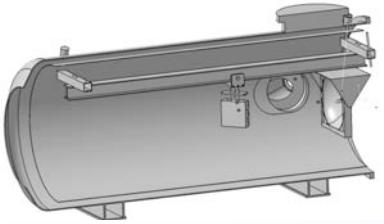
1. 10 TEC CP2 31 10L 18.8 W

2. 2 TEC CP2 127 10L 77.1 W

3. 2 Thermoelectric Temperature Controller
MTTC 1410

- $\pm 0.1^{\circ}\text{C}$ temperature stability
- DC output voltages: 3, 7, 12, 14 VDC (PWM)
- Maximum output current 10A
- Control range: -100°C to 200°C
- Temperature sensor: 2-wire PT1000 RTD
- PID control





The Software Package

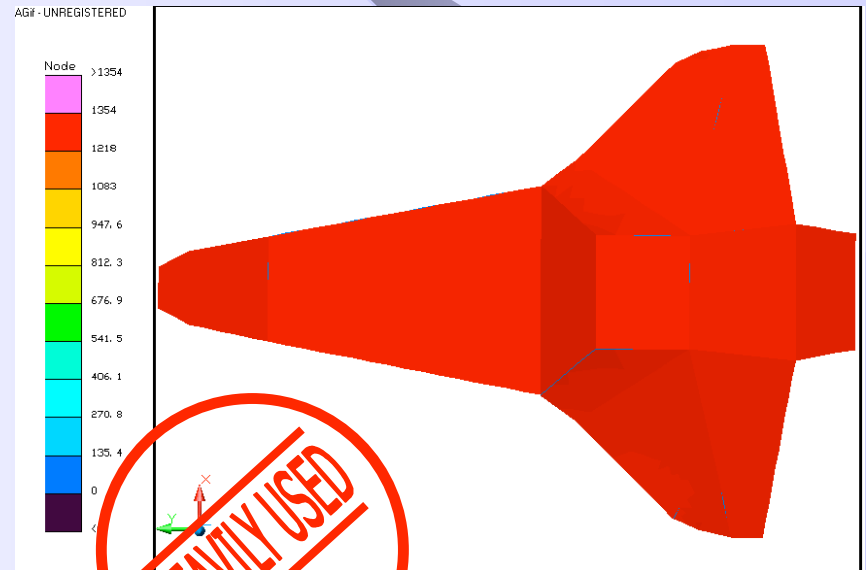
Thermaldesktop®, Radcad®, Sinda/Fluint®

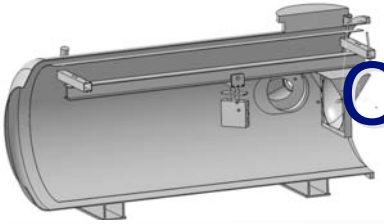


Main features:

1. FE-FD-Monte Carlo modellers
2. Definition of optical properties vs. spectrum
3. Orbital heat rates simulator

On next release (early 2007)
volumetric absorption available





Optical tests equipment: lasers

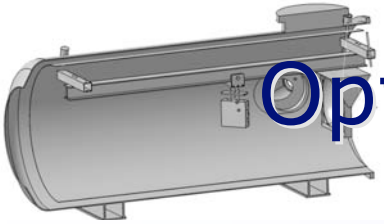
Optical bench (1.5 X 2.5 m²) and optical equipment available from the Labs' gravitational wave group. We bought the lasers and the beam profilers



Laser MONOLAS -532-100-SM (Nd-Yag, 532 nm, diode pumped) Class IIIB 100 mW

Laser He-Ne 1145 (633 nm, gas) Class IIIB 22.5 mW



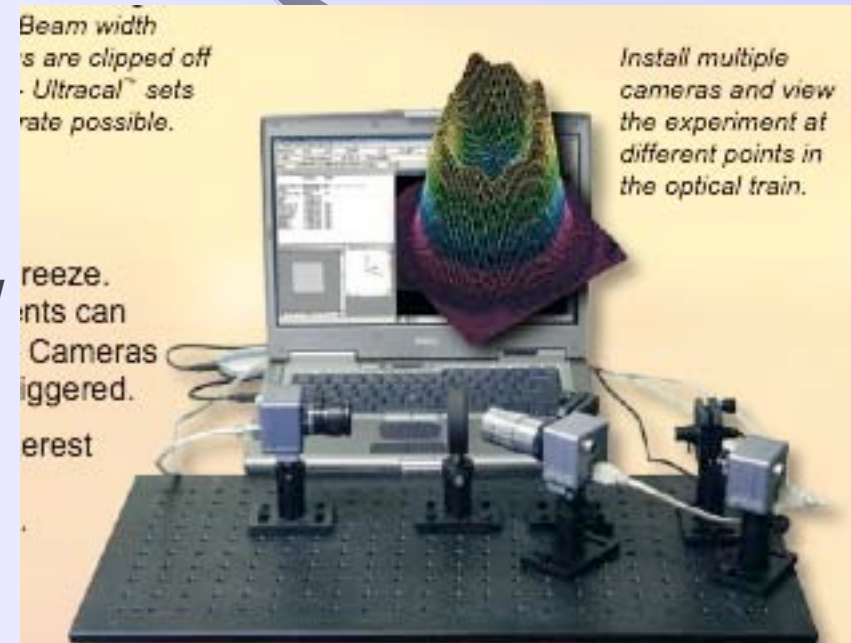


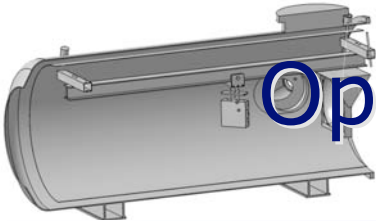
Optical pre-launch characterization

Test 1: measurement of the Far-Field Diffraction Pattern (FFDP).

- Optical bench
- Prototype (LAGEOS, LARES, GPS3...)
- Lasers
- Spyricon laser beam profilers (software and camera, PC firewire system)

Repeat test above with the prototypes inside the SCF...





Optical pre-launch characterization

Test 2: ranging test.

Close cooperation with NASA-GSFC and ILRS (will also contact G. Bianco/ASI for help on the pulsed laser)

- Laser timing unit (start time)
- Microchannel plate photomultiplier (or equivalent device for stop time). Streak Camera in use @ LNF!
- Mirror to widen the laser beam to typical dimensions in space at LAGEOS or GPS3 size

Repeat test above with the prototypes inside the SCF...

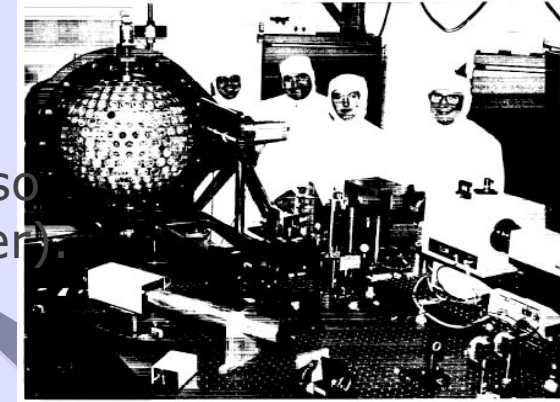
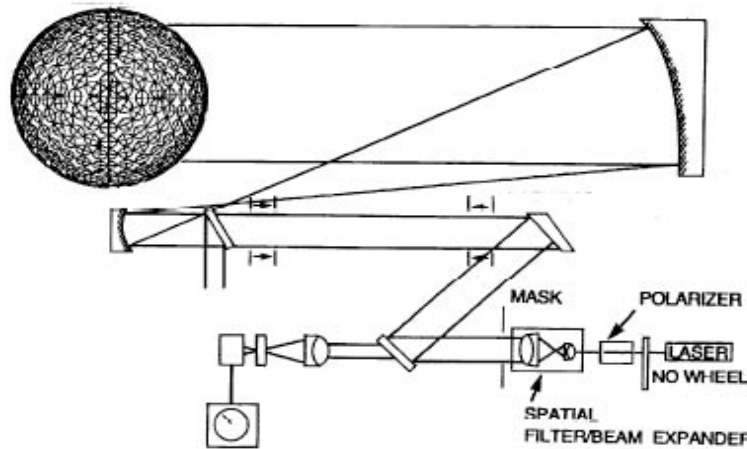


Figure 1.1-1. The Laser Geodynamic Satellite (LAGEOS-2).

NASA
Technical
Paper
3400

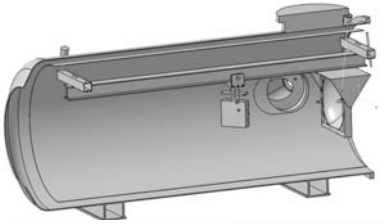
1993

Prelaunch Optical
Characterization of the
Laser Geodynamic Satellite
(LAGEOS 2)

Peter O. Minott and
Thomas W. Zagwodzki
Goddard Space Flight Center
Greenbelt, Maryland

Thomas Varghese and
Michael Seldon
Allied Signal Aerospace Company
Seabrook, Maryland



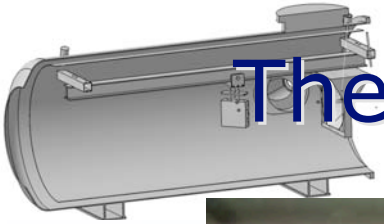


Testing LAGEOS

LAGEOS I/II are orbiting the Earth since many years. They are mainly bulk spheres with lots of CCRs.

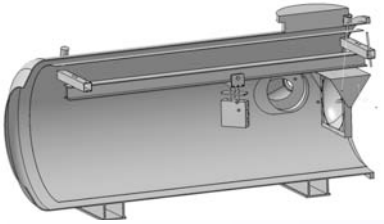
The temperature distribution of each component of the satellites is crucial for the evaluation of the Thermal Trusts (TTs), in order to measure the Lense-Thirring effect (LT) better than 1%.



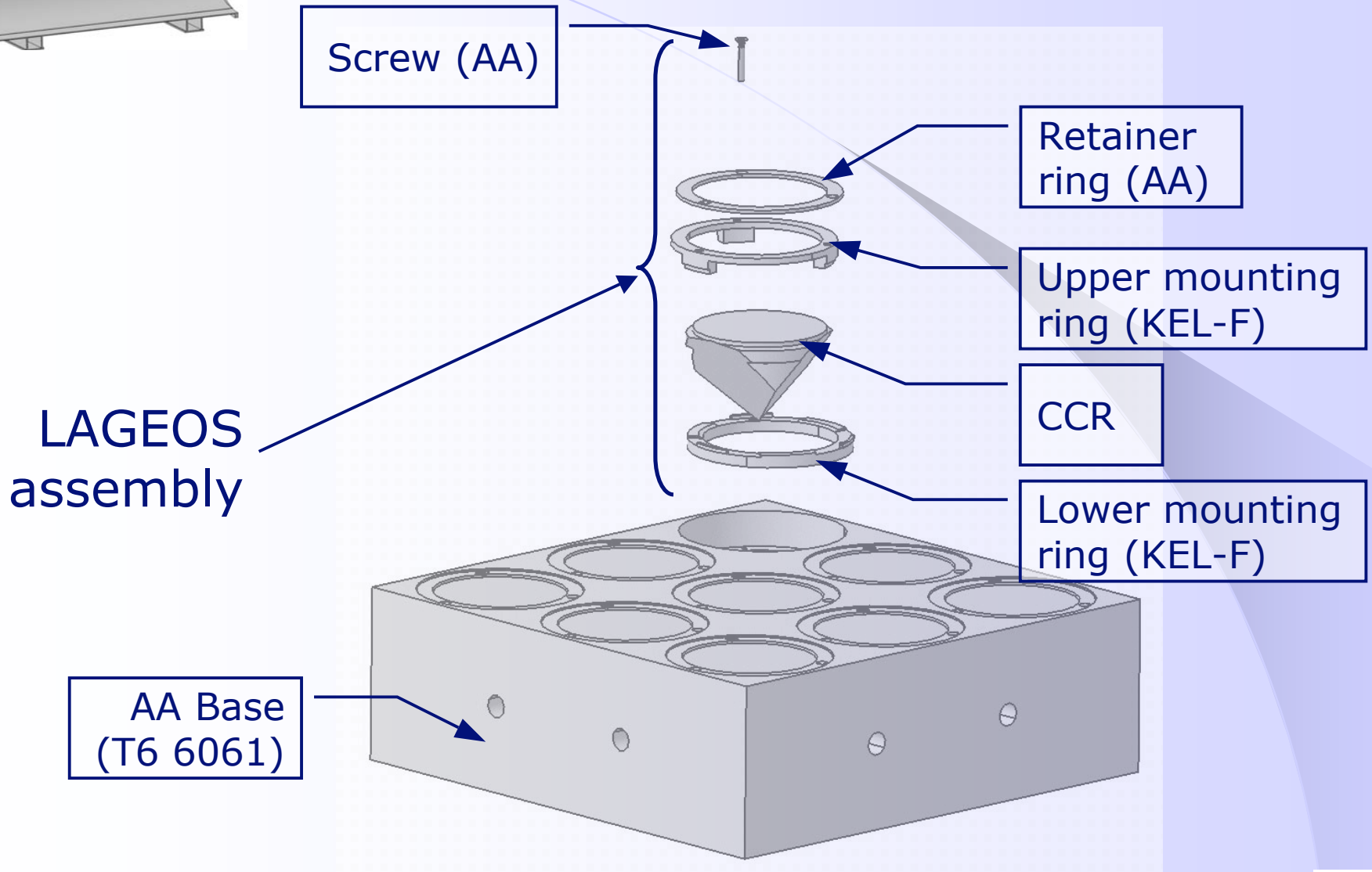


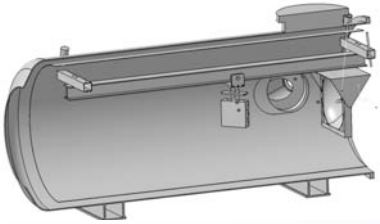
The LAGEOS Prototype: CCRs matrix





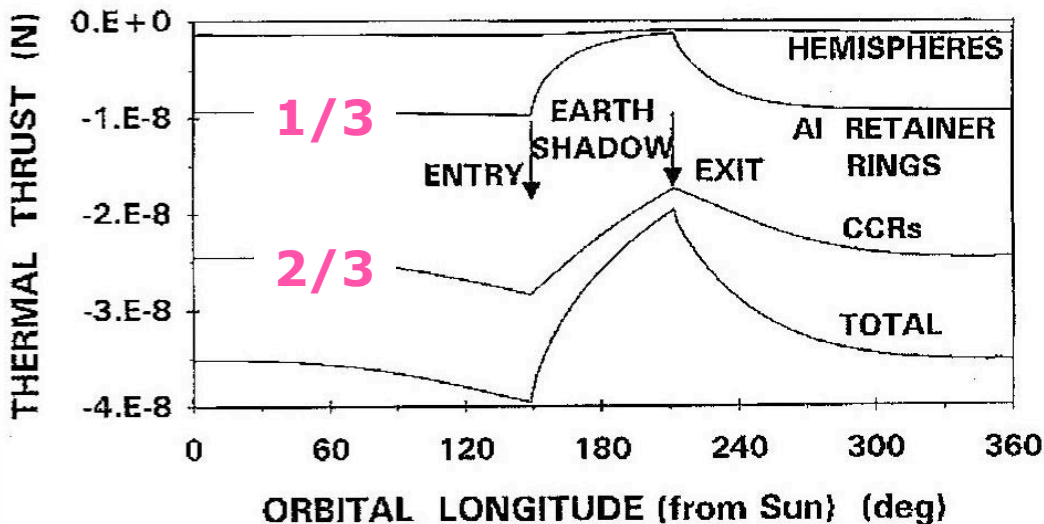
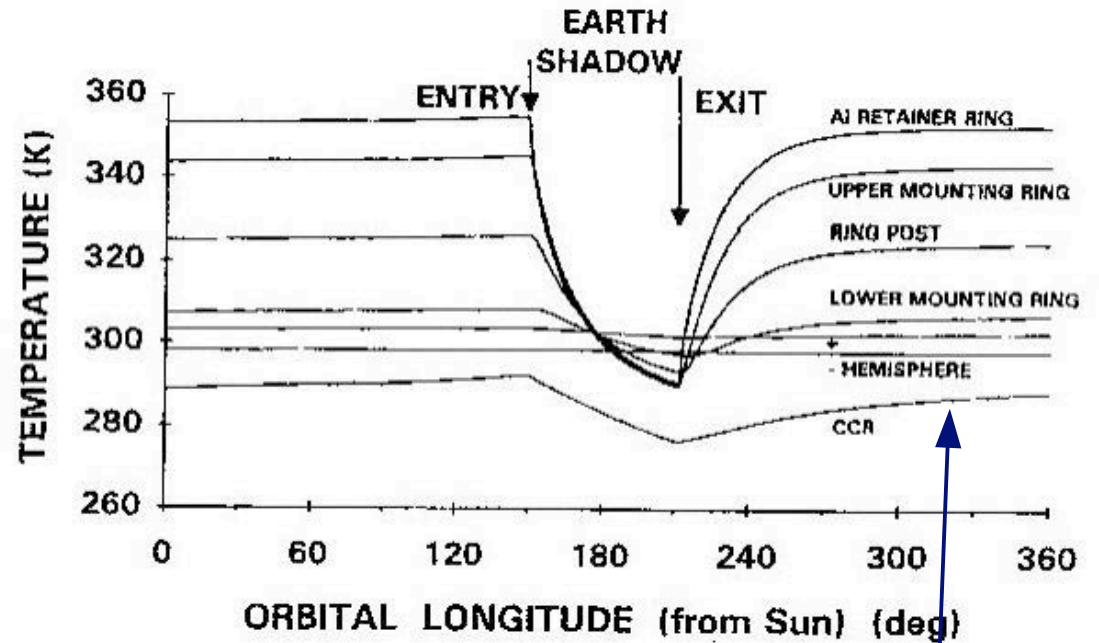
The LAGEOS CCR assembly



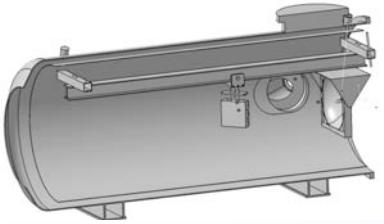


Thermal gradients & thrusts

Sunlit pole of LAGEOS
 Figures and calculations
 by Victor J. Slabinski,
 Cel. Mech. Dyn. Astr.
 vol.66, 131-179 (1997)



CCR thermal relaxation time, τ_{CCR}

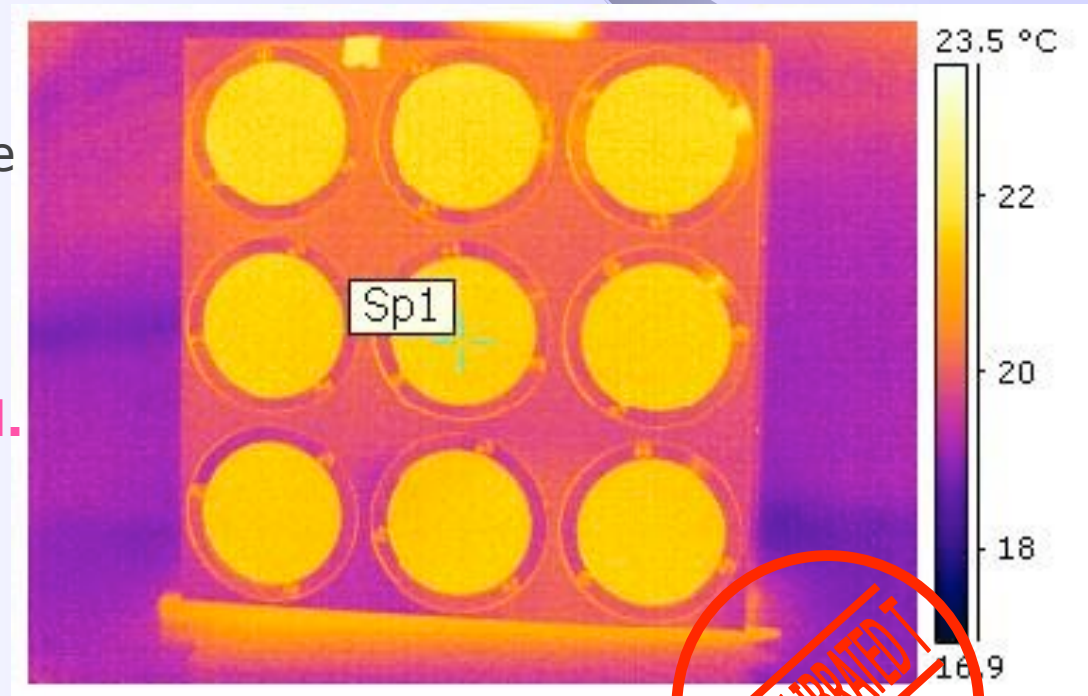


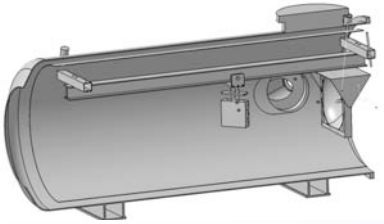
The 3x3 LAGEOS CCR matrix

The bulk of the satellite can be considered at constant temperature (matrix inside the SCF will be thermalized at 300 K with TEC)

The CCR assembly is exactly the same of LAGEOS to evaluate its thermal behaviour

T measurement of the base with IR camera is not crucial.



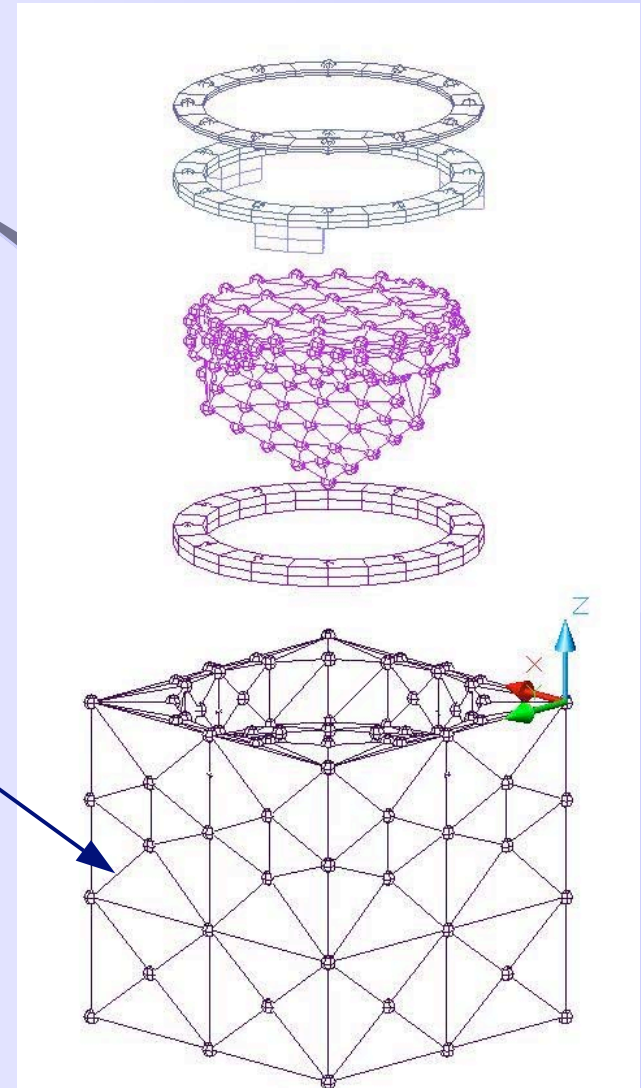


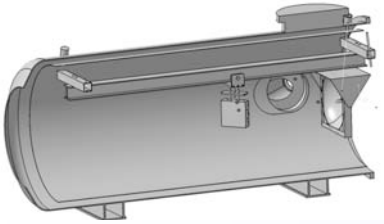
The Thermal Model

Preliminary.

1. Volumetric IR absorption in the CCR not yet simulated (sw modification 2007)
2. Thermal resistance of all interfaces simulated. Critical. It really needs to be measured

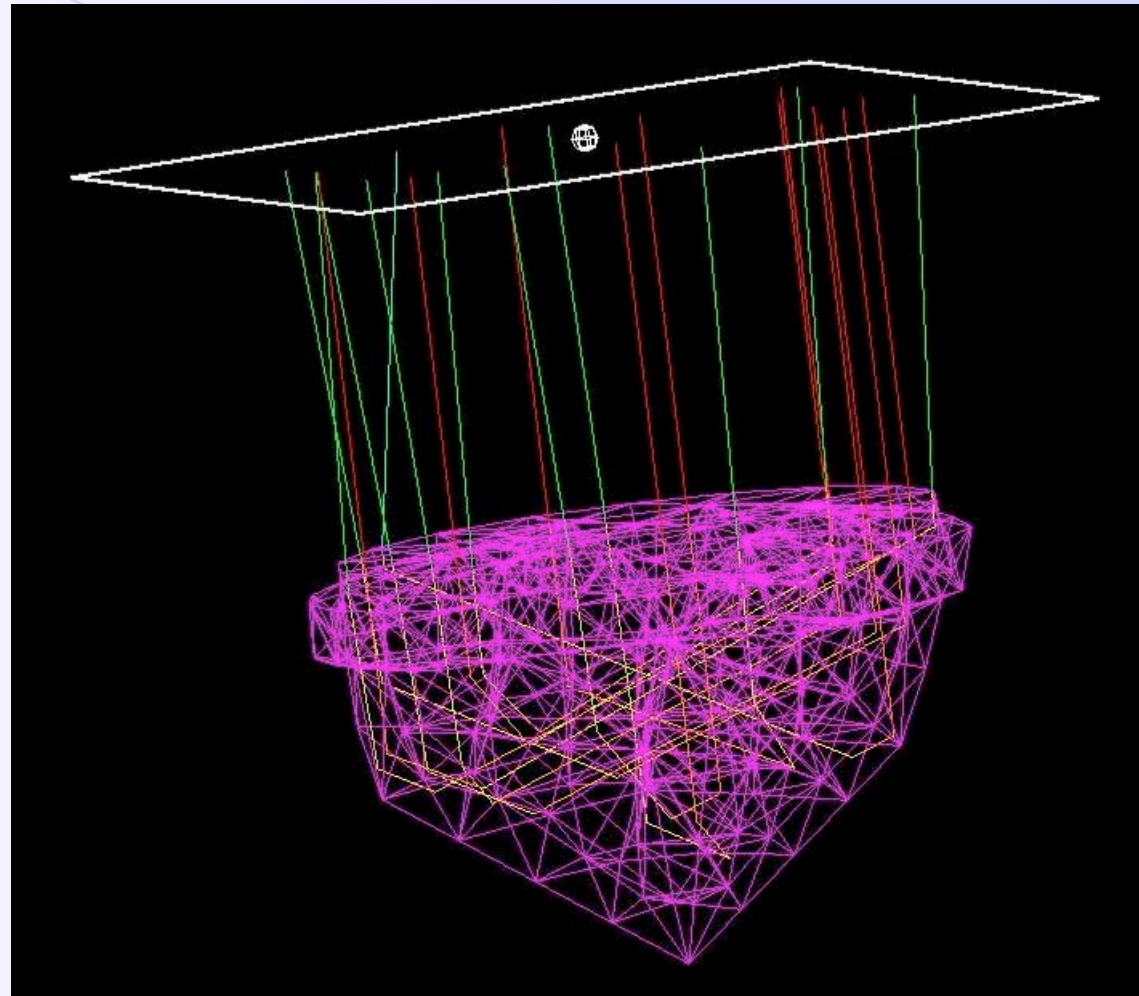
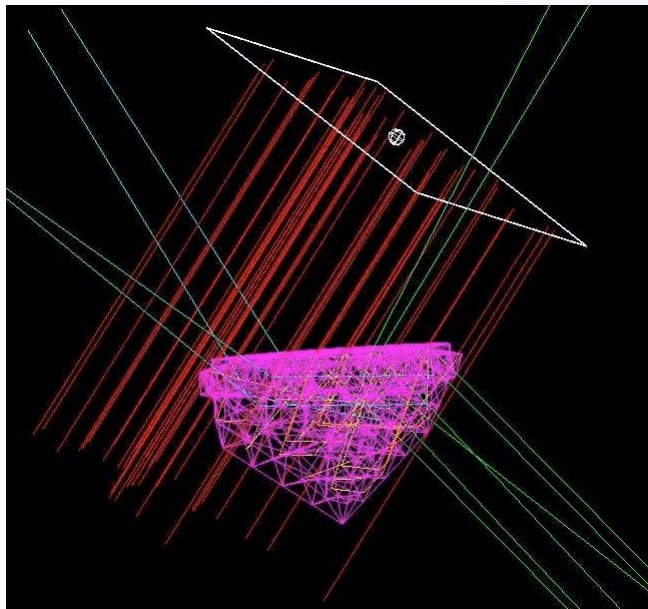
Temperature of AA Base fixed (CCR IR emission evaluation)

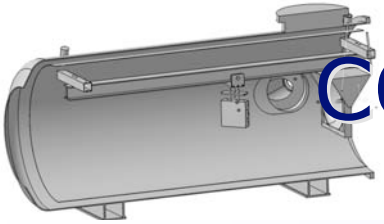




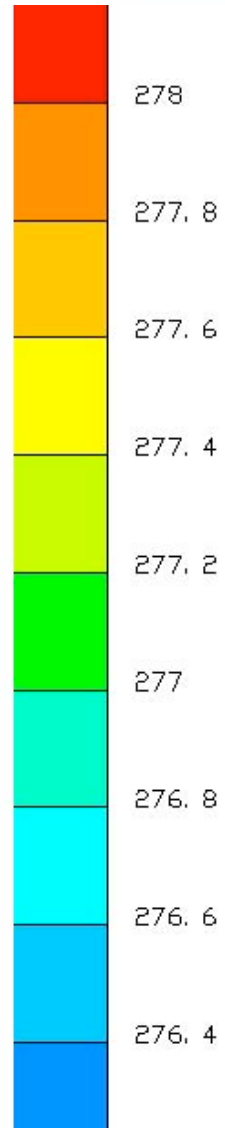
Optical property simulation

RadCad module
simulates total internal
reflection

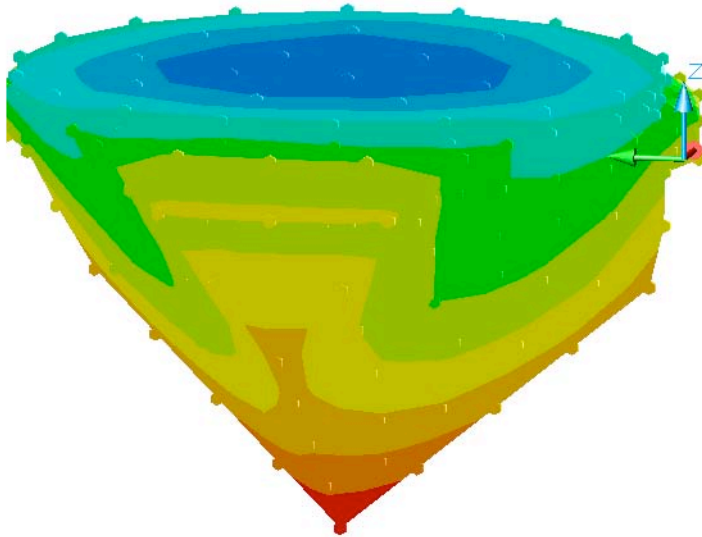




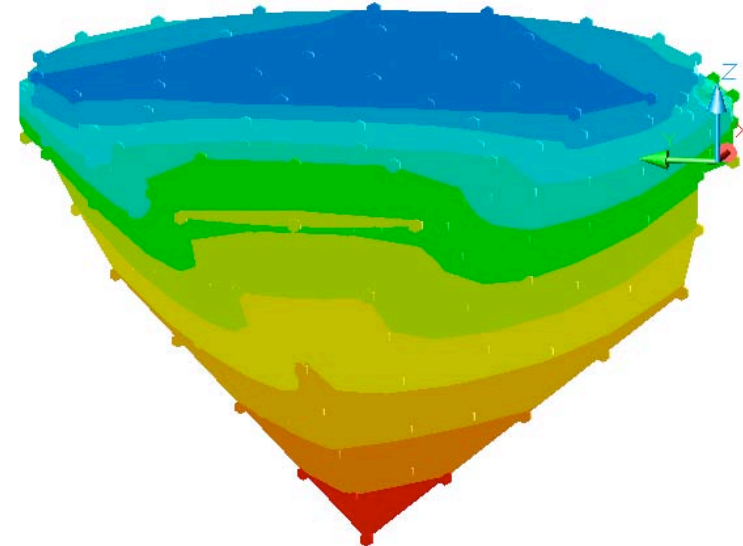
CCR T plot, $T_{\text{base}} = 300 \text{ K}$, Sun on

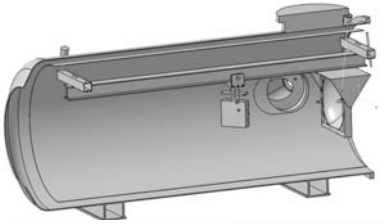


T (K) at $t = 2800 \text{ sec}$



T (K) at $t = 12000 \text{ sec}$



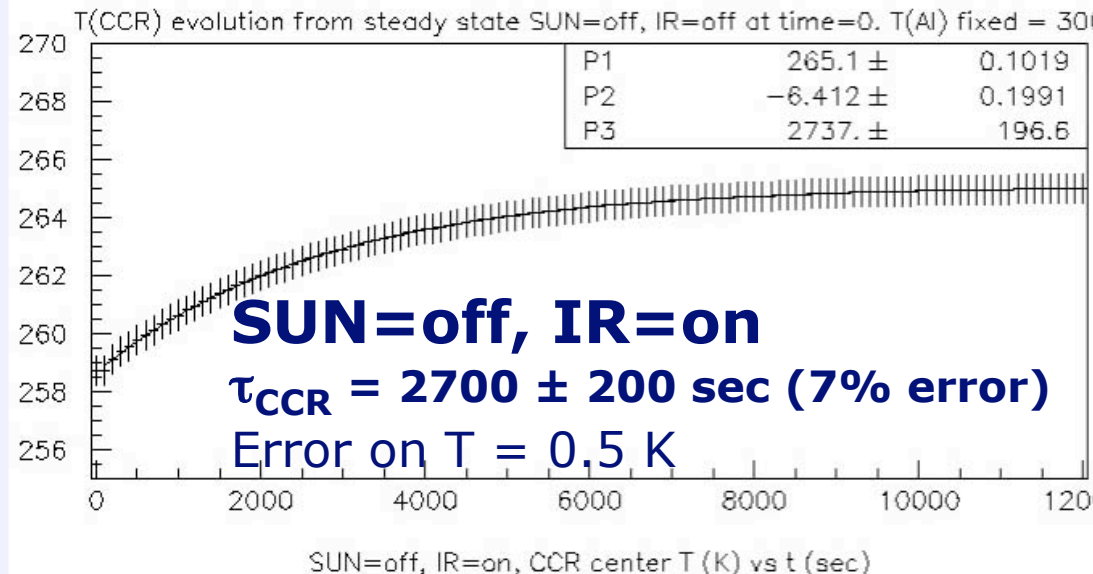
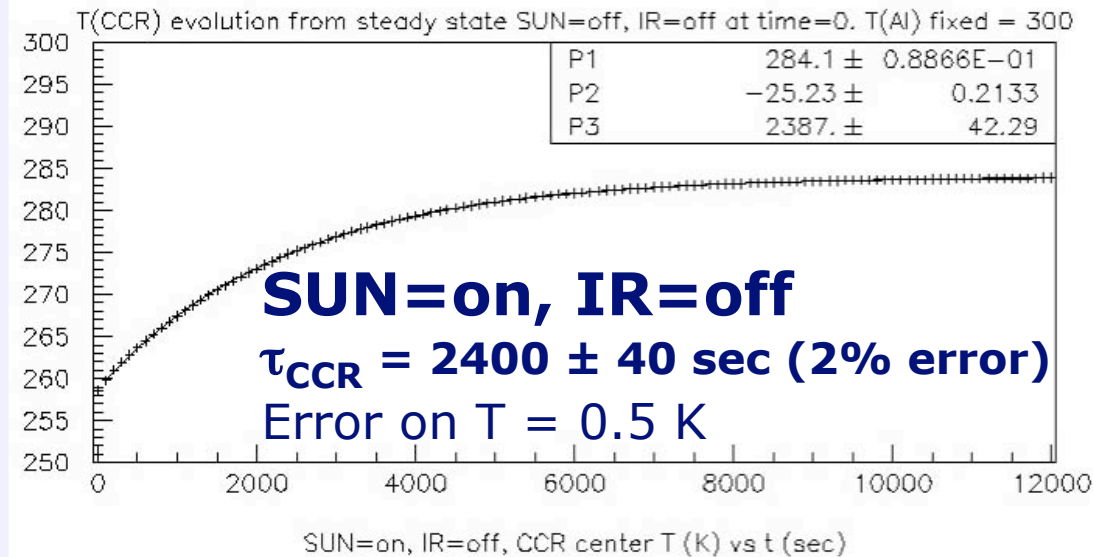


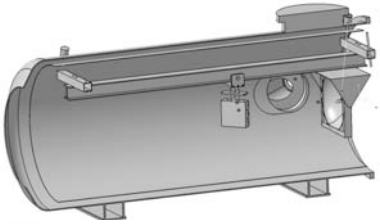
Transient simulation Temp (K) vs time (sec)

The LAGEOS τ_{CCR} has never been measured. In the literature estimates vary from 2000 sec to 7000 sec, ie by **250%**. This implies a **2%** error on the LT effect due the TTs (I. Ciufolini).

Our goal: measure τ_{CCR} at **5% accuracy**. This will give a **0.04%** error on LT due to TTs.

With a ≤ 0.5 K accuracy on thermometry this goal is within (**statistical**) reach.





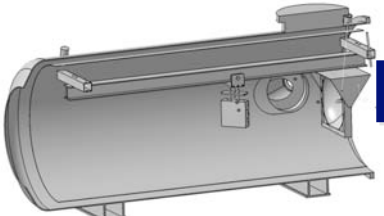
LARES new design: "shell over the core"



The idea is to bring some of the solar radiation (the parts which are not reflected by the CCR) to the "night side" of the satellite.

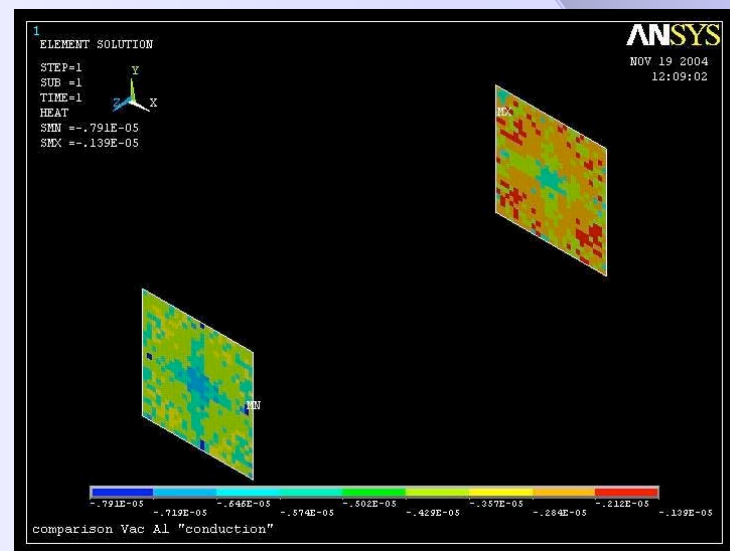
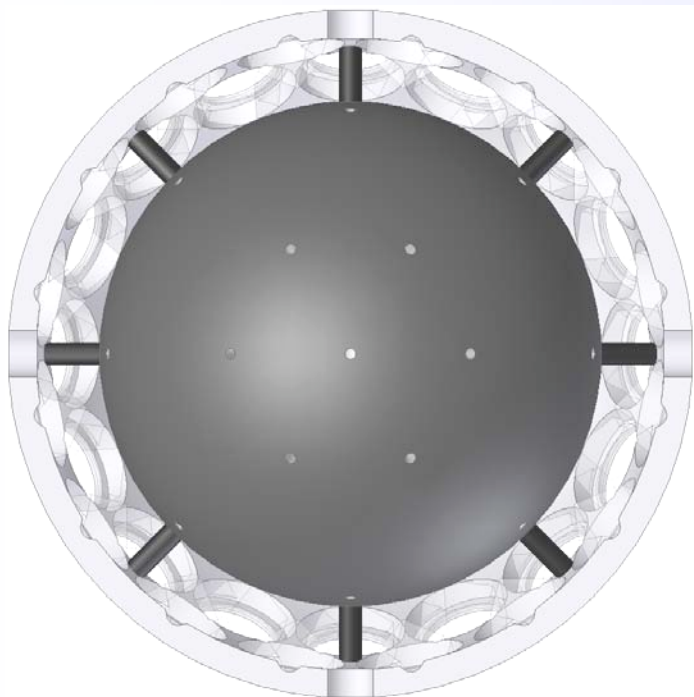
Also the IR radiation re-emitted by the back of each CCR propagates to the night side due to the new geometry

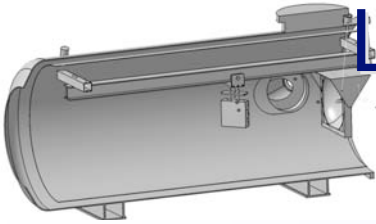
The outer shell houses the CCRs, while the inner sphere (Tungsten made) gives mass and support to the shell. Total weight is ~ 100 Kg



LARES "shell over the core"

The void between shell and sphere puts the corner side of all CCRs in "radiative contact" (vacuum conducts better than Al). This should lead to a more uniform temperature among the CCRs and a lower thermal gradient along the CCR axis

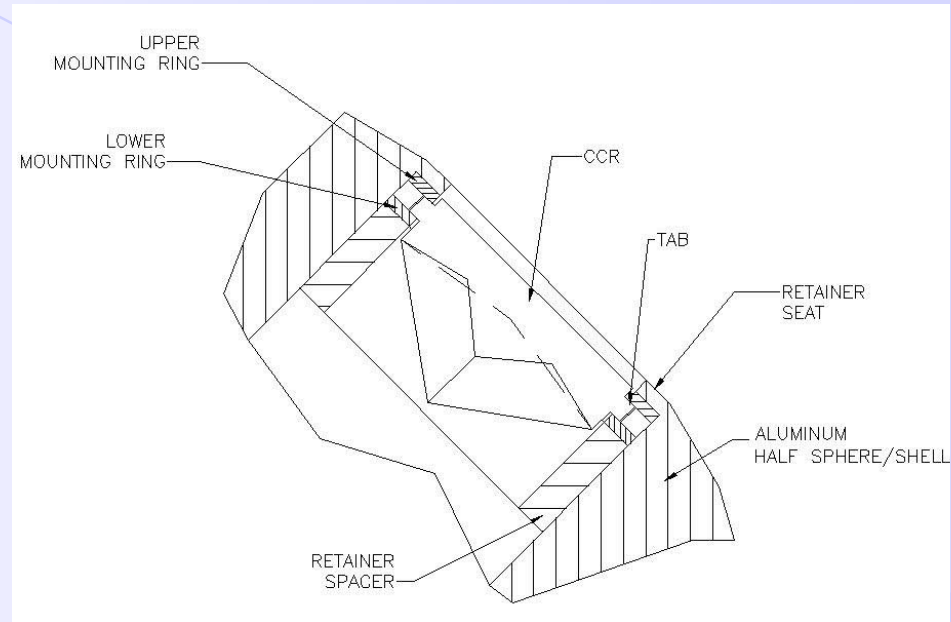




LARES "shell over the core": back mounting

This design allows the CCR
"back mounting" option too.

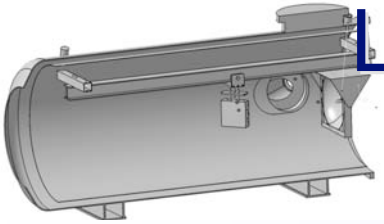
The retainer ring is replaced by
a retainer seat machined
directly on the shell. This
removes **1/3** of the TTs
according to the Slabinski
paper.



Details can be found in: www.inf.infn.it/acceleratori/lares:

G. Delle Monache: *LARES satellite thermal design: proposal for the limitation of thermal trust* – INFN LNF LARES tech note 2

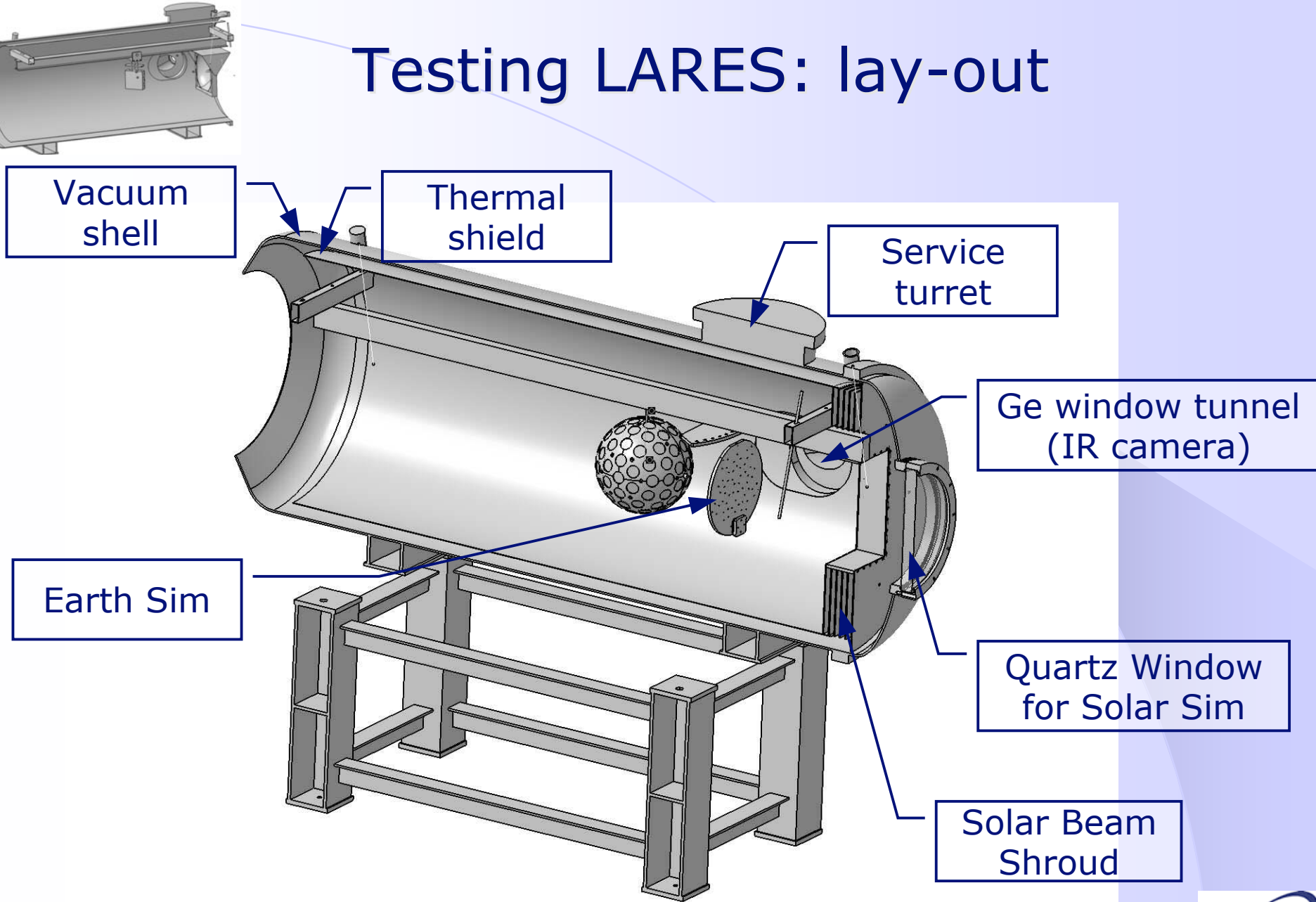
G. Delle Monache: *LARES thermal design: comparison between Al and Vacuum "conduction" between two plates* - INFN LNF LARES tech note 1

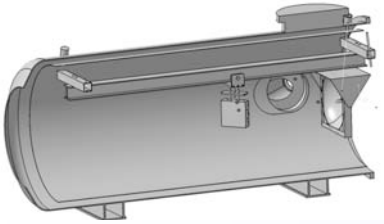


LARES "shell over the core": 1/2 size prototype



Testing LARES: lay-out

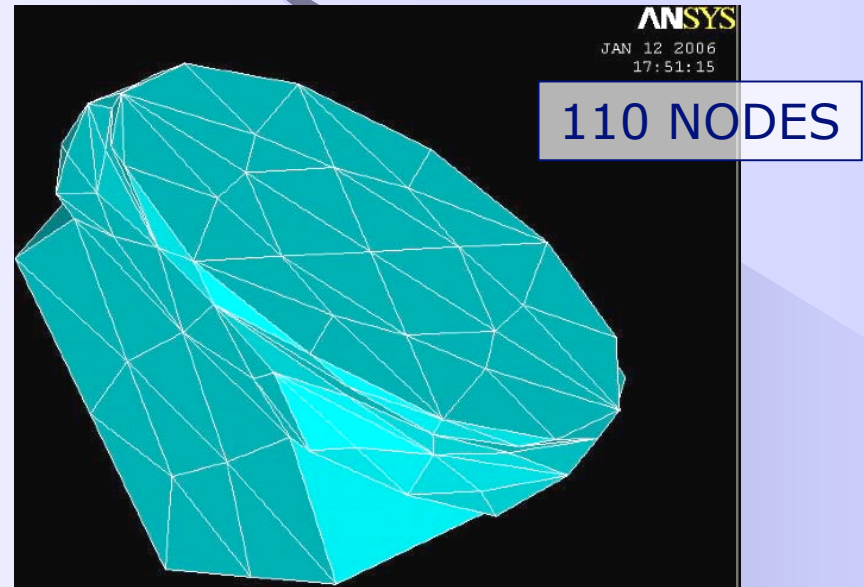


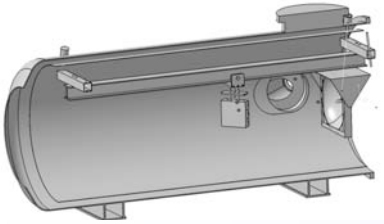


Modeling LARES

C&R declared that their customers never run a model with more than **20.000** nodes. Considering that the spacecraft sets 102 CCRs, the goal is to model each reflector with 100 nodes.

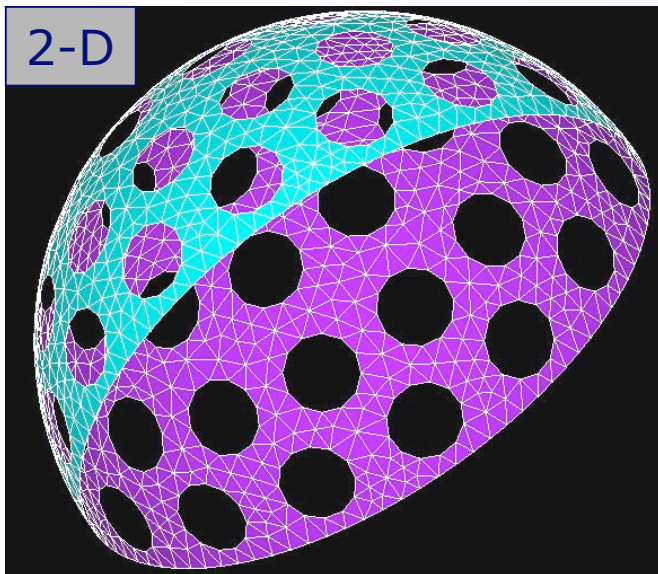
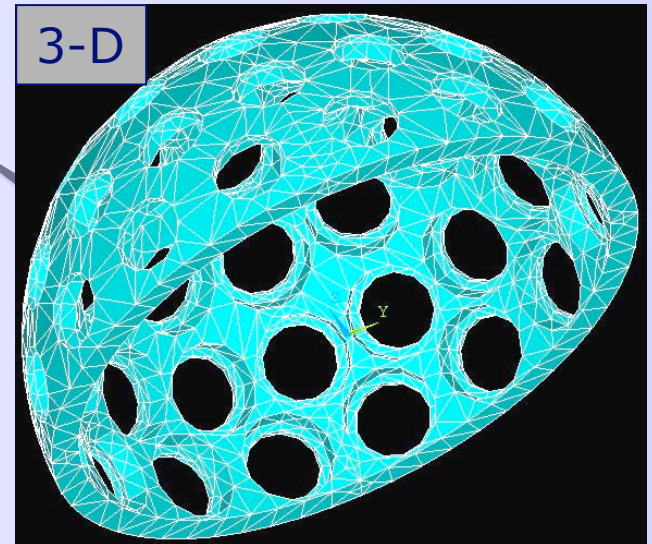
The mesh has been really **“hand made”** to (almost) reach the goal





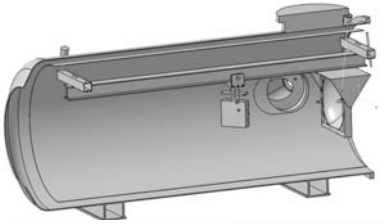
Modeling LARES

We are preliminary studying the mesh to figure out various options which simplify the geometry without relevant effects on the thermo-optical behavior of the model.



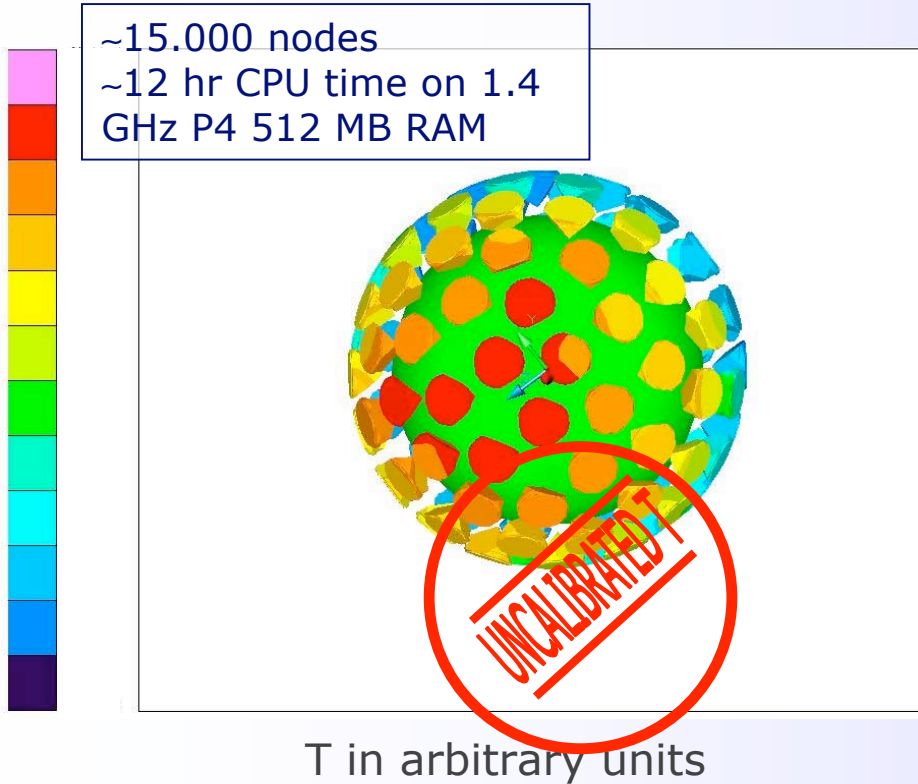
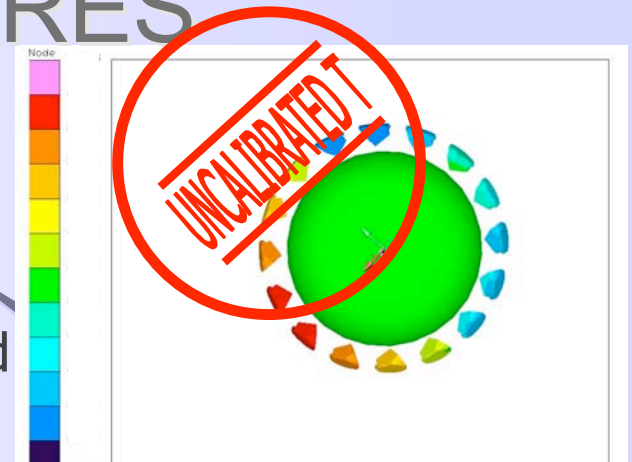
Once the model is done and tuned on the prototype tested in the SCF we can:

1. Optimize optical properties of the satellite components to **"uniform"** its temperature thus limiting TTs
2. Help on the evaluation of the **residual** TTs



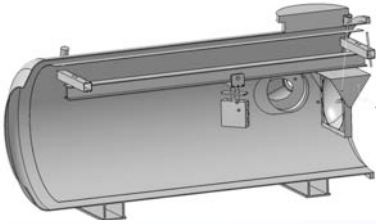
Modeling LARES

Even if the project is at an early stage a model of a consistent mesh has been run to evaluate the impact of such complicated model on the sw/hw architecture



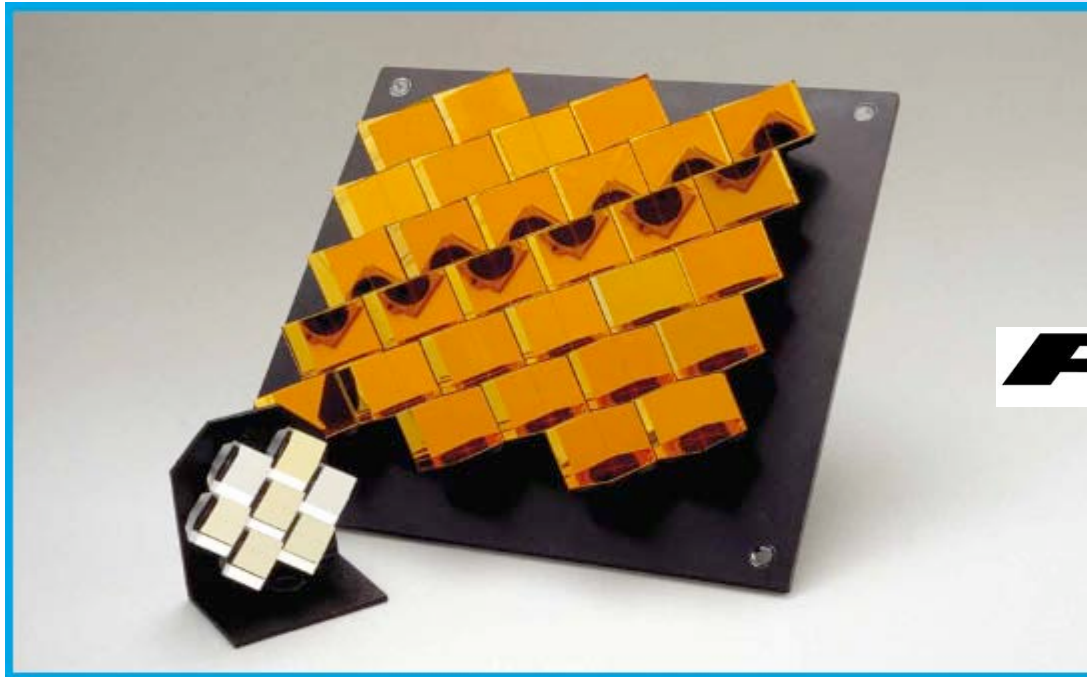
The test was successful. Even if the result shows just "a couple" of modeling bugs somewhere, the sw/hw system works!





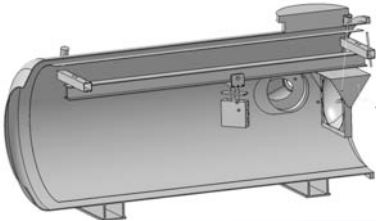
Beryllium Hollow Cube RR for GPS3

ILRS, NASA-GSFC proposal for retroreflector (RR) arrays on the GPS3 system to be flown from 2011 on. Be hollow RR previously used in space to be tested according to new orbital conditions.



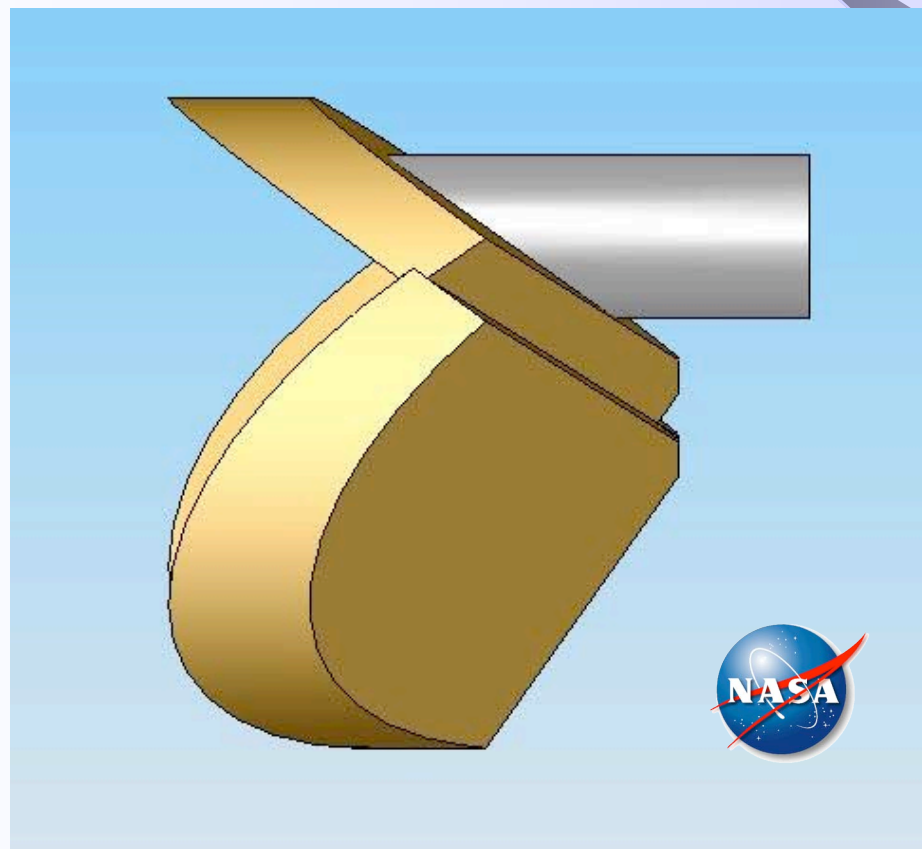
PLX

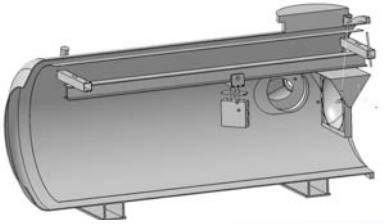




Beryllium Hollow Cube RR for GPS3

The hollow cube RR could also be integrated in the Lares "shell over the core" design





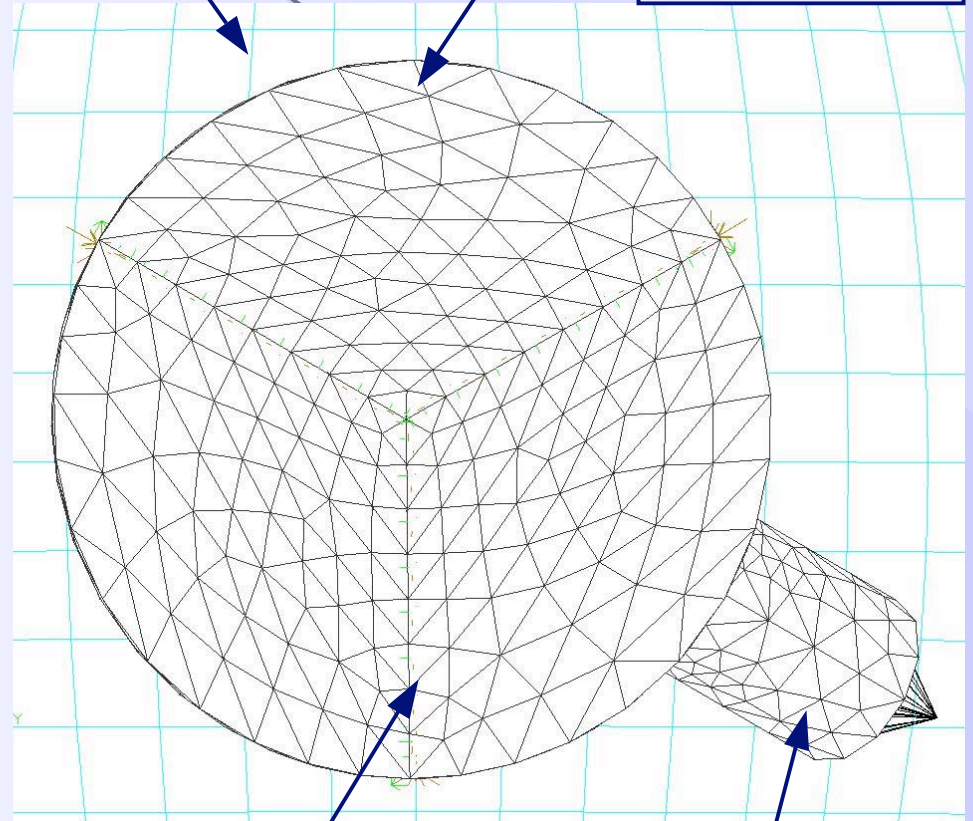
Beryllium Hollow Cube RR for GPS3

"Fake"
spacecraft

Be plane

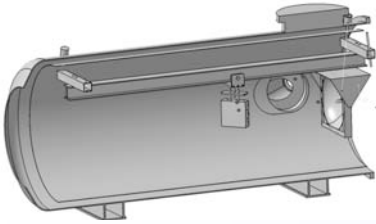
RR modeled with
ThermalDesktop; bonding
effects between the 3
planes and the post
modeled

Very crude spacecraft model:
an Al half-sphere
surrounding the RR



Stycast bonding
(10W/K)

Post



Beryllium Hollow Cube RR for GPS3

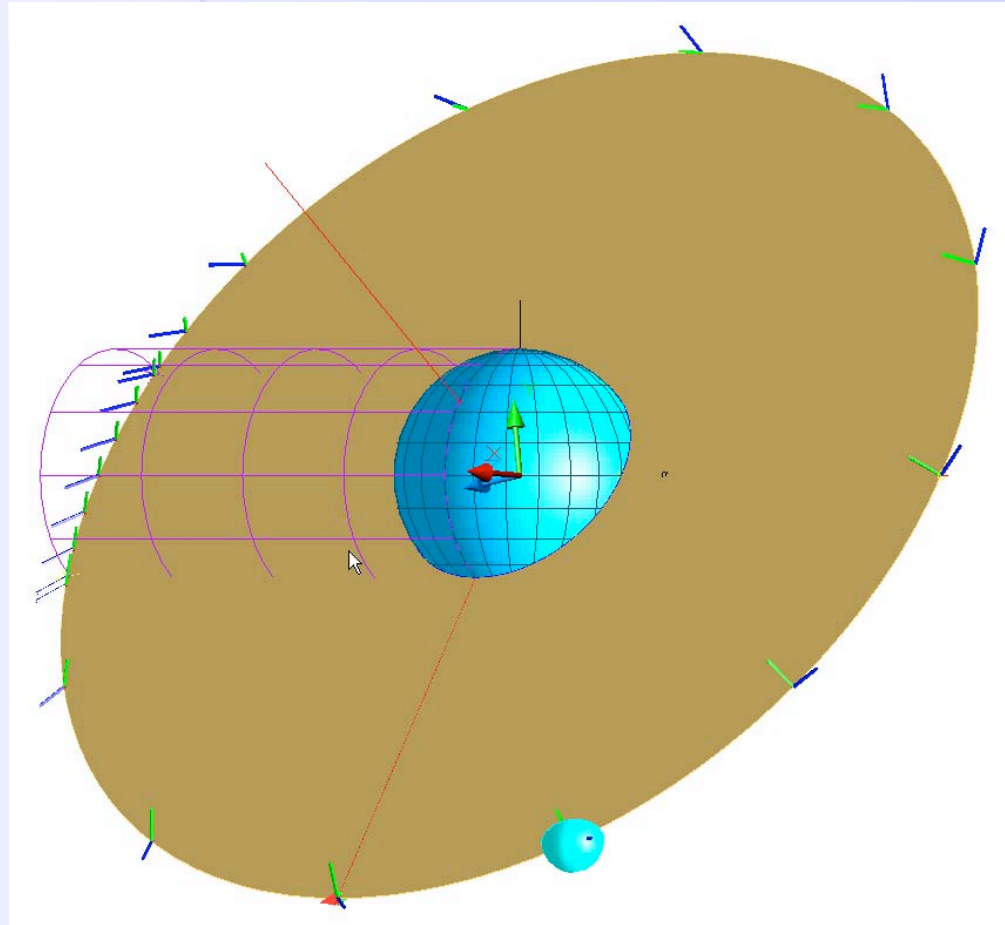
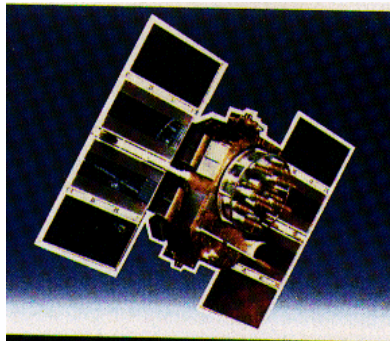
Orbital heat rate evaluated on
GPS-35 orbit:

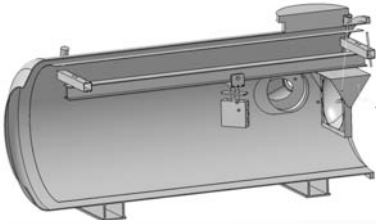
Orbit incl.: 54°

Max altitude: 20195 km

Eccentricity: 0

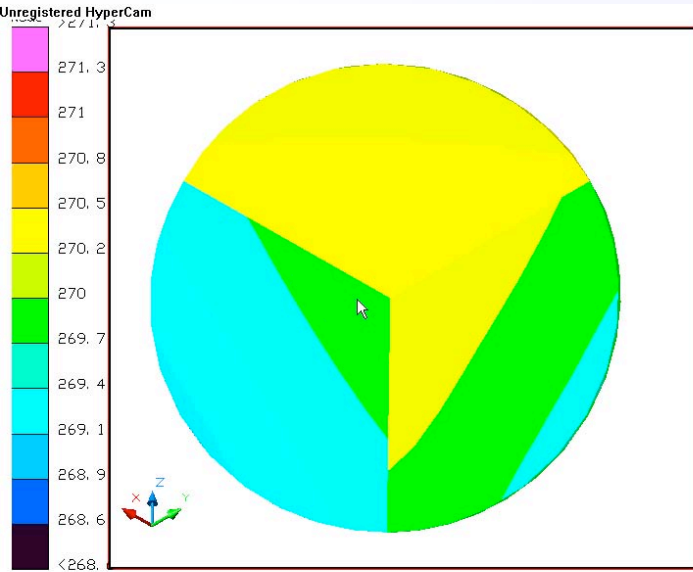
Ar. Periapsis: 270°





Beryllium Hollow Cube RR for GPS3

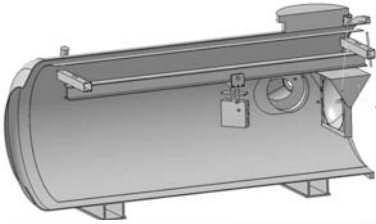
Environment and thermo-optical parameters



	Conductivity (W/m K)	Specific Heat (J/kg K)	Density Kg/m ³	C _p x ρ (J/m ³ K)
Be I-70	216.0	1920.0	1850.0	3.552 x 10 ⁶
AA 6061-T6	167.0	900.0	2700.0	2.430 x 10 ⁶
Zerodur	1.6	810.0	2530.0	2.049 x 10 ⁶

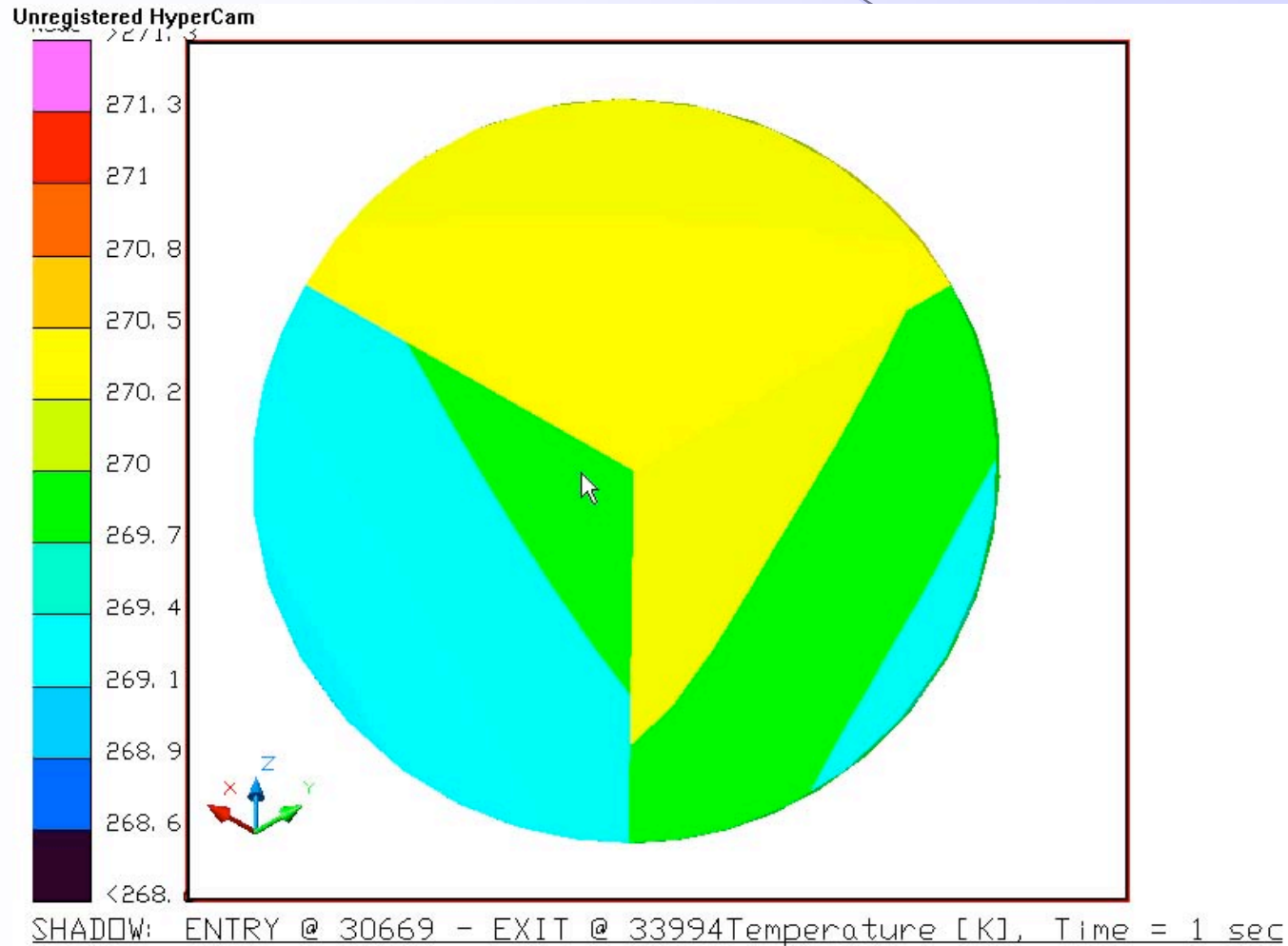
Solar (W/m ²)	Planetary IR (W/m ²)	Albedo
1420	240	0.35

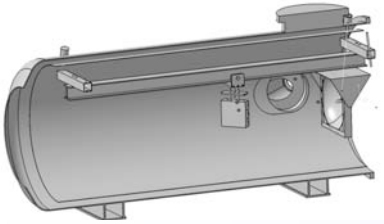
Finish	Location	BOL α	BOL ε	EOL α	EOL ε
VDS	Front RR	0.04	0.05	0.08	0.03
White Paint	Back of RR	0.17	0.92	0.40	0.87
Black Paint	Inside of Shiel.	0.95	0.95	0.95	0.95



Beryllium Hollow Cube RR for GPS3

Preliminary results; next step is to collect more detailed information about RR/spacecraft heat exchange





Conclusions

The group is building an SCF to characterize high-accuracy laser-ranged test masses to probe gravity in near Earth orbits.

The group is designing a new prototype of LARES to drastically decrease Thermal Trusts

In the simulation we evaluated τ_{CCR} with a preliminary 3% statistical accuracy. We verified that τ_{CCR} scales as $1/T^3$

If we reduce and control TTs as planned then also the perigee might be useful to measure the LT and to search for new physics

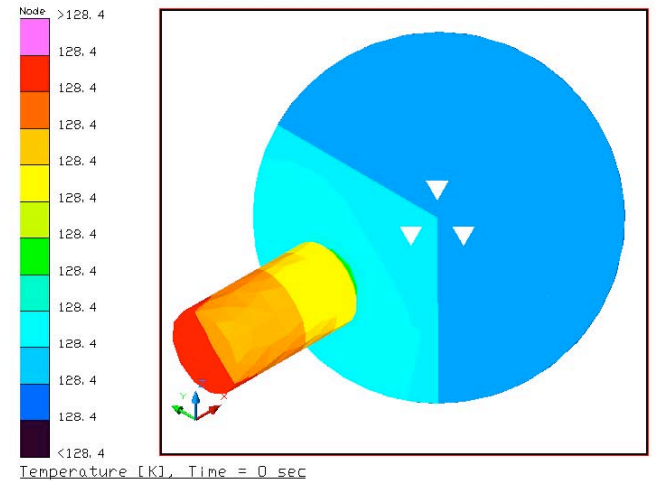
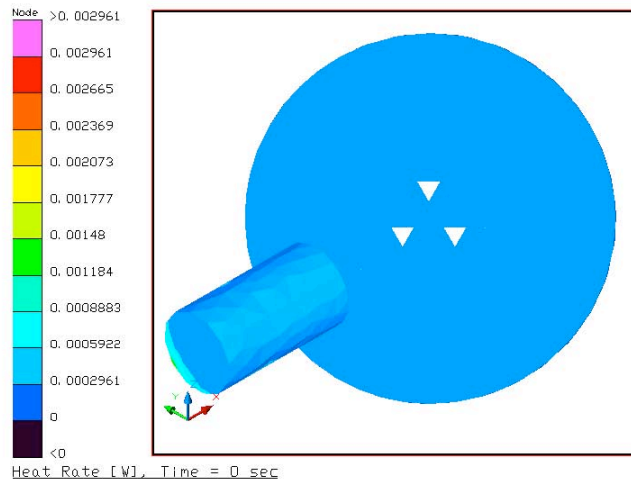
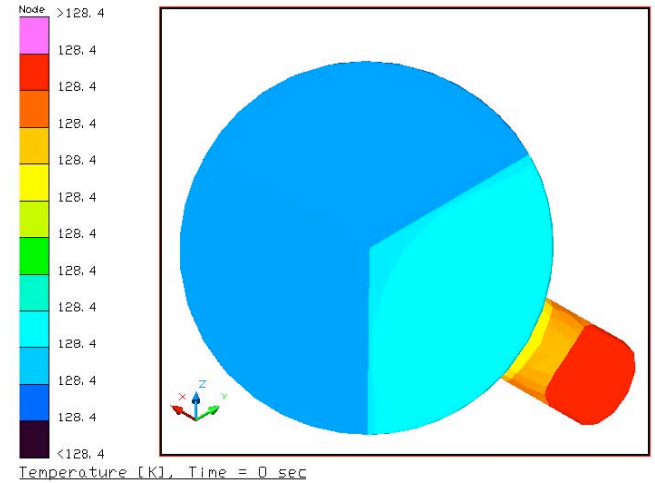
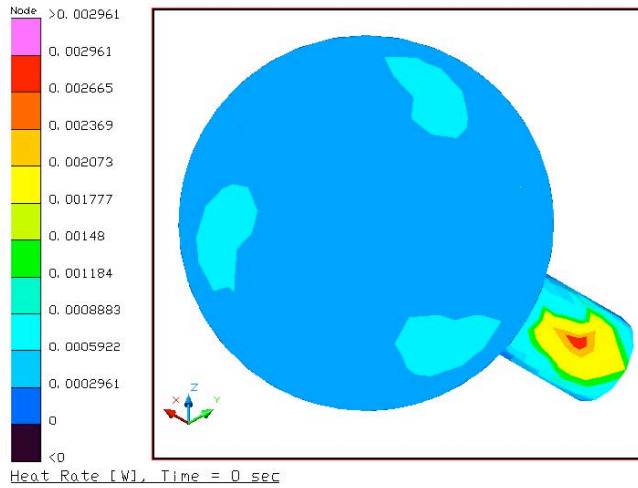
The SCF is also well suited to study the performance of hollow retro-reflectors for GNSS constellations

Steady State Analysis Earth (CCR front) radiation

Q [W]

BOL

T [K]



Orbital Analysis CCR central node

BOL



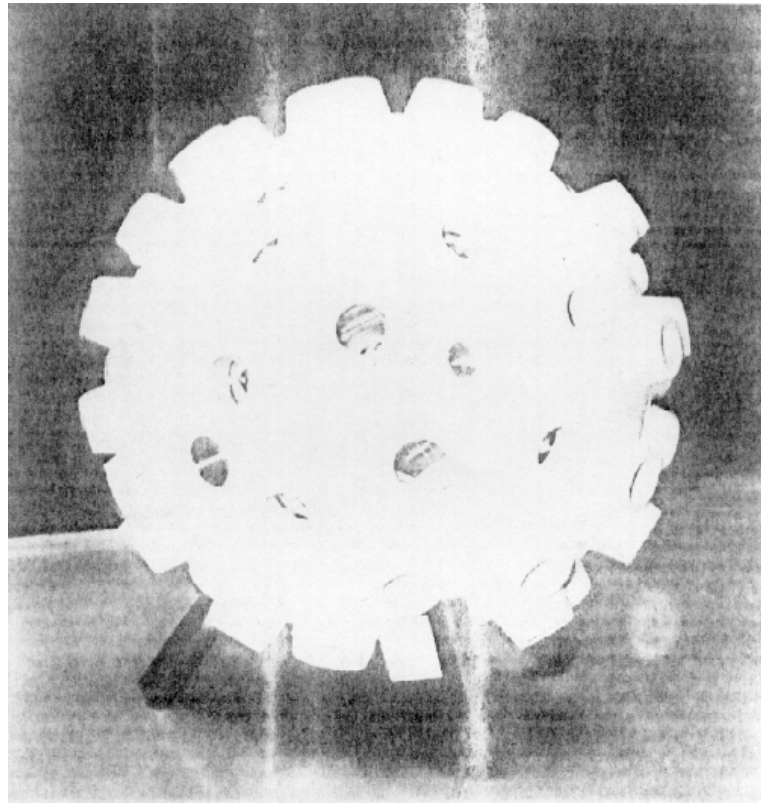
WESTPAC DESIGN

Launched 10 July 1998

First returns from REAL Westpac on 23 July
1998

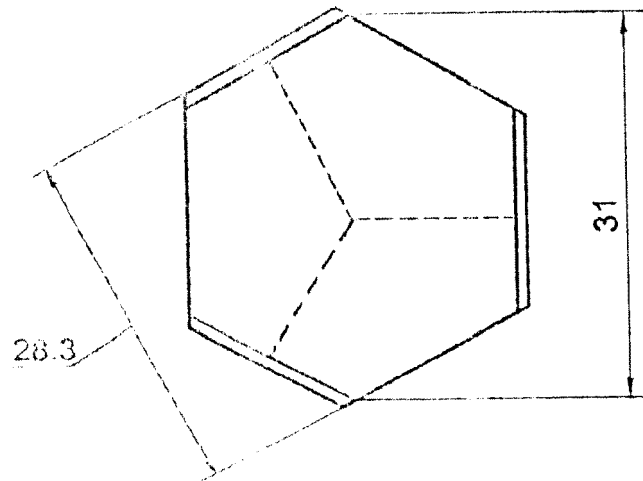
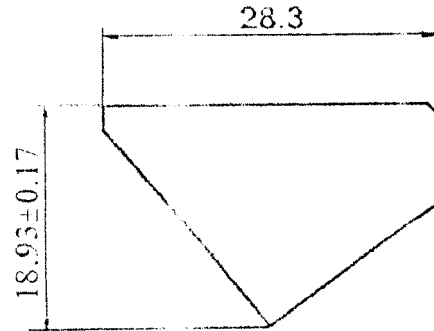
WESTPAC RETROS WERE DESIGNED TO EXPLORE THE “FIZEAU EFFECT”

Best photo available on my computer yesterday – sorry!

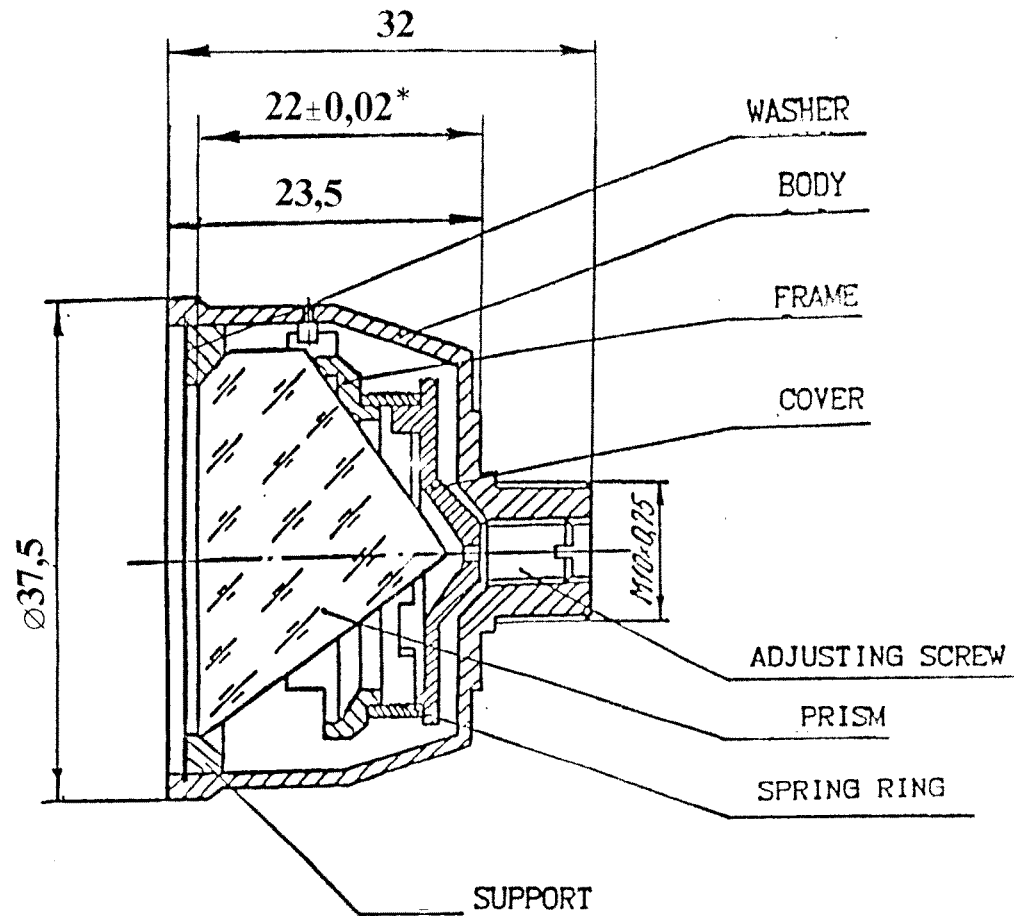


Diagrams from RISDE Tech Manual

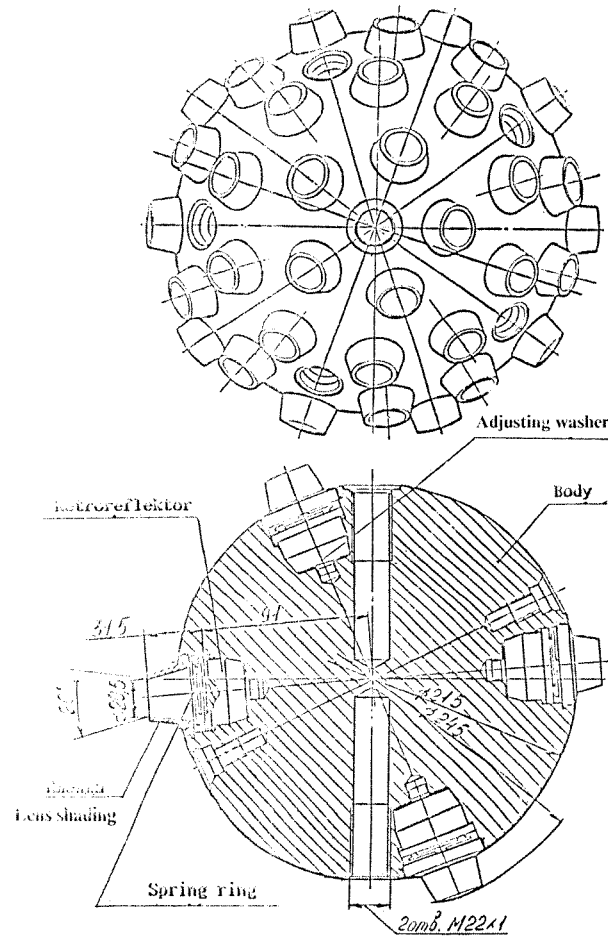
Retroreflector glass is Fused Silica KY-1



Retroreflector in its holder



Arrangement of retroreflectors and baffles



OPTUS B RETROREFLECTOR DESIGN

Geostationary Orbits

Longitudes 156 and 160 deg East

Optus B1 launched 24 August 1992

Optus B2 crashed in China after launch

Optus B3 launched 1993

RETRO SPECS

- Flat tray 20 cm x 18 cm containing 14 solid corner-cube retroreflectors.
- Retro front face is tri-roundular with inscribed diameter 38 mm.
- Rear faces: Dihedral angle offset 0."8 +/- 0."3 to allow for velocity aberration 3."7 due to 2.7 km/sec speed relative to Orroral SLR/LLR station.
- Herseus fused silica, Amasil grade.

COATING

- Front face coated with Indium Tin Oxide over an anti-reflection dielectric layer.
- Rear faces coated with Indium Tin Oxide without compromising total internal reflection.
- The I.T.O. coatings actually enhance the cross section (don't ask me why, they just do!)
- Mounted to tray via Vespel O-rings.
- The I.T.O. (resistivity $< 10^9 \Omega/\text{m}^2$) and Vespel rings conduct nasty electrostatic build-up away to the bus.

PERFORMANCE

- Specific Intensity 4.5×10^6 m²/steradian (i.e. cross section give or take that 4π factor)
- Return rate from Orroal SLR on clear nights >100 returns/minute for extended periods:
- 1.5 metre telescope, 10 shots/sec at 200 mJ per shot in 150 ps, Schreiber APD detector.
- Still got returns after turning off one of the 2 laser power amplifiers (x 20?) and inserting ND's
- Returns received from Stromlo 1 (0.75 m, <100 mJ, CSPAD)

SATELLITE SPEEDS AND POINT-AHEAD, RELATIVE TO STROMLO

GLONASS retroreflector array position relative to CoM

Table 1

	X ± Δ X	Y ± ΔY	Z ± ΔZ
GLONASS-87, 89	-1582,6 ± 2	0 ± 10	0 ± 2
GLONASS-95	-1901.6 ± 3	-137 ± 3	3 ± 3

SC reference frame: zero in the SC CoM, X-axis direction – opposite to direction towards the Earth center, Y-axis direction – towards the Sun.

The array position reference point is the center of the input optical aperture (prism face plane). The prism face plane is normal to the X-axis.

The range to SC CoM determined in accordance to Table 1 is to be reduced by the optical correction value δ calculated from the following expression

$$\delta = \frac{h \cdot n}{\sqrt{1 - \frac{\sin^2 \varepsilon}{n^2}}}$$

where ε is the light incidence angle (between the beam and the perpendicular to the prism face plane), h is the prism height, and n is the prism refraction index.

At $\lambda = 532 \text{ nm}$ $n = 1.4607$; $h = 19.1 \text{ mm}$. Then

$$\delta = \frac{27.899}{\sqrt{1 - \frac{\sin^2 \varepsilon}{2.1336}}}$$

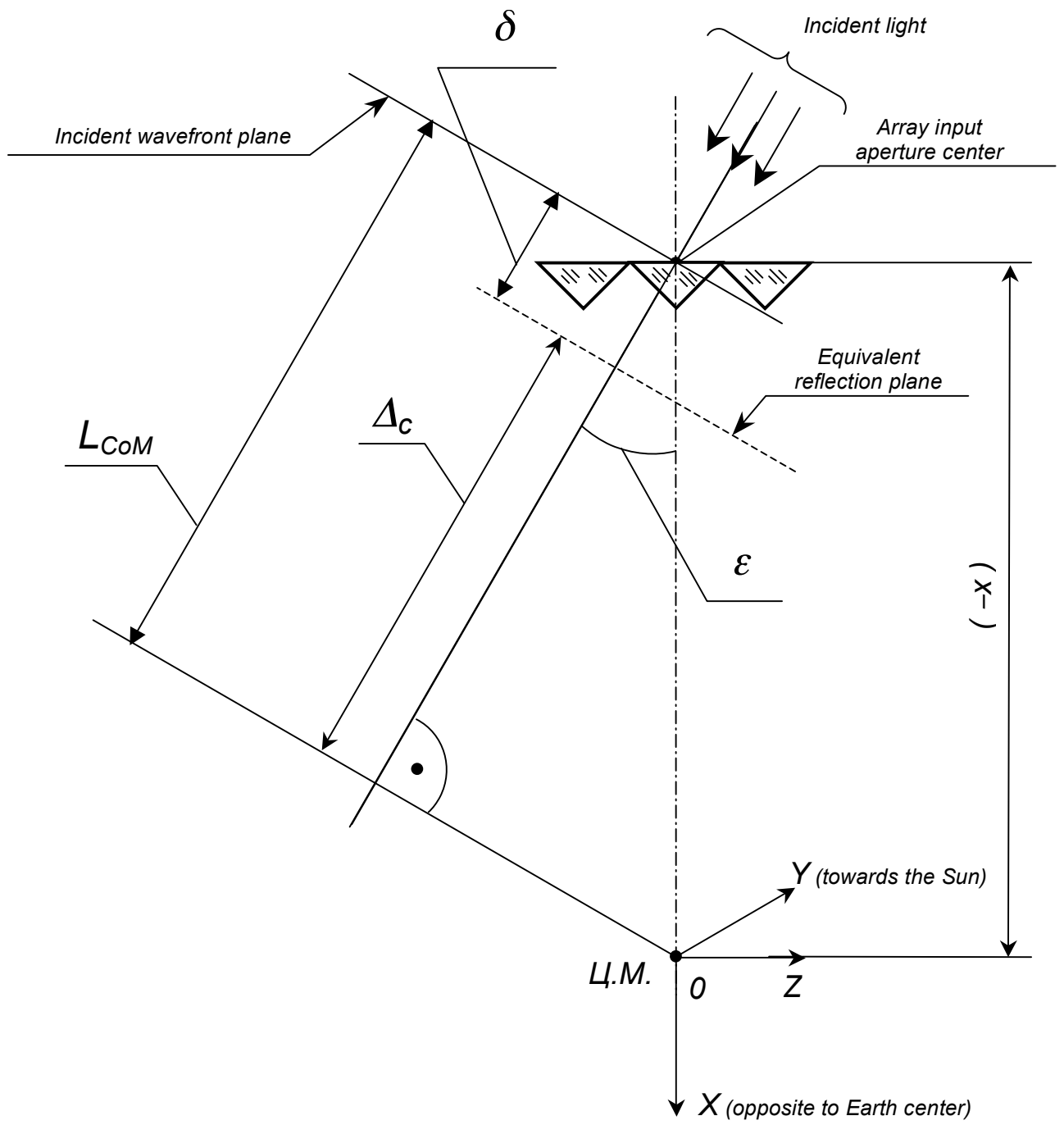
Table 2

ϵ , deg	δ , mm	ϵ , deg	δ , mm
0	27.899	8	28.03
1	27.901	9	28.06
2	27.91	10	28.10
3	27.92	11	28.14
4	27.93	12	28.19
5	27.95	13	28.24
6	27.97	14	28.29
7	28.00	15	28.35

The range to the SC to CoM is the measured range plus total correction value $\Delta_c = L_{CoM} - \delta$, where L_{CoM} is the SC CoM distance from the array input plane, and δ is the optical correction value.

For example, when the SC CoM and the array aperture center are on the X-axis (see also Figure 1): $L_{CoM} = -X \cdot \cos \epsilon$, where X is from Table 1, and $\Delta_c = -X \cdot \cos \epsilon - \delta$

Figure 1. Range reduction to the SC CoM



SPEED (m/s) and POINT AHEAD (PAH) ANGLES, SECONDS OF ARC

Azimuths are raw, and NOT multiplied by Cos(Elevation)

$$\text{"On-Sky"} = \sqrt{[(\Delta\text{az}.\cos\text{El})^{**2} + (\Delta\text{El})^{**2}]}$$

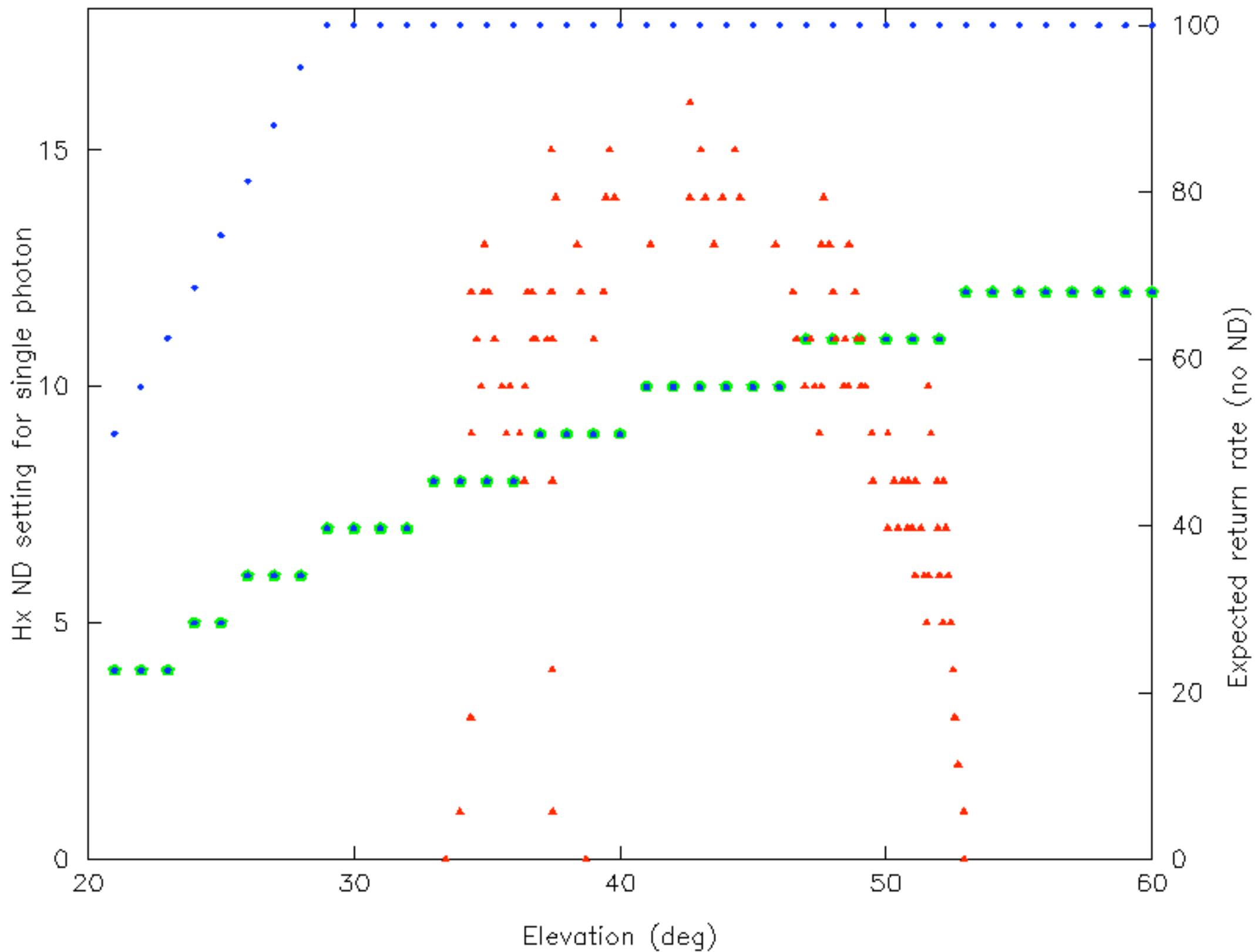
Speed and PAH angles computed for Stromlo SLR station (-35.3deg) from one CPF file per satellite.

Speeds are relative to the station, average of min and max.

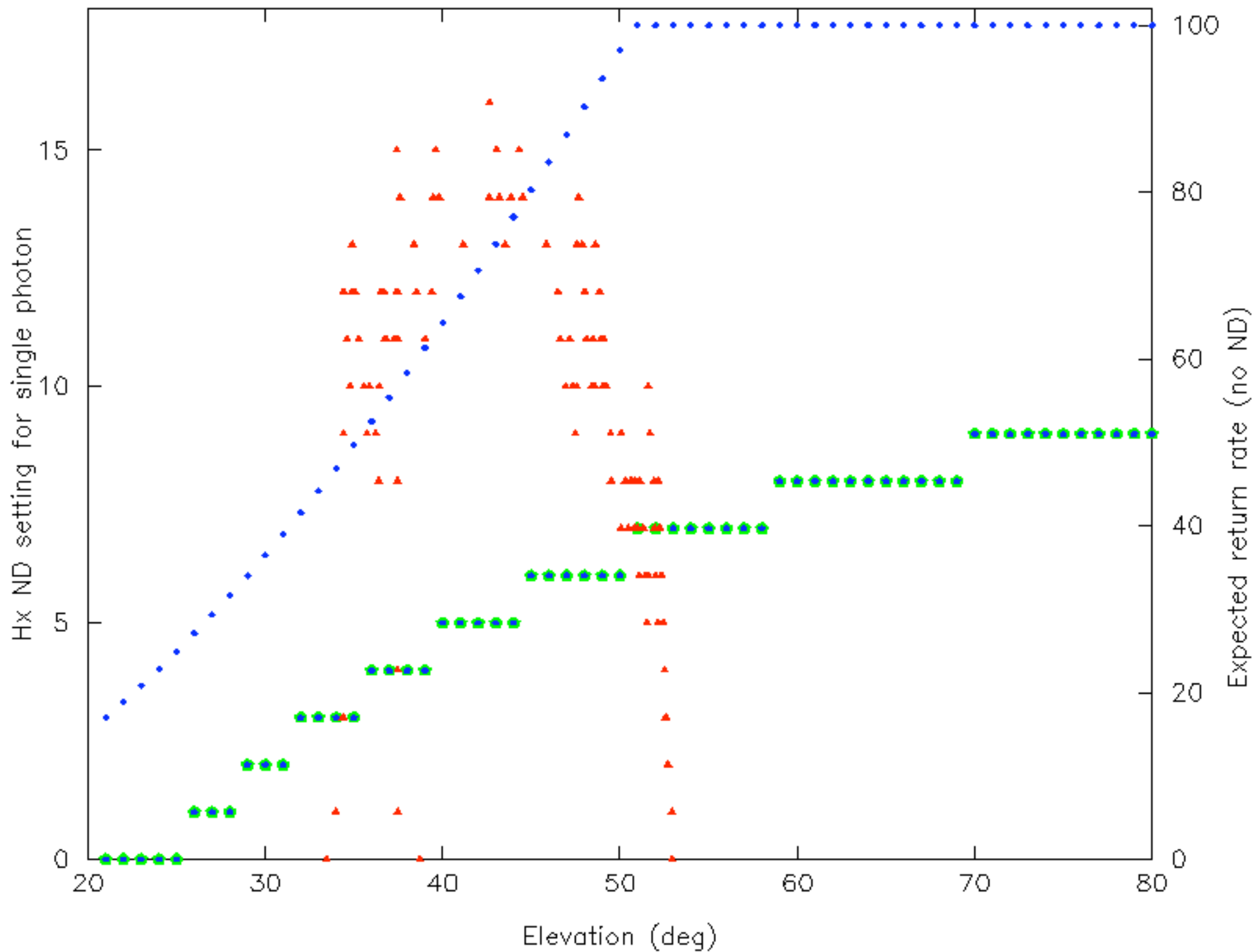
Relative

Satellite	CPF	Perigee Alt	Incl	Speed	On-Sky PAH (")		Azimuth PAH		Elevation PAH	
		(km)	(deg)	(m/sec)	Min	Max	Min	Max	Min	Max
GraceA	gfz	450	89.0	7590	4.0	10.6	-14.4	13.7	-6.9	6.7
Larets	sgf	691	98.2	7540	4.6	10.5	-25.0	14.9	-6.7	7.5
Envisat	sgf	800	98.5	7470	4.7	10.5	-25.2	12.6	-7.8	7.7
Jason1	sgf	1336	66.0	6970	5.6	9.8	-28.0	17.7	-8.7	8.7
Lageos1	sgf	5850	109.8	5740	6.6	8.3	-58.4	107.7	-7.6	7.8
Etalon1	sgf	19105	65.3	3930	4.9	5.8	-19.8	14.2	-5.1	5.2
Glonass95	cod	19140	64.0	3920	4.9	5.9	-31.5	20.9	-5.2	5.2
GPS35	cod	20195	54.2	3840	4.9	5.6	-1.5	31.9	-4.8	4.9
OptusB	jmckl	37180	0.0	2700	3.7	3.7	5.5	5.5	-0.6	-0.6
Apollo15	utx	356400	5.1	835	0.9	1.4	0.2	1.1	-1.4	1.0

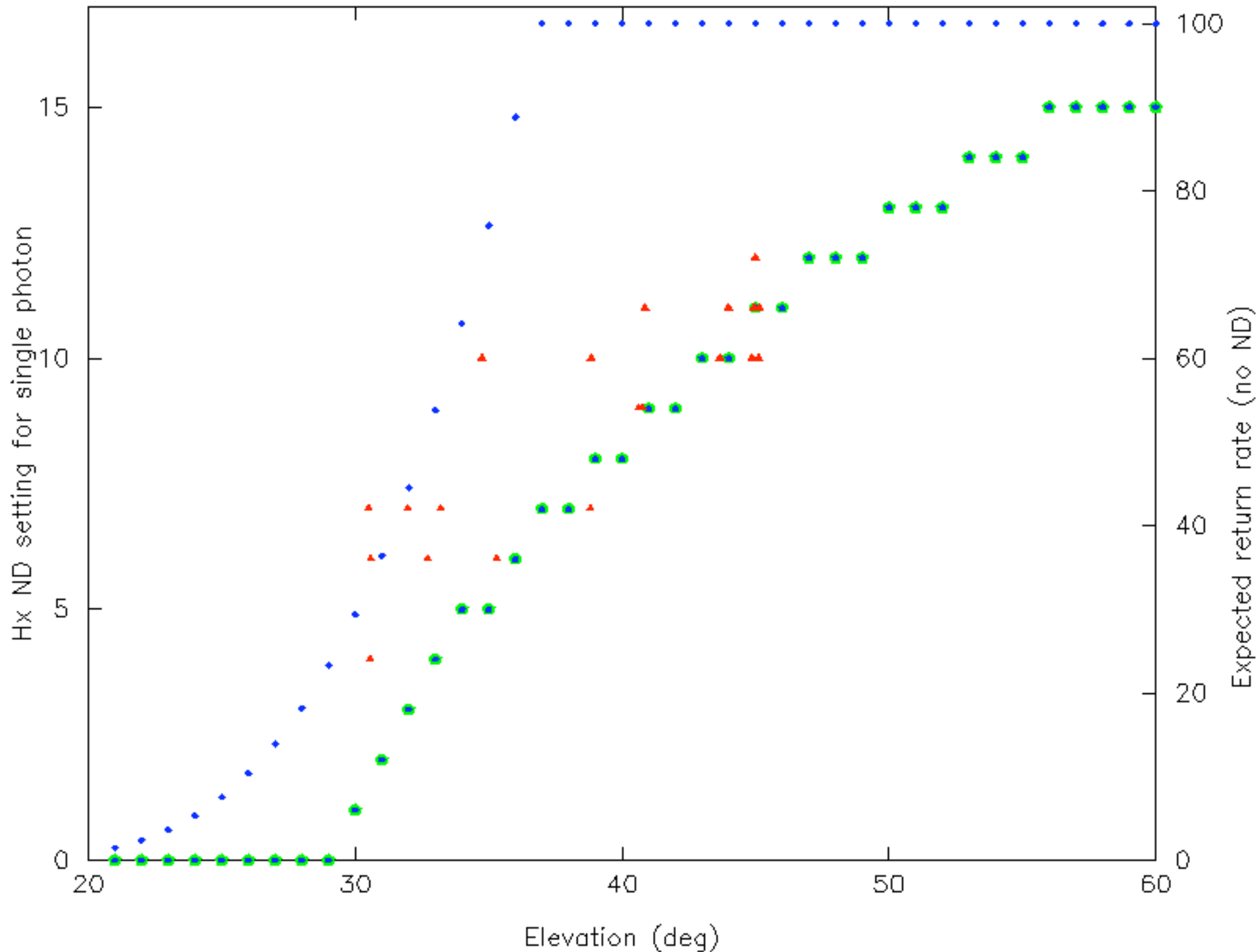
Link return stats lga



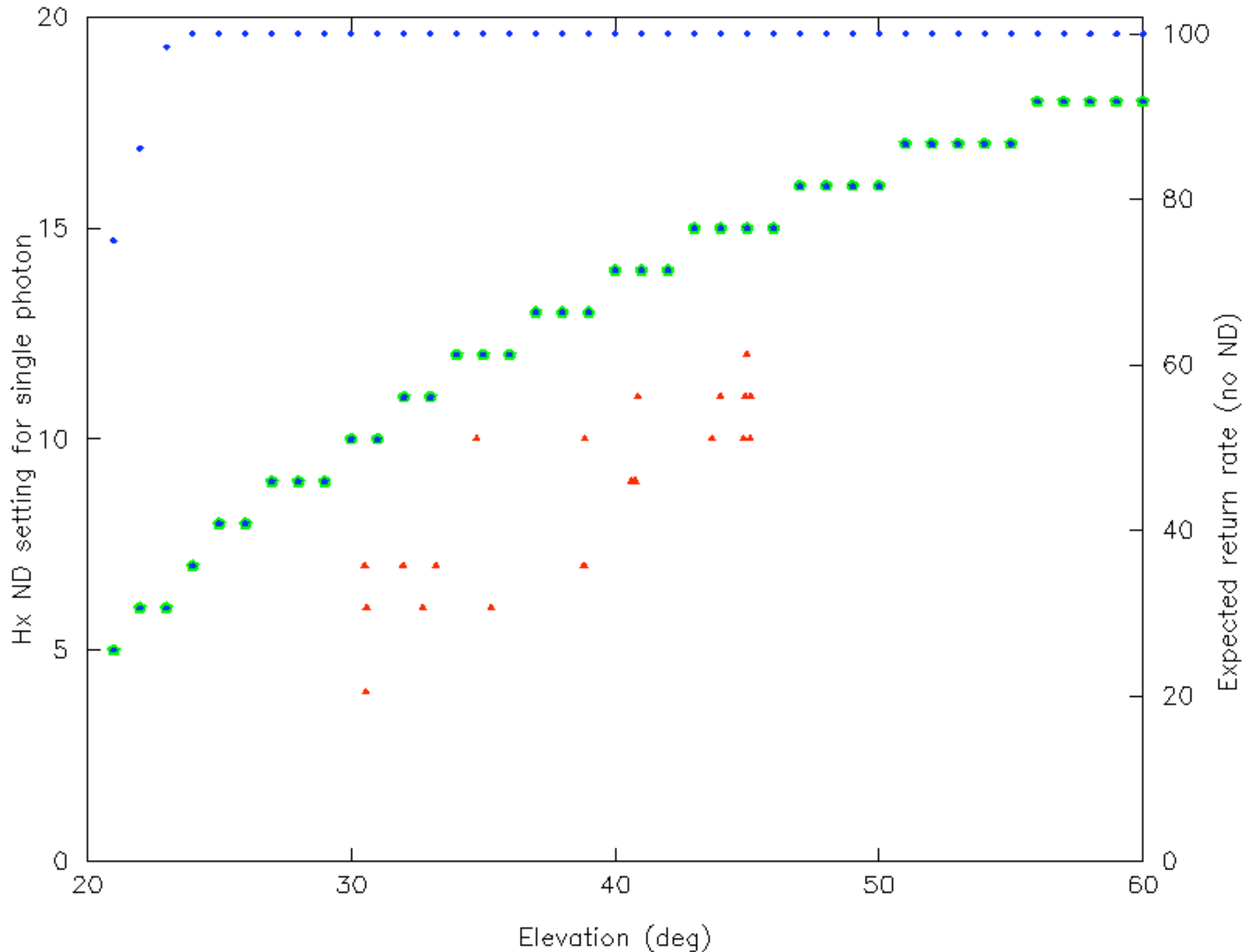
Link return stats lga



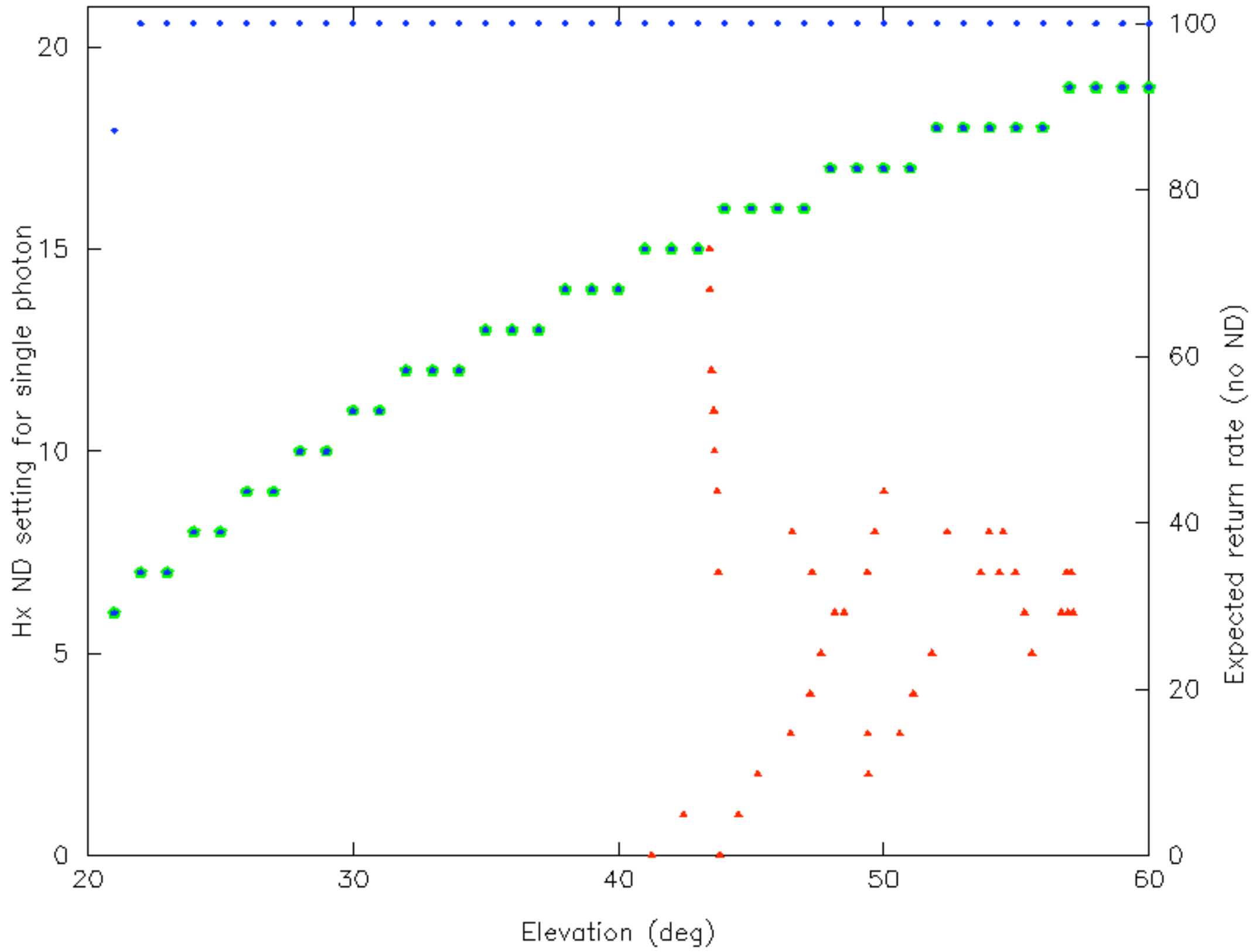
Link return stats str



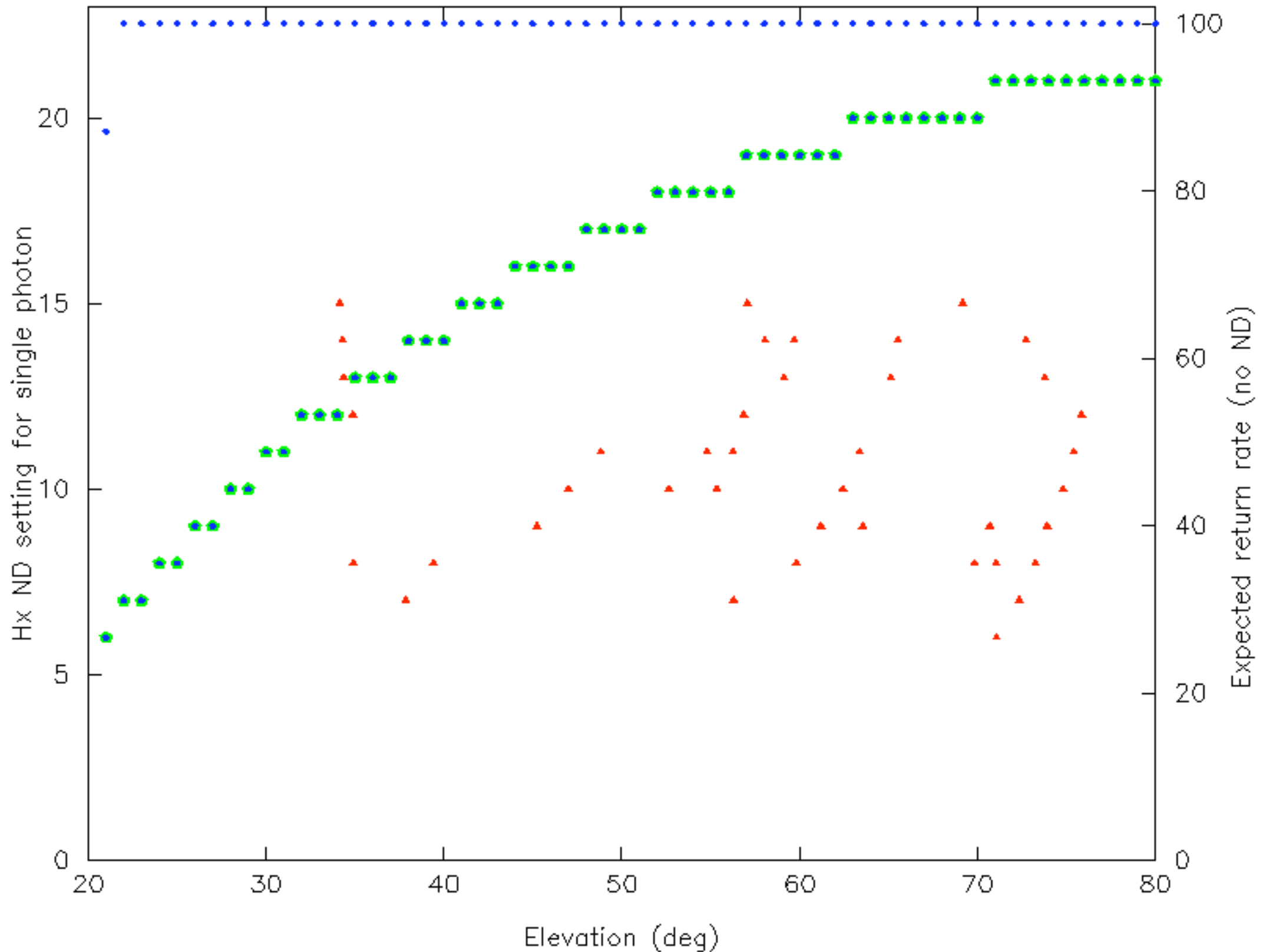
Link return stats str



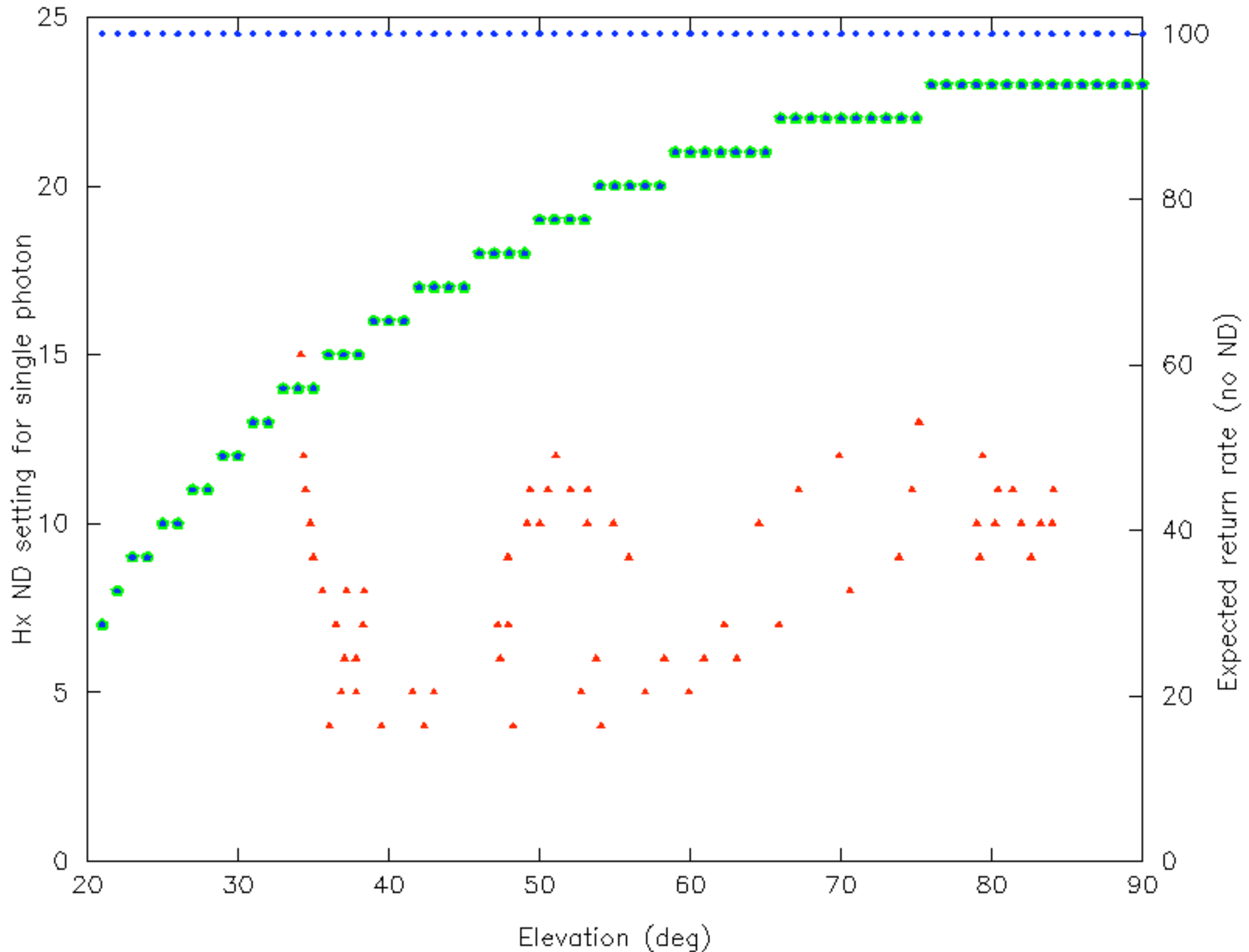
Link return stats aji



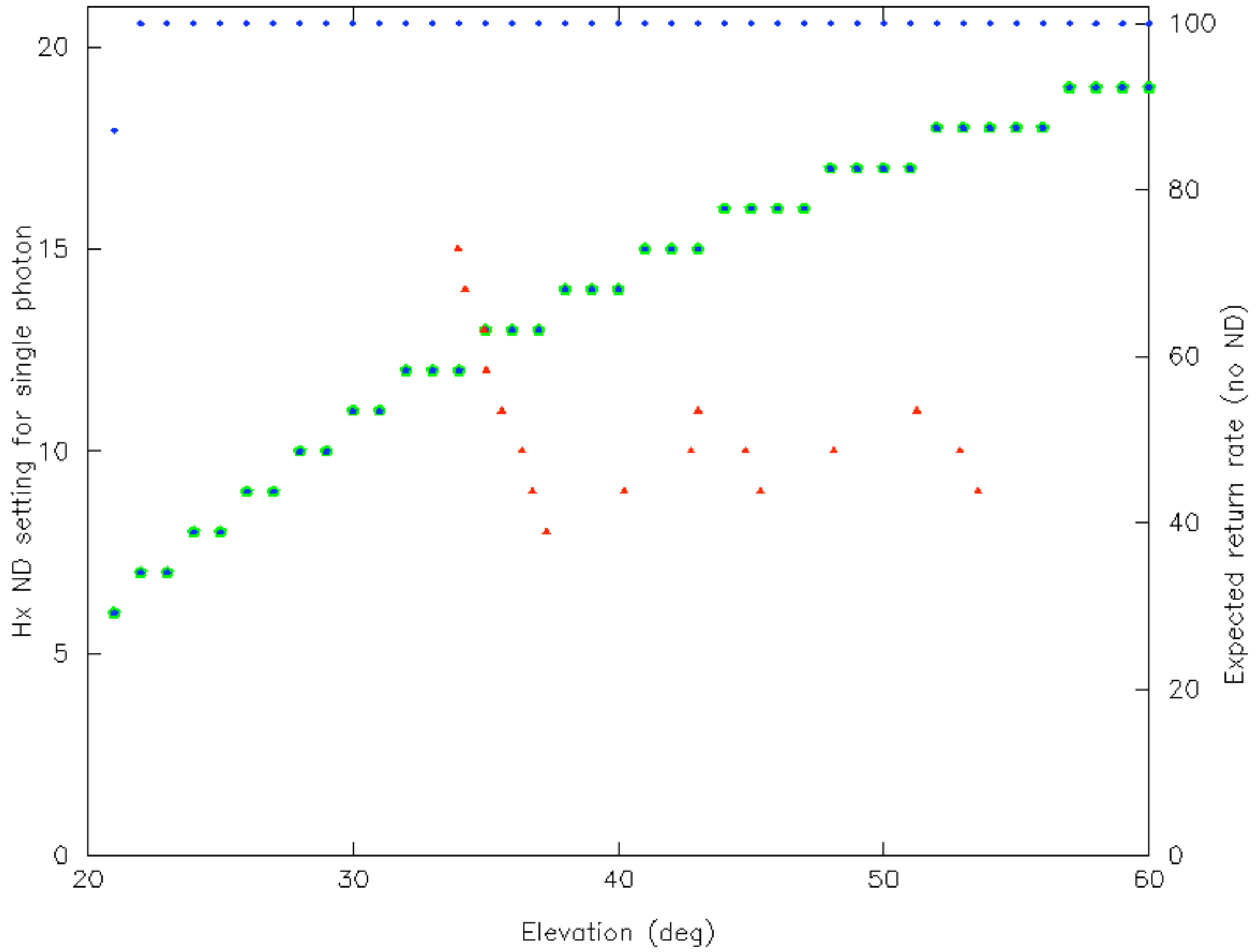
Link return stats aji



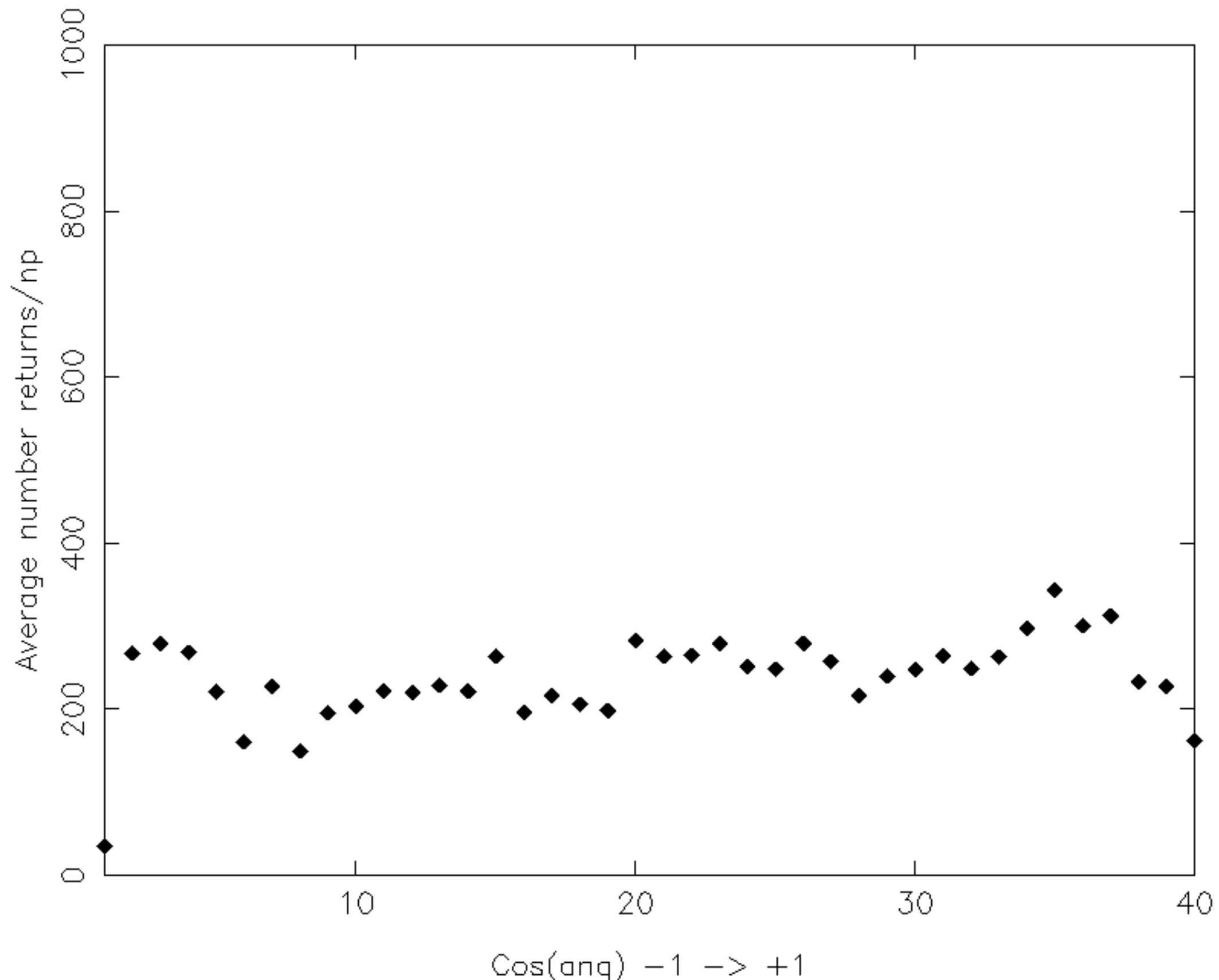
Link return stats aji



Link return stats aji



GPS tracking data



ILRS stations - System configuration and CoM corrections for LAGEOS

<i>Stn pad ID</i>	<i>Name</i>	<i>Pulselength</i>	<i>Detector</i>	<i>Regime</i>	<i>Processing</i>	<i>Calib.</i>	<i>LAGEOS</i>	<i>LAGEOS</i>
		<i>(ps)</i>		<i>(single, few, multi)</i>	<i>level</i>	<i>St. error (mm)</i>	<i>St. error (mm)</i>	<i>CoM (mm)</i>
1873	Simeiz	350	PMT	No Control	2.0 sigma	60	70	248-244
1884	Riga	130	PMT	Controlled s->m	2.0 sigma	10	15	252-248
7080	Mc Donald	200	MCP	Controlled s->m	3.0 sigma	8.5	13	250-244
7090	Yaragadee	200	MCP	Controlled f->m	3.0 sigma	4.5	10	250-244
7105	Greenbelt	200	MCP	Controlled f->m	3.0 sigma	5	10	250-244
7110	Monument Peak	200	MCP	Controlled f->m	3.0 sigma	5	10	250-244
7124	Tahiti	200	MCP	Controlled f->m	3.0 sigma	6	10	250-244
7237	Changchung	200	CSPAD	Controlled s->m	2.5 sigma	10	15	250-245
7249	Beijing	200	CSPAD	No Control, m	2.5 sigma	8	15	250-248
7355	Urumqui	30	CSPAD	No Control	2.5 sigma	15	30	255-247
7405	Conception	200	CSPAD	Controlled s	2.5 sigma	15	20	246-245
7501	Harteb.	200	PMT	Controlled f->m	3.0 sigma	5	10	250-244
7806	Metsahovi	50	PMT	?	2.5 sigma	15	17	254-248
7810	Zimmerwald	300	CSPAD	Controlled s->f	2.5 sigma	20	23	250-244
7811	Borowiec	40	PMT	No Control f	2.5 sigma	16	23	256-250
7824	San Fernando	100	CSPAD	No Control s->m	2.5 sigma	30	25	252-246
7825	Stromlo	10	CSPAD	Controlled s->m	2.5 sigma	4	10	257-247
7832	Riyadh	100	CSPAD	Controlled s->m	2.5 sigma	10	15	252-246
7835	Grasse	50	CSPAD	Controlled s->m	2.5 sigma	6	15	255-246
7836	Potsdam	35	PMT	Controlled s->m	2.5 sigma	10	20	256-252
7838	Simosato	100	MCP	Controlled s->m	3.0 sigma	20	40	252-248
7839	Graz	35	CSPAD	No Control m	2.2 sigma	3	9	255-250
7839	Graz kHz	10	CSPAD	No Control s->f	2.2 sigma	3	9	?
7840	Herstmonceux	100	CSPAD	Controlled s	3.0 sigma	8	17	246-244
7841	Potsdam 3	50	PMT	Controlled s->f	2.5 sigma	10	18	254-248
7941	Matera	40	MCP	No Control m	3.0 sigma	1	5	254-248
8834	Wettzell	80	MCP	No Control f->m	2.5 sigma	10	20	252-248